

2011

## Blind Estimation of OFDM System Parameters for Automatic Signal Identification

Qian Chen

Follow this and additional works at: <https://ir.lib.uwo.ca/digitizedtheses>

---

### Recommended Citation

Chen, Qian, "Blind Estimation of OFDM System Parameters for Automatic Signal Identification" (2011). *Digitized Theses*. 3277.  
<https://ir.lib.uwo.ca/digitizedtheses/3277>

This Thesis is brought to you for free and open access by the Digitized Special Collections at Scholarship@Western. It has been accepted for inclusion in Digitized Theses by an authorized administrator of Scholarship@Western. For more information, please contact [wlsadmin@uwo.ca](mailto:wlsadmin@uwo.ca).

# **Blind Estimation of OFDM**

## **System Parameters for**

### **Automatic Signal Identification**

(Spine title: Blind Estimation of OFDM System Parameters)

(Thesis format: Monograph Article)

by

**Qian Chen**

**Graduate Program  
in  
Engineering Science  
Electrical and Computer Engineering**

**A thesis submitted in partial fulfillment  
of the requirements for the degree of  
Master of Engineering Science**

**School of Graduate and Postdoctoral Studies  
The University of Western Ontario  
London, Ontario, Canada**

© Qian Chen 2011

# Certificate of Examination

THE UNIVERSITY OF WESTERN ONTARIO  
SCHOOL OF GRADUATE AND POSTDOCTORAL STUDIES  
CERTIFICATE OF EXAMINATION

Chief Advisor:

Dr. Xianbin Wang

Examining Board:

Dr. Liying Jiang

Dr. Ilia Polushin

Dr. Jagath Samarabandu

The thesis by

**Qian Chen**

entitled:

**Blind Estimation of OFDM**

**System Parameters for**

**Automatic Signal Identification**

is accepted in partial fulfillment of the

requirements for the degree of

**Master of Engineering Science**

Date: \_\_\_\_\_

Chair of Examining Board

Dr. Serguei L. Primak

## Abstract

Orthogonal frequency division multiplexing (OFDM) has gained worldwide popularity in broadband wireless communications recently due to its high spectral efficiency and robust performance in multipath fading channels. A growing trend of smart receivers which can support and adapt to multiple OFDM based standards automatically brings the necessity of identifying different standards by estimating OFDM system parameters without *a priori* information. Consequently, blind estimation and identification of OFDM system parameters has received considerable research attentions. Many techniques have been developed for blind estimation of various OFDM parameters, whereas estimation of the sampling frequency is often ignored. Furthermore, the estimated sampling frequency of an OFDM signal has to be very accurate for data recovery due to the high sensitivity of OFDM signals to sampling clock offset. To address the aforementioned problems, we propose a two-step cyclostationarity based algorithm with low computational complexity to precisely estimate the sampling frequency of a received oversampled OFDM signal. With this estimated sampling frequency and oversampling ratio, other OFDM system parameters, i.e., the number of subcarriers, symbol duration and cyclic prefix (CP) length can be estimated based on the cyclic property from CP sequentially. In addition, modulation scheme used in the OFDM can be classified based on the higher-order statistics (HOS) of the frequency domain OFDM signal.

All the proposed algorithms are verified by a lab testing system including a vector signal generator, a spectrum analyzer and a high speed digitizer. The evaluation results confirm the high precision and efficacy of the proposed algorithm in realistic scenarios.

**Key Words:** OFDM, sampling frequency, cyclostationary, oversampling ratio, blind parameter estimation, modulation scheme classification.

## Acknowledgements

This research would not have been possible without the support of many people. I am heartily thankful to those people who helped me and inspired me during my research.

In the first place I gratefully thank my professor Dr. Xianbin Wang for giving me the confidence to explore my research interests and the guidance to avoid getting lost in my exploration. It has been a true fortune and privilege to work with him.

I also owe my deepest gratitude to Dr. Serguei Primak, Dr. Raveendra Rao, and Dr. Hanif Ladak for those courses greatly improved my research in theoretical analysis, understanding of communication systems, and simulation works.

I am indebted to Dr. Weikun Hou for helping me complete my thesis. His lively discussions and constructive feedbacks improved my knowledge and enlarged my prospects. His patient instructions and guidance will benefit me for my future study and work all the time.

My deepest gratitude goes to my family for their unflagging love and support throughout my life. I have been blessed with the most wonderful and supportive family any one can wish for. Despite of the geographical distance, my family was always nearby and giving me confidence and encouragements consistently during my study.

Last but not least, I would like to thank my boyfriend for his advice on my research and also for all his encouragements when I got frustrated.

# Table of Contents

Certificate of Examination . . . . .	ii
Abstract . . . . .	iii
Acknowledgements . . . . .	iv
List of tables . . . . .	viii
List of figures . . . . .	ix
Acronyms . . . . .	xi
<b>1 Introduction . . . . .</b>	<b>1</b>
1.1 Background . . . . .	1
1.2 Motivations and Objectives . . . . .	3
1.3 Thesis Contributions . . . . .	5
1.4 Thesis Organization . . . . .	6
<b>2 Review of OFDM Systems . . . . .</b>	<b>8</b>
2.1 FDM and OFDM . . . . .	8
2.2 Basics of OFDM . . . . .	10
2.2.1 Analog Representation of OFDM Signals . . . . .	10
2.2.2 Digital Representation of OFDM Signals . . . . .	11
2.2.3 Cyclic Prefix . . . . .	12
2.3 OFDM System Structure . . . . .	13
2.3.1 Transmitter Structure . . . . .	15
2.3.2 Receiver Structure . . . . .	15
2.4 Impairments of Non-ideal Transmission . . . . .	18
2.4.1 Multipath Channel . . . . .	18
2.4.2 CFO and SFO . . . . .	19
2.5 Wireless Communication Standards Based on OFDM System . . . . .	24
2.5.1 OFDM Advantages and Disadvantages . . . . .	24
2.5.2 Current Standards Using OFDM . . . . .	25
2.6 Summary . . . . .	31

<b>3</b>	<b>Algorithms for Blind Estimation of OFDM System Parameters</b>	<b>33</b>
3.1	Signal Cyclostationarity	33
3.1.1	Cyclostationary Process	34
3.1.2	An Interpretation of the Cyclic Correlation Function	37
3.2	Second-Order Cyclostationarity of Received Oversampled OFDM Signals	38
3.2.1	Signal Model	38
3.2.2	Cyclostationarity in Oversampled OFDM Signals	40
3.2.3	Cyclic Frequency Estimator	42
3.3	Sampling Frequency Estimation by A Two-Step Algorithm	43
3.3.1	Conventional One-Step CF Estimation	43
3.3.2	Zoom Fast Fourier Transform	45
3.3.3	Proposed Two-Step CF Estimator Based on ZFFT	51
3.4	Estimation of Other System Parameters	54
3.4.1	Estimation of the Number of Subcarriers	54
3.5	Complexity Analysis of the Proposed Algorithm for Oversampling Ratio Estimation	57
3.6	Simulation Results	59
3.6.1	Simulation Setup	59
3.6.2	Numerical Results	59
3.7	Summary	60
<b>4</b>	<b>Modulation Scheme Classification for OFDM Systems</b>	<b>64</b>
4.1	Digital Modulation Techniques	65
4.1.1	Phase Shift Keying (PSK)	65
4.1.2	Quadrature Amplitude Modulation (QAM)	67
4.2	Review of Existing Modulation Classification Methods	69
4.2.1	Likelihood-based Methods	69
4.2.2	Feature-based Methods	70
4.3	HOS Basics	70
4.3.1	Moments	70
4.3.2	Cumulants	71
4.4	Proposed Modulation Classification Algorithm for OFDM Systems	74
4.4.1	Signal Model	74
4.4.2	Theoretical Cumulants for Different Constellations	75
4.4.3	Proposed Algorithm for OFDM Subcarrier MS	76
4.5	Simulation Results	77
4.5.1	Simulation Setup	78
4.5.2	Numerical Results	78
4.6	Summary	79

*Table of Contents*

---

<b>5</b>	<b>Lab Testing for Algorithm Verification . . . . .</b>	<b>82</b>
5.1	Introduction of lab testing system . . . . .	82
5.1.1	Hardware and Software Specifications . . . . .	82
5.1.2	Equipment Setup for Testing System . . . . .	84
5.2	Workflow of the Lab Testing . . . . .	85
5.2.1	Signal Generation . . . . .	86
5.2.2	Signal Validation . . . . .	91
5.2.3	Signal Reception . . . . .	92
5.3	Verification of the Proposed Algorithm . . . . .	93
5.4	Summary . . . . .	96
<b>6</b>	<b>Conclusion . . . . .</b>	<b>100</b>
6.1	Research Contributions . . . . .	100
6.2	Future Work . . . . .	101
	<b>References . . . . .</b>	<b>103</b>
	<b>Appendices</b>	
<b>A</b>	<b>Time-varying ACF, CCF and CS of OFDM Signals . . . . .</b>	<b>109</b>
	<b>Curriculum Vitae . . . . .</b>	<b>115</b>



## List of Tables

2.1	OFDM parameters in WiMAX . . . . .	30
2.2	Summary of OFDM based wireless standards . . . . .	32
3.1	Computational complexity comparisons between the proposed algorithm and the conventional algorithm . . . . .	58
4.1	Theoretical cumulants for constellations under constraints of unit variance. . . . .	76
5.1	Hardware specifications for the testing platform . . . . .	84
5.2	Software specifications for the testing platform . . . . .	84
5.3	System parameter of IEEE 802.11a used in the testing . . . . .	88
5.4	Modulation schemes and data rates in IEEE 802.11a . . . . .	88
5.5	Signal configurations in WinQSIM . . . . .	89

## List of Figures

1.1	Application of blind estimation of OFDM system parameters in smart receivers. . . . .	2
1.2	Example of blind signal parameter estimation in military application. . . . .	4
2.1	OFDM exploits subcarrier orthogonality for spectral efficiency. . . . .	9
2.2	One OFDM symbol with CP. . . . .	12
2.3	Elimination of ISI by CP. . . . .	13
2.4	OFDM transmitter structure. . . . .	14
2.5	Example of 5 subcarriers in one OFDM symbol in the frequency domain. . . . .	16
2.6	Example of 5 subcarrier signals in one OFDM symbol in the time domain. . . . .	16
2.7	OFDM receiver structure. . . . .	17
2.8	Phase rotation between two adjacent OFDM subcarriers due to CFO and SFO. . . . .	23
2.9	DTT broadcasting standards around the world. . . . .	25
2.10	OFDMA signal structure specified in WiMAX. . . . .	28
2.11	Frequency range and data rate specified by typical OFDM based wireless standards. . . . .	31
3.1	Cyclic spectrum of an oversampled OFDM signal. . . . .	41
3.2	Block diagram of ZFFT. . . . .	45
3.3	The frequency spectrum of $U(e^{j\omega})$ . . . . .	46
3.4	The spectrum of $v(n)$ after frequency shifting of $u(n)$ . . . . .	47
3.5	The ideal lowpass filter $H_{LP}(e^{j\omega})$ . . . . .	47
3.6	The spectrum of $u_0(n)$ after decimation. . . . .	48
3.7	The spectrum of $u_0(n)$ after decimation. . . . .	49
3.8	Spectrum of a signal with closely spaced frequency components processed with a)FFT and b)ZFFT. . . . .	50
3.9	Block diagram of blind estimation of OFDM system parameters. . . . .	51
3.10	Computational complexity of the proposed algorithm compared to the conventional algorithm with the same estimation accuracy. . . . .	62
3.11	NMSE of oversampling ratio estimated from the proposed algorithm and conventional algorithm versus SNR under AWGN and multipath channels. . . . .	62
3.12	Correct estimation probability of number of subcarriers and CP length in multipath channel with AWGN under different SNRs. . . . .	63

3.13	NMSE of the CFO estimation versus SNR under both AWGN and multipath channels. . . . .	63
4.1	Binary data and the corresponding waveform of a BPSK signal. . . .	66
4.2	Binary data and the corresponding waveform of a QPSK signal. . . .	66
4.3	The constellation of 16QAM modulation scheme. . . . .	68
4.4	Binary data and the corresponding waveform of a 16QAM signal. . .	68
4.5	Correct classification probability of the proposed algorithm versus SNR. 80	
4.6	Correct classification probability of the proposed algorithm with different number of samples when SNR=10 dB. . . . .	80
4.7	Estimated SERs compared with the theoretical SERs of four MSs. . .	81
5.1	R&S® SMJ100A vector signal generator. . . . .	83
5.2	R&S FSP spectrum analyzer. . . . .	83
5.3	National instruments PXI 5105 high speed digitizer. . . . .	83
5.4	Instrument setup for the algorithm evaluation. . . . .	85
5.5	R&S® WinIQSIM configurations for generating IEEE 802.11a signals. 86	
5.6	Multipath configuration panel. . . . .	89
5.7	Frequency offset configuration panel. . . . .	90
5.8	Configuration of waveform generation in WinIQSIM. . . . .	91
5.9	Setup for signal waveform transmission on R&S® SMJ100A. . . . .	91
5.10	Transmit spectrum mask according to IEEE 802.11a standard. . . . .	92
5.11	Power spectrum of the transmitted signal observed from spectrum analyzer. . . . .	92
5.12	Configuration window of the signal waveform reception. . . . .	93
5.13	Lab testing system for the verification of the blind estimation algorithm. 94	
5.14	Power spectrum of the IEEE 802.11a signal received by NI PXI 5105 high speed digitizer. . . . .	97
5.15	Correlation peaks in the estimation of the number of subcarriers. . . .	97
5.16	NMSE of oversampling ratio estimation of the proposed algorithm versus SNR under both AWGN and multipath channels. . . . .	98
5.17	Probability of correct estimation of the number of subcarriers and CP length under both AWGN and multipath channels versus SNR. . . . .	98
5.18	NMSE of the CFO estimation versus SNR under both AWGN and multipath channels. . . . .	99
5.19	Modulation scheme classification versus SNR under both AWGN and multipath channels. . . . .	99

## Acronyms

ACF	<i>Autocorrelation Function</i>
ADC	<i>Analog-to-Digital Converter</i>
ARB	<i>Arbitrary Waveform Generator</i>
AWGN	<i>Additive White Gaussian Noise</i>
BPSK	<i>Binary Phase Shift Keying</i>
BWA	<i>Broadband Wireless Access</i>
CCF	<i>Cyclic Correlation Function</i>
CF	<i>Cyclic Frequency</i>
CFO	<i>Carrier Frequency Offset</i>
CP	<i>Cyclic Prefix</i>
CR	<i>Cognitive Radio</i>
CS	<i>Cyclic Spectrum</i>
DA	<i>Data-Aided</i>
DAC	<i>Digital-to-Analog Converter</i>
DC	<i>Direct Current</i>
DD	<i>Decision-Directed</i>
DFT	<i>Discrete Fourier Transform</i>
DSL	<i>Digital Subscriber Line</i>
DTT	<i>Digital Terrestrial Television</i>
DVB	<i>Digital Video Terrestrial Broadcasting</i>
FB	<i>Featured-Based</i>
FDM	<i>Frequency Division Multiplexing</i>
FFT	<i>Fast Fourier Transform</i>
HOS	<i>Higher-order Statistics</i>
ICI	<i>Intercarrier Interference</i>
IDFT	<i>Inverse Discrete Fourier Transform</i>
IEEE	<i>Institute of Electrical and Electronics Engineers</i>
IFFT	<i>Inverse Fast Fourier Transform</i>

<b>ISI</b>	<i>Inter Symbol Interference</i>
<b>LB</b>	<i>Likelihood-Based</i>
<b>LNA</b>	<i>Low-Noise Amplifier</i>
<b>LoS</b>	<i>Line-of-Sight</i>
<b>M-C</b>	<i>Moment-to-Cumulant</i>
<b>MIMO</b>	<i>Multiple Input Multiple Output</i>
<b>MS</b>	<i>Modulation Scheme</i>
<b>NDA</b>	<i>Non-Data-Aided</i>
<b>NI</b>	<i>National Instruments</i>
<b>NLoS</b>	<i>Non-Line-of-Sight</i>
<b>NMSE</b>	<i>Normalized Mean Square Error</i>
<b>OFDM</b>	<i>Orthogonal Frequency Division Multiplexing</i>
<b>OFDMA</b>	<i>Orthogonal Frequency Division Multiple Access</i>
<b>PHY</b>	<i>Physical Layer</i>
<b>P/S</b>	<i>Parallel-to-Serial</i>
<b>QAM</b>	<i>Quadrature Amplitude Modulation</i>
<b>QPSK</b>	<i>Quadrature Phase Shift Keying</i>
<b>RF</b>	<i>Radio Frequency</i>
<b>PRBS</b>	<i>Pseudo Random Binary Sequence</i>
<b>R&amp;S</b>	<i>Rohde&amp;Schwarz<sup>®</sup></i>
<b>SCM</b>	<i>Single Carrier Modulations</i>
<b>SFN</b>	<i>Single Frequency Networks</i>
<b>SFO</b>	<i>Sampling Frequency Offset</i>
<b>SNR</b>	<i>Signal-to-Noise Ratio</i>
<b>S&amp;R</b>	<i>Surveillance and Reconnaissance</i>
<b>S/P</b>	<i>Serial-to-Parallel</i>
<b>WLAN</b>	<i>Wireless Local Area Network</i>
<b>WSSUS</b>	<i>Wide Sense Stationary Uncorrelated Scattering</i>
<b>ZFFT</b>	<i>Zoom Fast Fourier Transform</i>

# Chapter 1

## Introduction

### 1.1 Background

Multi-carrier transmission has been deployed for broadband wireless communications in order to overcome hostile signal propagation environments. As a special form of multi-carrier transmission, orthogonal frequency division multiplexing (OFDM) is becoming a popular modulation scheme by the adoption of a group of orthogonal subcarriers. Due to its high spectrum efficiency and robust performance in multipath fading channels, OFDM system has been adopted in many wireless applications, including IEEE 802.11 wireless local area network (WLAN) [1] and Digital Video Terrestrial Broadcasting (DVB) [2].

The dramatic increase of OFDM based global wireless applications poses a looming challenge of developing smart receivers that can support and adapt to multiple standards automatically using the cognitive radio (CR) technology. It is expected that such software-defined radio receivers are capable of intelligently detecting and identifying radio signals so that interference identification, signal confirmation and spectrum management can be performed to optimize the system performance as well as spectrum utilization efficiency.

Fig. 1.1 shows the block diagram of a smart receiver for OFDM systems. Basically, a smart receiver consists of three main blocks: a receiver frontend for down converting the received signal to baseband from radio frequency; an estimator that

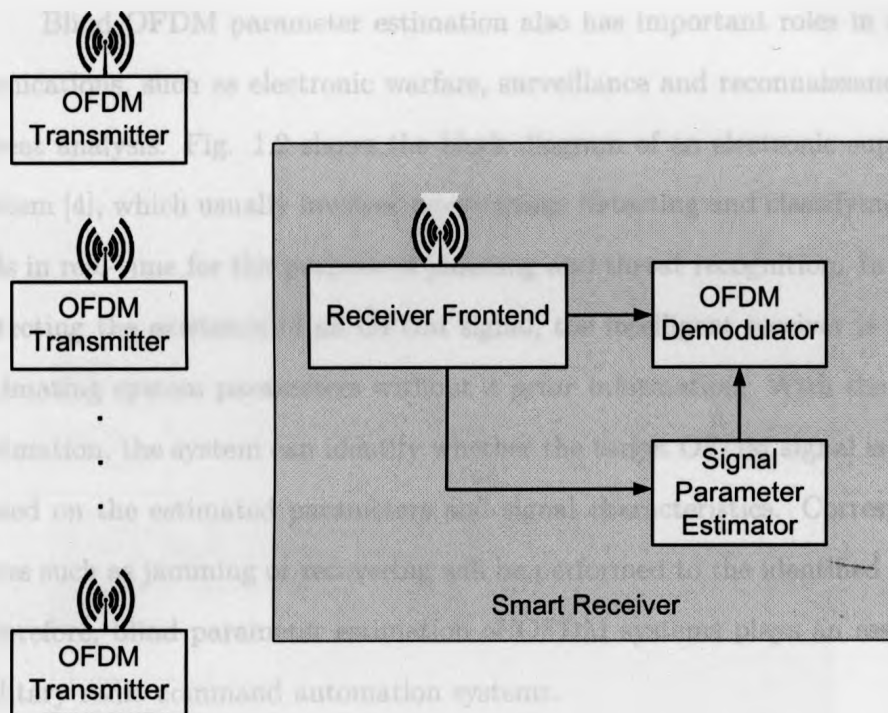


Figure 1.1: Application of blind estimation of OFDM system parameters in smart receivers.

blindly estimates OFDM system parameters and a demodulator that recovers the signal.

The OFDM system parameter estimator shown in Fig. 1.1 is an indispensable component in the smart receiver. By estimating OFDM system parameters without *a priori* knowledge, the receiver is able to automatically adapt its receiving algorithm to various wireless applications. Furthermore, based on the estimation results, wireless service provider may detect and suppress the interference, monitor the spectrum usage and trace unlicensed transmitters in wireless networks for dynamic spectrum sharing. Therefore, blind estimation and identification of OFDM signals is expected to be one of the most important components for cognitive radio (CR) system design and dynamic spectrum sharing [3].

Blind OFDM parameter estimation also has important roles in military communications, such as electronic warfare, surveillance and reconnaissance (S&R) and threat analysis. Fig. 1.2 shows the block diagram of an electronic support measure system [4], which usually involves intercepting, detecting and classifying received signals in real-time for the purpose of jamming and threat recognition. In general, after detecting the existence of an OFDM signal, the intelligent receiver is responsible of estimating system parameters without *a priori* information. With the help of blind estimation, the system can identify whether the target OFDM signal is hostile or not based on the estimated parameters and signal characteristics. Corresponding measures such as jamming or recovering will be performed to the identified hostile signal. Therefore, blind parameter estimation of OFDM systems plays an essential part in military radio command automation systems.

## 1.2 Motivations and Objectives

The wide deployment of different OFDM systems in broadband wireless communications raises new challenges for blind system identification and parameter estimations. However, most existing blind signal parameter estimation algorithms in literature are focused on single carrier modulations (SCM) where only carrier frequency and modulation schemes are blindly estimated. These algorithms are not directly applicable for OFDM signals due to significant differences between SCM and OFDM in signal formats.

Although some blind estimation algorithms have been proposed for OFDM systems [5] [6] [7] [8], most of which [5] [6] focus on the synchronization parameter estimation or the bandwidth estimation [7] [8]. Moreover, one of the common weaknesses of these algorithms is the assumption of a perfectly known sampling frequency



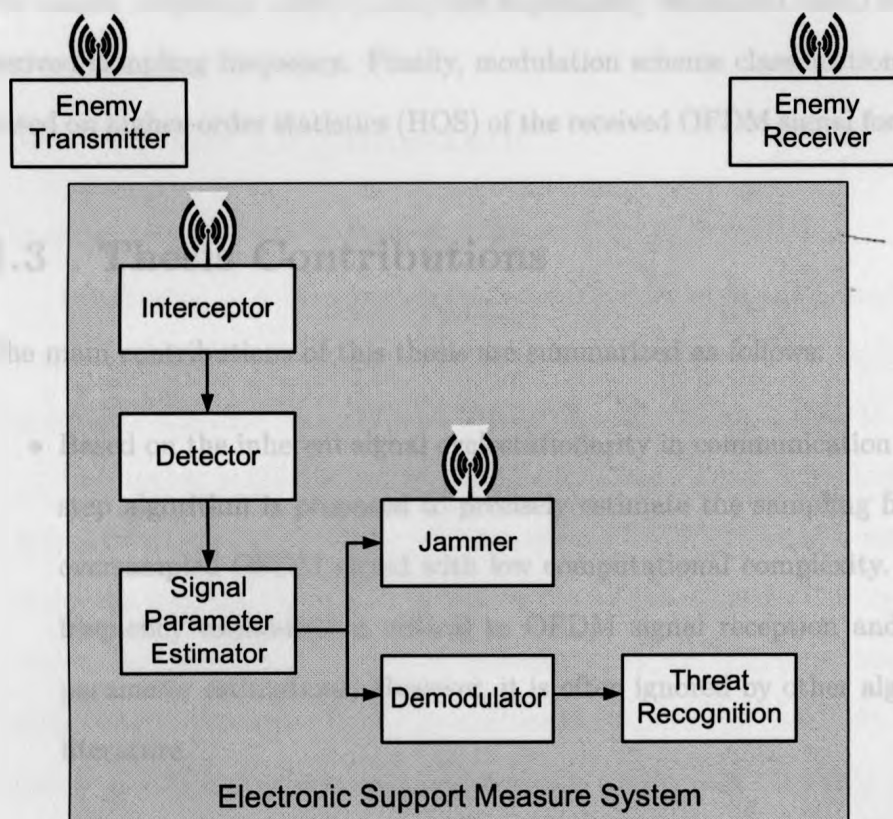


Figure 1.2: Example of blind signal parameter estimation in military application.

which is not available in realistic scenarios.

In this thesis, to achieve blind OFDM system parameter estimation, a two-step algorithm is first proposed for precisely estimating sampling frequency of a received oversampled OFDM signal. Following this, various parameters of OFDM signals, including the number of subcarriers, symbol duration, length of cyclic prefix (CP) and the carrier frequency offset (CFO) are sequentially estimated based on the previous derived sampling frequency. Finally, modulation scheme classification is carried out based on higher-order statistics (HOS) of the received OFDM signal for data recovery.

### 1.3 Thesis Contributions

The main contributions of this thesis are summarized as follows:

- Based on the inherent signal cyclostationarity in communication signals, a two-step algorithm is proposed to precisely estimate the sampling frequency of an oversampled OFDM signal with low computational complexity. The sampling frequency estimation is critical to OFDM signal reception and other system parameter estimations. However, it is often ignored by other algorithms in the literature.
- All remaining OFDM system parameters, i.e., the number of subcarriers, symbol duration, length of CP and CFO are blindly estimated based on the previously estimated sampling frequency of the received signal.
- The modulation scheme employed by OFDM system is classified using the HOS of the signal. The subcarrier based algorithm can classify the modulation scheme of each OFDM subcarrier which is useful for adaptive OFDM systems where different modulation schemes may be employed by different subcarriers.

- The proposed algorithm for blind OFDM system parameter estimations are verified by a lab testing system which includes Rohde&Schwarz (R&S®) SMJ100A vector signal generator, National Instruments (NI) PXI 5105 high speed digitizer, MATLAB and LABVIEW simulation softwares. The evaluation results confirm the precision and efficacy of the proposed algorithm in realistic scenarios.

## 1.4 Thesis Organization

The organization of this thesis is as follows:

In Chapter 2, a brief introduction to OFDM systems is provided. The basic concept of OFDM, the corresponding transceiver structure, the main implementation impairments together with different industrial applications of OFDM are presented.

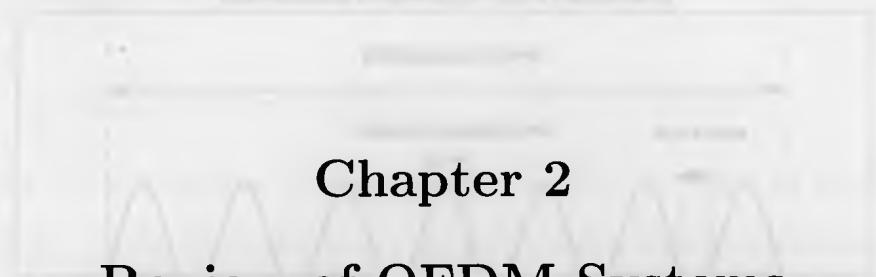
In Chapter 3, OFDM system parameters (i.e., the sampling frequency, number of subcarriers, symbol duration, CP length and CFO) are blindly estimated by exploiting the inherent characteristics of the oversampled signal. The cyclostationarity of an oversampled OFDM signal is investigated in the beginning under a time dispersive channel corrupted by additive white Gaussian noise (AWGN). The analytical expressions for the cyclic correlation function (CCF) and the cyclic spectrum (CS) are derived to prove the existence of cyclostationarity in OFDM signals. By using the inherent cyclostationarity, a two-step algorithm for sampling frequency and oversampling ratio estimation is proposed subsequently. Other OFDM parameters, i.e., the number of subcarriers, symbol duration, CP length and CFO are estimated in the sequel. Finally, the complexity of the proposed algorithm is analyzed and performances of the proposed estimation algorithm are evaluated.

In Chapter 4, a subcarrier based modulation scheme classification algorithm is presented. Various modulation schemes commonly employed in OFDM systems are introduced at the beginning of this chapter. Following this, a review of the existing algorithms for modulation scheme classification in the literature is given. Basic principles of HOS of stationary random variables and processes are discussed sequentially. The classification algorithm based on the HOS of the frequency domain signal is then proposed, by which four modulation schemes mainly used in OFDM systems, namely, BPSK, QPSK, 16QAM and 64QAM can be classified. Finally, simulation results are presented to validate the analysis and the performance of the proposed algorithm.

In Chapter 5, a lab testing system for algorithm evaluations are presented. The evaluations of the proposed algorithm are carried out on an oversampled OFDM signal from vector signal generator and the results confirm the high precision of the proposed algorithm. Finally, conclusions are drawn and future works are discussed in Chapter 6.

## 2.1 FDM and OFDM

The goal of using OFDM for both data and transmission is to avoid the interference between different subcarriers. OFDM is an extension to the conventional FDM with complex orthogonal design. In OFDM, every subcarrier carries one substream and transmitting to different frequency bands. In different cases, different modulation schemes can be used for each subcarrier. In this chapter, we will focus on the OFDM system for data transmission.



## Chapter 2

# Review of OFDM Systems

OFDM is a wideband digital communications technique in which high-rate data is transmitted in parallel via multiple orthogonal subcarriers. In 1966, the idea of multi-carrier transmission was first brought out by Chang in [9]. Weinstein and Ebert subsequently proposed a complete digital OFDM system that used discrete Fourier transform (DFT) and inverse DFT (IDFT) for baseband modulation and demodulation in 1971 [10]. From then on, OFDM systems have been investigated for wideband communications over various channels [11]. In this chapter, the principle of OFDM system is explained compared with conventional frequency division multiplexing (FDM). The basics of OFDM are introduced, including the analog and digital presentations. The transmitter and receiver structures for OFDM systems are presented in the sequel. Finally, the main merits and drawbacks of OFDM system are summarized, followed by the major applications of OFDM systems.

### 2.1 FDM and OFDM

The idea of using OFDM for high data rate transmissions has been investigated due to its simple structure and bandwidth efficiency. OFDM is an extension to the conventional FDM with respect to spectrum usage. In FDM, many parallel carriers are modulated and transmitted in different frequency bands to different users simultaneously. To avoid inter-band interference caused by spectral leakage in conventional

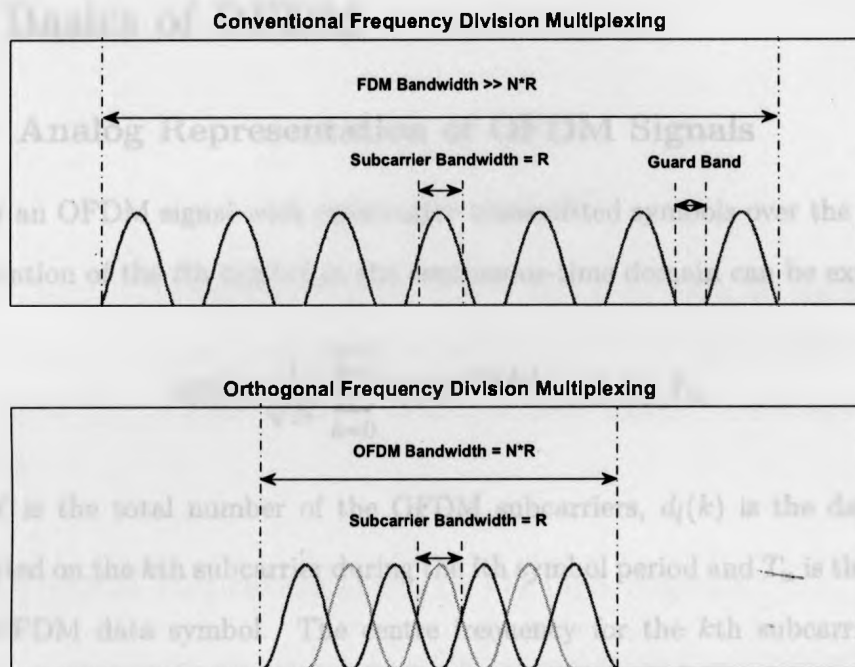


Figure 2.1: OFDM exploits subcarrier orthogonality for spectral efficiency.

FDM, guard bands are inserted between two adjacent frequency bands. However, the utilization rate of available frequency spectrum drops due to the insertion of guard bands. To cope with this inefficient bandwidth usage, OFDM technique was proposed, in which adjacent subcarriers are overlapped orthogonally without interfering each other.

For illustration purpose, Fig. 2.1 shows the spectrum usage of both conventional FDM and OFDM systems. Compared to the conventional FDM with guard band interval between adjacent carriers, OFDM can utilize the frequency band efficiently by exploiting the subcarrier orthogonality, which saves the scarce bandwidth resource significantly. In the next section, the principle of orthogonality in OFDM will be presented in detail.

## 2.2 Basics of OFDM

### 2.2.1 Analog Representation of OFDM Signals

Consider an OFDM signal with consecutive transmitted symbols over the time. The representation of the  $l$ th symbol in the continuous-time domain can be expressed as

$$s(t) = \frac{1}{\sqrt{N}} \sum_{k=0}^{N-1} d_l(k) e^{j2\pi f_k t}, \quad 0 \leq t \leq T_u, \quad (2.1)$$

where  $N$  is the total number of the OFDM subcarriers,  $d_l(k)$  is the data symbol transmitted on the  $k$ th subcarrier during the  $l$ th symbol period and  $T_u$  is the duration of one OFDM data symbol. The centre frequency for the  $k$ th subcarrier can be expressed as  $f_k = f_0 + k\Delta f$ , where  $\Delta f$  is the subcarrier spacing of the OFDM symbol which satisfies  $T_u \Delta f = 1$ .

The orthogonality among any subcarriers can be proved by computing the integral of the product of the  $k$ th subcarrier and the  $l$ th subcarrier within the  $l$ th symbol as follows [12],

$$\begin{aligned} & \frac{d_l(k)d_l(l)}{T_u} \int_0^{T_u} e^{j2\pi f_k t} (e^{j2\pi f_l t})^* dt \\ &= \frac{d_l(k)d_l(l)}{T_u} \int_0^{T_u} e^{j2\pi(f_k - f_l)t} dt \\ &= \frac{d_l(k)d_l(l)}{T_u} \int_0^{T_u} e^{j2\pi(k-l)\Delta f t} dt \\ &= d_l(k)d_l(l)\delta(k-l), \end{aligned} \quad (2.2)$$

where  $\delta(k - l)$  is a delta function defined as

$$\delta(k - l) = \begin{cases} 1, & k = l, \\ 0, & \text{otherwise.} \end{cases} \quad (2.3)$$

Therefore, any two subcarriers are orthogonal to each other since the integral of their product is zero. The orthogonality allows simultaneous data transmission on multiple subcarriers in a more tight frequency spacing without mutual interference compared with FDM.

### 2.2.2 Digital Representation of OFDM Signals

Assume that the continuous-time domain OFDM signal  $s(t)$  is sampled at an interval of  $T = \frac{T_u}{N}$ , the corresponding discrete-time baseband OFDM signal is then given by

$$s(n) = \frac{1}{\sqrt{N}} \sum_{k=0}^{N-1} d_l(k) e^{j2\pi f_k n T}, \quad n = 0, 1, \dots, N-1. \quad (2.4)$$

Without loss of generality, let  $f_0 = 0$ , (2.4) therefore turns into

$$\begin{aligned} s(n) &= \frac{1}{\sqrt{N}} \sum_{k=0}^{N-1} d_l(k) e^{j2\pi \frac{k}{T_u} \frac{n T_u}{N}} \\ &= \frac{1}{\sqrt{N}} \sum_{k=0}^{N-1} d_l(k) e^{j2\pi n \frac{k}{N}}, \quad n = 0, 1, \dots, N-1. \end{aligned} \quad (2.5)$$

The frequency domain symbol  $d_l(k)$  can be inversely represented by

$$d_l(k) = \sum_{n=0}^{N-1} s(n) e^{-j2\pi n \frac{k}{N}}, \quad n = 0, 1, \dots, N-1. \quad (2.6)$$

It is shown that (2.5) and (2.6) are identical to the expressions of IDFT and



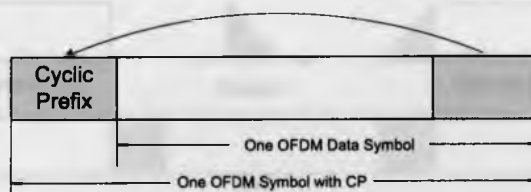


Figure 2.2: One OFDM symbol with CP.

DFT which provide a method to efficiently implement OFDM modulation and demodulation.

### 2.2.3 Cyclic Prefix

When a series of OFDM symbols pass through a multipath fading channel, intersymbol interference (ISI) will be introduced due to the dispersive nature of the channel. The impact of ISI will destroy the orthogonality among subcarriers in OFDM systems. By adding CP as a guard interval, ISI between OFDM symbols can be gracefully eliminated. A CP typically is a copy of the last part of one OFDM data symbol and appended at the beginning of that symbol. Fig. 2.2 illustrates one complete OFDM symbol with CP.

Provided that the length of the CP is longer than the maximum channel duration, multipath components from current OFDM symbol will not interfere the subsequent symbol. This is because CP converts the linear convolution between the OFDM signal and the channel impulse response into a cyclic convolution. Therefore, multipath components from the previous symbol are limited within the CP part. As a result, ISI can be avoided and the orthogonality among subcarriers is maintained. Fig. 2.3 illustrates how the ISI is removed in OFDM symbols. It is shown in the figure that when the length of CP is longer than the channel duration, the multipath interference from the preceding symbol can be absorbed by the CP of the current

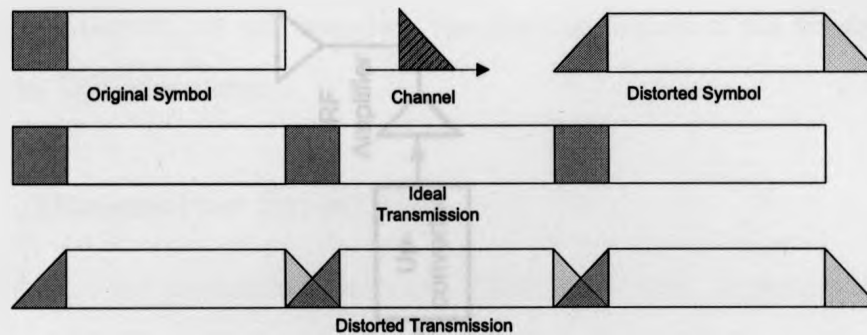


Figure 2.3: Elimination of ISI by CP.

symbol. Consequently, ISI can be eliminated efficiently by removing the CP before OFDM symbol demodulation.

Adding CP, on the other hand, will decrease the bandwidth efficiency due to the additional transmission time taken by the CP for each symbol. Therefore, a good system design will control CP as short as possible while maintaining sufficient length for multipath protection.

## 2.3 OFDM System Structure

As described in Section 2, from (2.5) and (2.6), OFDM modulation and demodulation can be implemented by IDFT and DFT respectively. For efficient implementation, the inverse fast Fourier transform (IFFT) and fast Fourier transform (FFT) can be applied to achieve the IDFT and DFT operations.

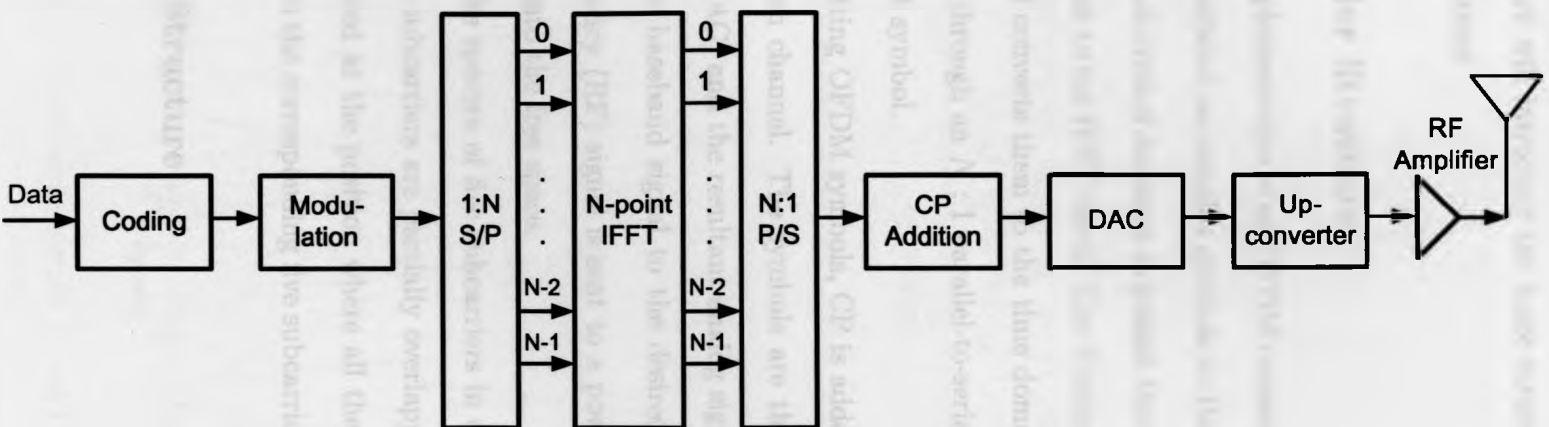


Figure 2.4: OFDM transmitter structure.

In this section, we will introduce the basic structures of the transmitter and receiver for OFDM systems.

### 2.3.1 Transmitter Structure

Fig. 2.4 depicts the implementation of an OFDM transmitter. Incoming data bits are encoded and then modulated as complex symbols in the first two blocks in Fig. 2.4. Following this, the serial symbol sequence is passed through a  $1 : N$  serial-to-parallel (S/P) converter and sent to the IFFT block. The  $N$ -point IFFT block takes the input frequency symbols and converts them to the time domain. The complex outputs of IFFT are then passed through an  $N : 1$  parallel-to-serial (P/S) converter, forming a complex-valued OFDM symbol.

Prior to transmitting OFDM symbols, CP is added to each symbol to prevent ISI caused by multipath channel. The symbols are then passed through a digital-to-analog converter (DAC) and the resultant analog signal is fed to the upconverter. After upconverting the baseband signal to the desired carrier frequency  $f_{RF}$ , the modulated radio frequency (RF) signal is sent to a power amplifier and radiated by the transmit antenna into the free space.

Fig. 2.5 shows the spectra of five subcarriers in one OFDM signal. As shown in the figure, different subcarriers are partially overlapped and the spectral peak of each subcarrier is located at the position where all the other subcarriers' spectrum are zero. Fig. 2.6 shows the corresponding five subcarrier signals in the time domain.

### 2.3.2 Receiver Structure

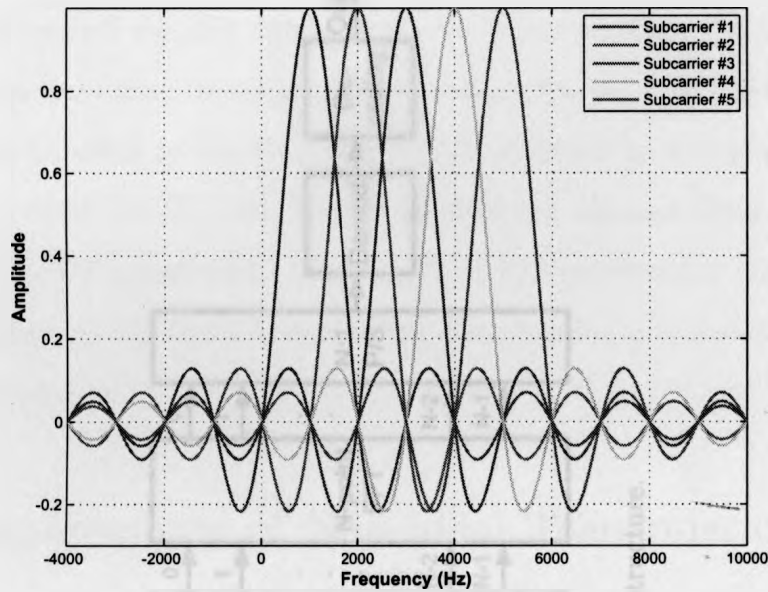


Figure 2.5: Example of 5 subcarriers in one OFDM symbol in the frequency domain.

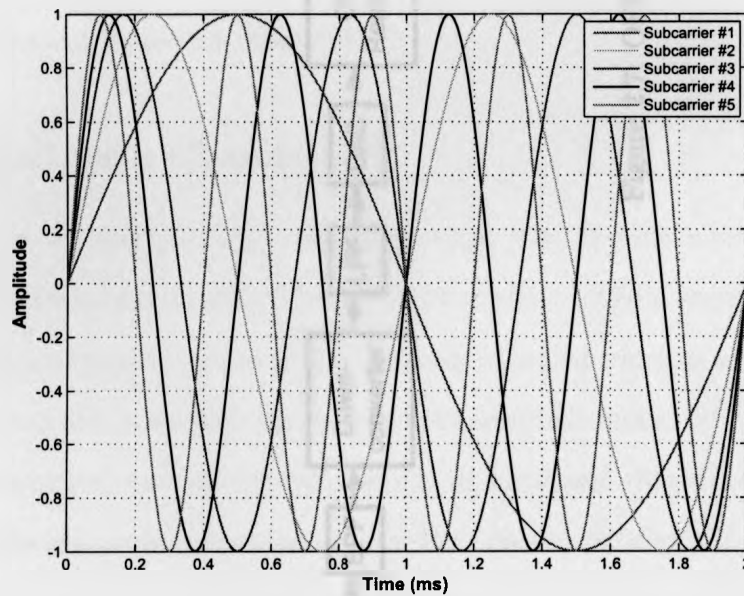


Figure 2.6: Example of 5 subcarrier signals in one OFDM symbol in the time domain.

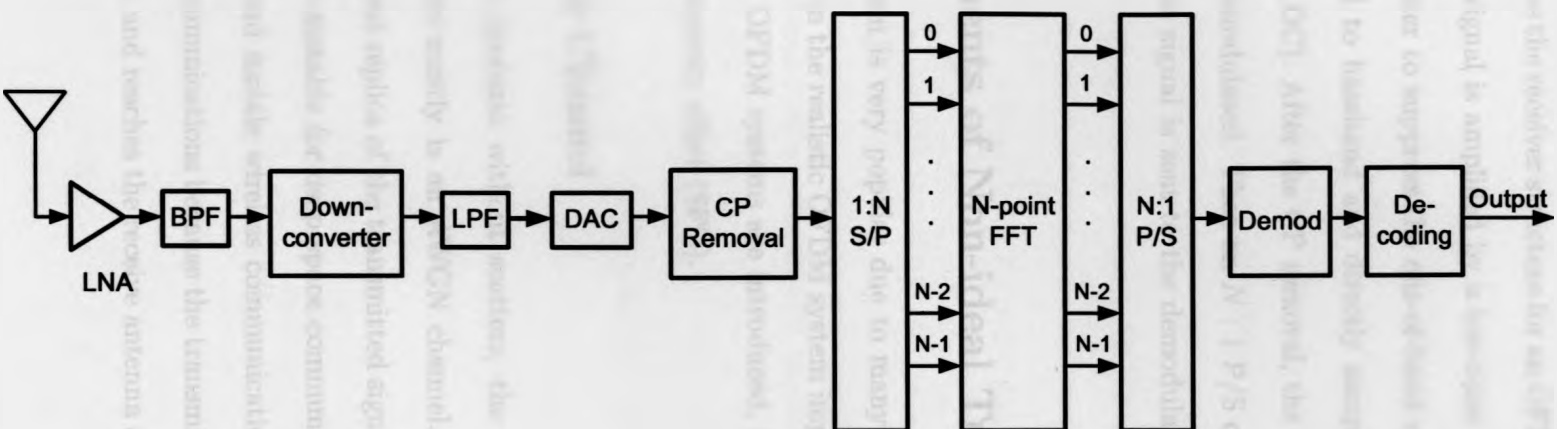


Figure 2.7: OFDM receiver structure.

Fig. 2.7 illustrates the receiver structure for an OFDM system. After the receive antenna, the received signal is amplified by a low-noise amplifier (LNA) and passed through a bandpass filter to suppress the out-of-band noise. The filtered RF signal is then downconverted to baseband and directly sampled by a high-speed analog-to-digital converter (ADC). After the CP removal, the sampled signal is  $1 : N$  S/P converted and FFT demodulated. Then an  $N : 1$  P/S conversion is carried out over each subcarrier and the signal is sent to the demodulation and decoding blocks for further processing.

## 2.4 Impairments of Non-ideal Transmission

Although OFDM system is very popular due to many attractive advantages, there are some impairments in the realistic OFDM system implementation. In this section, major impairments in OFDM systems are introduced, including multipath channel, CFO and sampling frequency offset (SFO).

### 2.4.1 Multipath Channel

In the simple wireless scenario without scatters, the channel model employed in OFDM system analysis mostly is an AWGN channel. With such model, the receiver gets an attenuated replica of the transmitted signal which is only corrupted by AWGN. This model is suitable for deep space communications, but is not the right model for terrestrial and mobile wireless communications. Multipath fading is inevitable in wireless communications because the transmitted signal bounces off walls, doors or other objects, and reaches the receive antenna at various delays via different paths.

A multipath channel model with  $M_c$  paths can be characterized by

$$h(\xi_m, t) = \sum_{m=1}^{M_c} h(\xi_m) \delta(t - \xi_m), \quad (2.7)$$

with  $h(\xi_m)$  as the channel coefficient at delay  $\xi_m$ ,  $m = 1, \dots, M_c$ . Based on the wide sense stationary uncorrelated scattering (WSSUS) assumption, channel taps are assumed to be uncorrelated with each other. The transmitted signal  $s(t)$  after passing through the multipath fading channel without AWGN can be expressed as

$$r(t) = \sum_{m=1}^{M_c} h(\xi_m) s(t - \xi_m). \quad (2.8)$$

### 2.4.2 CFO and SFO

Considering the CP in each symbol, the OFDM baseband signal for the  $l$ th symbol can be described as [13] [14]

$$s(t) = \frac{1}{\sqrt{N}} \sum_{k=0}^{N-1} d_l(k) e^{j2\pi k \Delta f_k (t - (lN_s + N_{cp})T)}, \quad (2.9)$$

where  $T$  is the sampling period,  $l$  represents the  $l$ th symbol;  $k$  denotes the  $k$ th sub-carrier;  $N_{cp}$  is the number of samples in CP and  $N_s$  is the number of samples in one OFDM symbol which equals to  $N + N_{cp}$ . Note that  $N_{cp} \times T$  is the duration of the CP and it should be longer than the maximum channel delay spread.

Denote the carrier frequency as  $f'$  and the sampling period as  $T'$  at the receiver. Thus the CFO  $\Delta f_c$  and the relative SFO  $\eta$  are defined as

$$\Delta f_c = f - f' \quad (2.10)$$



and

$$\eta = (T' - T)/T. \quad (2.11)$$

Sampling the received signal at the receiver with a sampling clock  $T'$ , the  $l$ th OFDM symbol after CP removal can be represented by  $N$  samples

$$r_l(n) = r(t_n), \quad 0 \leq n \leq N - 1, \quad (2.12)$$

where  $t_n = (lN_s + N_{cp})T' + nT'$ .

In this thesis, channel fading is assumed to be unchanged during two consecutive OFDM symbols. By substituting (2.9) and (2.12) into (2.8), the  $l$ th received symbol  $r_l(n)$  with CFO and SFO impairments in multipath fading channel can be represented as [13] [15],

$$\begin{aligned} r_l(n) &= e^{j2\pi\Delta f_c t_n} \frac{1}{\sqrt{N}} \sum_m^{M_c} h(\xi_m) \sum_{k=0}^{N-1} \sum_{l=-\infty}^{\infty} d_l(k) e^{\frac{j2\pi k(t_n - (lN_s + N_{cp})T - \xi_m)}{NT}} + w_l(n) \\ &= e^{j2\pi\Delta f_c (lN_s + N_{cp})(1+\eta)T} e^{j2\pi\Delta f_c n(1+\eta)T} \sum_m^{M_c} h(\xi_m) \\ &\quad \times \sum_{l=-\infty}^{\infty} \frac{1}{\sqrt{N}} \sum_{k=0}^{N-1} d_l(k) e^{j2\pi k \frac{1}{NT} [(lN_s + N_{cp})T' + nT' - (lN_s + N_{cp})T - \xi_m]} + w_l(n), \end{aligned} \quad (2.13)$$

where  $w_l(n)$  is the AWGN.

Substituting (2.10) into (2.13), we have

$$\begin{aligned}
 r_l(n) &= e^{j2\pi\Delta f_c(lN_s+N_{cp})(1+\eta)T} e^{j2\pi\Delta f_c n(1+\eta)T} \\
 &\times \frac{1}{\sqrt{N}} \sum_{m=0}^{M_c} h(\xi_m) \sum_{l=-\infty}^{\infty} \sum_{k=0}^{N-1} d_l(k) e^{\frac{j2\pi k}{NT}[(LN_s+N_{cp})\eta T+n(1+\eta)T-\xi_m]} + \omega_l(n) \\
 &= e^{j2\pi\Delta f_c(lN_s+N_{cp})(1+\eta)T} e^{j2\pi\Delta f_c n(1+\eta)T} \sum_{m=0}^{M_c} h(\xi_m) \\
 &\times \frac{1}{\sqrt{N}} \sum_{l=-\infty}^{\infty} \sum_{k=0}^{N-1} d_l(k) e^{\frac{j2\pi k}{N}(lN_s+N_{cp})\eta} e^{\frac{j2\pi kn}{N}(1+\eta)} \phi^H + w_l(n), \quad (2.14)
 \end{aligned}$$

where  $\phi^H = e^{-\frac{j2\pi k\xi_m}{NT}}$  is the phase rotation caused by the delay of the  $m$ th path.

Considering the CFO and SFO, the received data symbol in the frequency domain after FFT can be expressed as follows [13] [15]

$$\begin{aligned}
 Z_{l,k} &= \sum_{n=0}^{N-1} r_l(n) e^{-j2\pi kn/N} + W_l(k) \\
 &= \frac{1}{\sqrt{N}} \sum_{n=0}^{N-1} e^{j2\pi\Delta f_c n} \sum_{k=0}^{N-1} d_l(k) H_k \phi^H e^{j2\pi \frac{k}{NT}(t_n - (LN_s+N_{cp})T)} e^{-j\frac{2\pi kn}{N}} + W_l(k) \\
 &= \frac{1}{\sqrt{N}} e^{j2\pi\Delta f_c(lN_s+N_{cp})(1+\eta)T} \sum_{n=0}^{N-1} e^{j2\pi\Delta f_c n(1+\eta)T} \\
 &\times \sum_{k=0}^{N-1} d_l(k) H_k \phi^H e^{j2\pi \frac{k}{N}[(LN_s+N_{cp})(1+\eta)+n(1+\eta)-(LN_s+N_{cp})]} e^{-j\frac{2\pi kn}{N}} + W_l(k) \\
 &= \frac{1}{\sqrt{N}} e^{j2\pi\Delta f_c(lN_s+N_{cp})(1+\eta)T} e^{\frac{j2\pi k(lN_s+N_{cp})\eta}{N}} d_l(k) H_k \phi^H \sum_{n=0}^{N-1} e^{j2\pi\Delta f_c n(1+\eta)T} \\
 &\times e^{j2\pi kn \frac{\eta}{N}} + \frac{1}{\sqrt{N}} \sum_{n=0}^{N-1} e^{j2\pi\Delta f_c(lN_s+N_{cp})(1+\eta)T} d_l(k) H_k \phi^H \\
 &\times \sum_{i=0, i \neq k}^{N-1} e^{\frac{j2\pi i(lN_s+N_{cp})\eta}{N}} e^{\frac{j2\pi i n \eta}{N}} + W_l(k), \quad (2.15)
 \end{aligned}$$

where  $W_l(k)$  is the AWGN at the  $k$ th subcarrier in the  $l$ th OFDM symbol. From (2.10) we have

$$\begin{aligned}
 \Delta f_c &= f' - f \\
 &= \frac{1}{NT'} - \frac{1}{NT} \\
 &= \frac{T - T'}{NT'T} \\
 &= -\frac{\eta}{(1 + \eta)NT}.
 \end{aligned} \tag{2.16}$$

Therefore, (2.15) can be rewritten as

$$\begin{aligned}
 Z_{l,k} &= \frac{1}{N} e^{j2\pi\Delta f_c(lN_s + N_{cp})(1+\eta)T} e^{\frac{j2\pi k(lN_s + N_{cp})\eta}{N}} d_l(k) H(k) \phi^H \sum_{n=0}^{N-1} e^{j2\pi\Delta f_c n(1+\eta)T} \\
 &\times e^{j2\pi\eta \frac{n}{N}} + \sum_{n=0}^{N-1} \frac{1}{N} e^{j2\pi\Delta f_c(lN_s + N_{cp})(1+\eta)T} \\
 &\times \sum_{i=0, i \neq k}^{N-1} e^{\frac{j2\pi k(lN_s + N_{cp})\eta}{N}} e^{\frac{j2\pi i n \eta}{N}} d_l(k) H(k) \phi^H + W_l(k) \\
 &= \frac{1}{N} e^{j2\pi\Delta f_c(lN_s + N_{cp})(1+\eta)T} e^{\frac{j2\pi k(lN_s + N_{cp})\eta}{N}} d_l(k) H(k) \phi^H \\
 &\times \sum_{n=0}^{N-1} e^{j2\pi(-\frac{\eta}{(1+\eta)NT})n(1+\eta)T} e^{j2\pi\eta + \frac{1}{N} \sum_{n=0}^{N-1} e^{j2\pi\Delta f_c(lN_s + N_{cp})(1+\eta)T} \frac{n}{N}} \\
 &\times \sum_{i=0, i \neq k}^{N-1} e^{\frac{j2\pi k(lN_s + N_{cp})\eta}{N}} e^{\frac{j2\pi i n \eta}{N}} d_l(k) H(k) \phi^H + W_l(k) \\
 &= e^{j2\pi\Delta f_c(lN_s + N_{cp})(1+\eta)T} e^{\frac{j2\pi k(lN_s + N_{cp})\eta}{N}} d_l(k) H(k) \phi^H \\
 &+ \underbrace{\frac{1}{N} \sum_{n=0}^{N-1} e^{j2\pi\Delta f_c(lN_s + N_{cp})(1+\eta)T} \sum_{i=0, i \neq k}^{N-1} e^{\frac{j2\pi k(lN_s + N_{cp})\eta}{N}} e^{\frac{j2\pi i n \eta}{N}} d_l(k) H(k) \phi^H}_{\text{intercarrier interference (ICI)}} + W_l(k).
 \end{aligned} \tag{2.17}$$

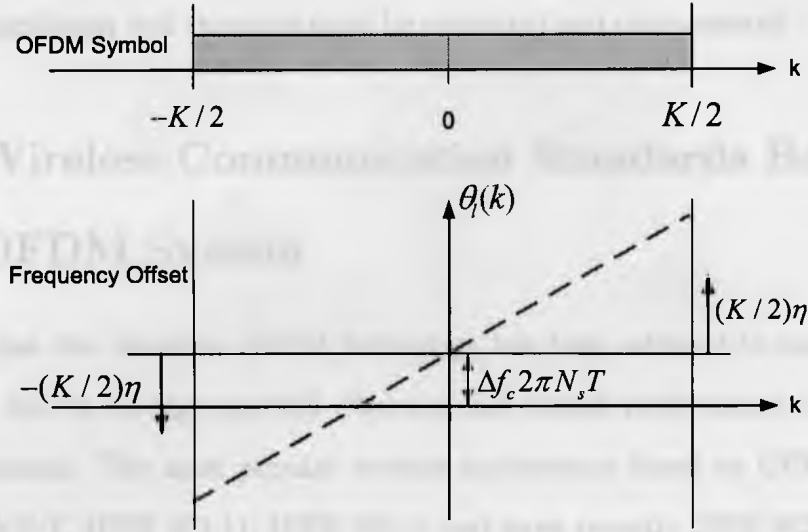


Figure 2.8: Phase rotation between two adjacent OFDM subcarriers due to CFO and SFO.

As illustrated in (2.17), the subcarrier phase rotation is [13] [15]

$$\varphi_l(k) = 2\pi\Delta f_c(lN_s + N_{cp})(1 + \eta)T + \frac{2\pi k}{N}(lN_s + N_{cp})\eta + \phi^H. \quad (2.18)$$

As the channel is slowly fading and for OFDM system with large  $N$  (i.e., constant from one OFDM symbol to the next,  $\phi_{l,k}^H = \phi_{l,k-1}^H$ ), the phase increment between neighboring OFDM symbols is given by,

$$\begin{aligned} \theta_l(k) &= \varphi_l(k) - \varphi_{l-1}(k) \\ &= 2\pi\Delta f_c N_s T + \frac{2\pi\Delta f_c N_s T \eta}{N} + \frac{2\pi N_s k \eta}{N} \\ &\approx 2\pi\Delta f_c N_s T + \frac{2\pi N_s k \eta}{N}. \end{aligned} \quad (2.19)$$

The phase rotation of each subcarrier is plotted in Fig. 2.8 according to (2.19). Depending on the number of subcarriers  $N$  and the total number of samples in one OFDM symbol  $N_s$ , the additional phase rotation introduced by frequency offsets

could be significant and therefore must be estimated and compensated.

## 2.5 Wireless Communication Standards Based on OFDM System

Over the last few decades, OFDM technology has been adopted in many wireless standards due to its high spectral efficiency and robust performance in multipath fading channels. The most popular wireless applications based on OFDM systems include DVB-T, IEEE 801.11, IEEE 802.16 and more recently IEEE 802.22. In this section, a brief introduction of these OFDM applications is presented. Before that, the advantages and disadvantages of OFDM systems are briefly summarized.

### 2.5.1 OFDM Advantages and Disadvantages

As discussed in the previous section, OFDM has many advantages over other transmission technologies. Main merits of OFDM systems are summarized as follows

- High efficiency of spectrum utilization.
- Robustness against ISI caused by multipath propagation.
- Simple implementation of modulation/demodulation by IFFT/FFT block.
- Adaptive modulation and flexible transmission power adjustment.

The main drawbacks of OFDM systems are as follows

- Transmission data rate loss due to the redundancy from CP.
- Vulnerability to CFO and SFO caused by the drifting between transmitter and receiver oscillators.



Figure 2.9: DTT broadcasting standards around the world.

- High peak-to-average power ratio (PAPR) from the drastically fluctuated magnitude in the OFDM signal.

### 2.5.2 Current Standards Using OFDM

Due to those advantages mentioned before, OFDM systems have been adopted as physic layer (PHY) modulation scheme in many standards. However, OFDM system parameters in different standards are not the same according to different system performances required by standards. For example, the OFDM system in DVB-T employs a larger number of subcarriers to increase the transmission efficiency in stationary scenario while DVB-H features a smaller number of subcarriers so that it is more robust in dynamic channel conditions. Hence, the knowledge of OFDM system parameters for different standards are imperative for automatic signal identification based on the estimated system parameters.

### 2.5.2.1 DVB

DVB-T [2] [16] is a television broadcasting standard where a set of specifications regulate the framing structure, channel coding, and modulation for digital terrestrial television (DTT) broadcasting. The DVB-T standard was originally designed for terrestrial transmission of digital TV services to fixed and portable receivers. But more services, such as mobile and handheld receiving, were introduced recently [16].

In order to deliver high quality video in a broadcast environment, OFDM is employed in DVB-T standard due to its data rate scalability and high multipath immunity. The DVB-T OFDM system PHY adopts the 2K (1705 subcarriers) and 8K (6817 subcarriers) transmission modes. The “2K mode” is suitable for single transmitter operation and for small single frequency networks (SFN) with limited transmitter distances. The “8K mode” can be used both for single transmitter operation and for small and large SFN networks. An OFDM symbol in DVB-T is composed of two parts: a useful data part and a CP part. Four different durations of CP can be used, i.e.,  $1/32$ ,  $1/16$ ,  $1/8$  and  $1/4$  of the data symbol duration. Various modulation schemes are also available in order to accommodate different transmission rates, including quadrature phase shift keying (QPSK), 16 quadrature amplitude modulation (QAM) and 64QAM.

As one popular digital TV broadcast standard, DVB-T has been adopted or proposed for digital television broadcasting by many countries and regions (see Fig. 2.9). Furthermore, DVB-T has been further evolved into more new standards, such as DVB-H for handheld terminals.

### 2.5.2.2 IEEE 802.11 Standards

In 1997, the institute of electrical and electronics engineers (IEEE) finalized the first WLAN standard - 802.11. Unfortunately, 802.11 at that time only supported a maximum network bandwidth of 2 Mbps which was too slow for most of the applications at that time. For this reason, old 802.11 wireless products are no longer manufactured. The IEEE 802.11 family used nowadays includes IEEE 802.11a [17], IEEE 802.11b [18], IEEE 802.11g [19] and more recently IEEE 802.11n [20]. Most of the standards apply OFDM technique except the IEEE 802.11b.

- 802.11a operates in 5 GHz band and uses a 52-subcarrier OFDM with a maximum raw data rate of 54 Mbit/s, which yields realistic net achievable throughput in the mid-20 Mbit/s. The data rate can be reduced to 48, 36, 24, 18, 12, 9 and 6 Mbit/s if necessary. 802.11a has been deployed worldwide for many different applications, particularly within the corporate workspace nowadays.
- 802.11g works in the 2.4 GHz band (like 802.11b) but can operate at a maximum data rate of 54 Mbit/s. The modulation scheme used in 802.11g is OFDM inherited from 802.11a with data rates of 54, 48, 36, 24, 18, 12, 9 and 6 Mbit/s. Even though 802.11g operates in the same frequency band as 802.11b, it can achieve higher data rate thanks to its heritage to 802.11a.
- 802.11n is the most recent Wi-Fi standard and is becoming commercially available. This standard significantly improves the maximum data rate from 54 Mbit/s to 600 Mbit/s. One of the most well known component of 802.11n is the multiple input multiple output (MIMO) technique. MIMO harnesses multipath with a technique known as space division multiplexing. The transmitting WLAN device splits a data stream into multiple spatial streams, and transmits



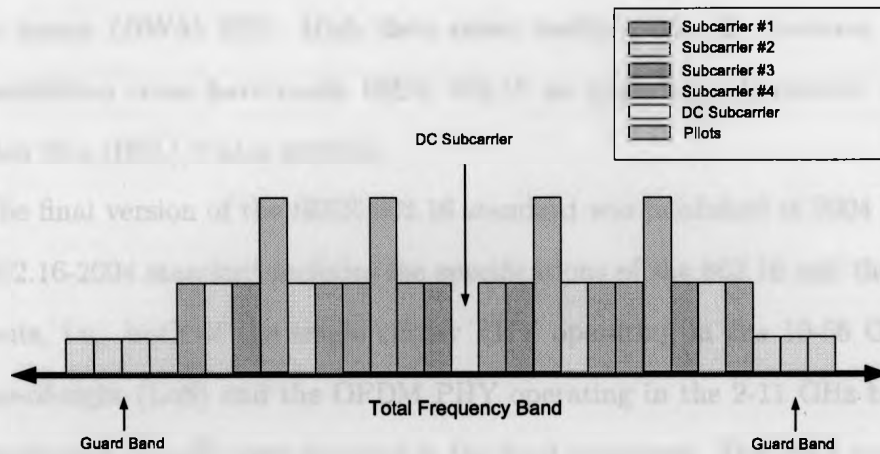


Figure 2.10: OFDMA signal structure specified in WiMAX.

each of them through separate antennas to corresponding antennas at the receiver. The current 802.11n provides up to four spatial streams. Doubling the number of spatial streams from one to two effectively doubles the data rate. There are trade-offs, however, such as increased power consumption and extra hardware cost. Doubling the width of a WLAN channel from 20 MHz to 40 MHz in the 802.11n also effectively doubles data rate. However, it leaves fewer channels available for other devices. In the case of the 2.4 GHz band, there is enough room for three non-overlapping 20 MHz channels while a 40 MHz channel does not leave much room for other devices to join the network or transmit in the same airspace. Therefore, intelligent and dynamic management is required to ensure that the 40 MHz channel option improves overall WLAN performances by balancing the high bandwidth demands from different clients.

### 2.5.2.3 IEEE 802.16 Standard

The IEEE 802.16 standard (also known as WiMAX) [21] for wireless metropolitan area networks is a wireless transmission system that falls into the category of broadband

wireless access (BWA) [22]. High data rates, mobility-friendly features, and low user installation costs have made IEEE 802.16 an appealing alternative to digital subscriber line (DSL)/Cable services.

The final version of the IEEE 802.16 standard was published in 2004 [23]. The IEEE 802.16-2004 standard includes the specifications of the 802.16 and the 802.16a documents, i.e., both of the single carrier PHY operating in the 10-66 GHz band with line-of-sight (LoS) and the OFDM PHY operating in the 2-11 GHz band with non-line-of-sight (NLoS) were included in the final document. The PHY standard of 802.16 also has two modes, i.e., OFDM and scalable orthogonal frequency division multiple access (OFDMA). The channel bandwidth in OFDMA can be an integer multiple of 1.25 MHz, 1.5 MHz, 1.75 MHz, 2MHz and 2.75 MHz with a maximum of 20 MHz. Binary phase shift keying (BPSK), QPSK, 16QAM and 64QAM modulation schemes are employed for each OFDM subcarrier.

The time domain OFDM symbol in WiMAX also consists of a useful data part and a CP part. The PHY can use variable CP length, i.e.,  $1/32$ ,  $1/16$ ,  $1/8$  and  $1/4$  of the data symbol duration, depending on the expected channel delay spread. In the frequency domain, there are three types of subcarriers in each OFDM symbol, namely

- Data subcarriers: subcarriers used to transmit user data;
- Pilot subcarriers: subcarriers used for channel estimation purposes;
- Null carriers: empty subcarriers for guard band and direct current (DC).

Fig. 2.10 illustrates the distribution of subcarriers in each IEEE 802.16 OFDM symbol. Among the 256 subcarriers in one symbol, 55 subcarriers are designated as guard bands, 28 subcarriers are in the lower frequency guard bands and 27 subcarriers are in

Table 2.1: OFDM parameters in WiMAX

Parameter	Value
IFFT/FFT Length	256
Number of Used Subcarriers	200
CP ratio	1/4, 1/8, 1/16, 1/32
Lower Frequency Guard Subcarriers	28 Subcarriers
Upper Frequency Guard Subcarriers	27 Subcarriers
Index of Lower Guard Subcarriers	-128, -127, ..., -101
Index of Upper Guard Subcarriers	+101, +102, ..., +127
Index of Pilot Subcarriers	-84, -60, -36, -12, 12, 36, 64, 84

the upper frequency guard bands. The IEEE 802.16 standard reserves 8 subcarriers to be used for channel estimation purposes. These subcarriers are known as pilot subcarriers. Table 2.1 summarizes the IEEE 802.16 standard OFDM parameters according to [23].

#### 2.5.2.4 IEEE 802.22 Standard

The IEEE 802.22 standard is a CR standard being developed to bring broadband access to less populated rural areas by using vacant TV channels. OFDMA is the modulation scheme for transmission in up- and downlink in the current draft 802.22 proposal. With OFDMA, it will be possible to achieve the flexibility for channel switching without errors in transmission and reception. By using just one TV channel, the approximate maximum bit rate is 19 Mbit/s at a 30 km distance. Another distinctive feature of IEEE 802.22 standard is the new technology Channel Bonding [24] which is employed to fulfill the speed and distance requirements of the standard.

Fig. 2.11 summarizes the frequency range and approximated data rate provided by different OFDM based wireless standards and Table 2.2 lists the key specifications of these standards. It is obvious that OFDM has been widely adopted in many state-of-art standards and has a promising future in the next generation of high speed

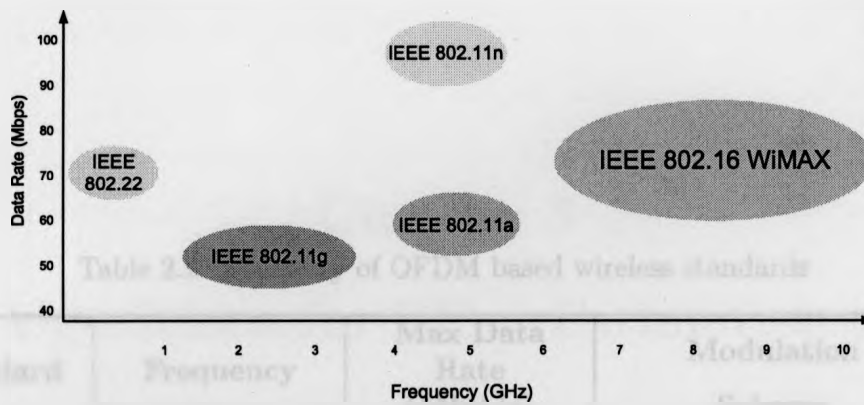


Figure 2.11: Frequency range and data rate specified by typical OFDM based wireless standards.

wireless communication technologies.

## 2.6 Summary

In this chapter, the principle of OFDM systems is introduced. In Section 1, conventional FDM and OFDM techniques for multi-carrier transmission are compared. The analog and digital representations of OFDM signals are both introduced in Section 2. In Section 3, the transmitter and receiver structures of OFDM systems are presented, followed by an introduction of the OFDM signal generation, transmission and reception procedures. The impairments of non-ideal transmission of OFDM systems, including the multipath fading and frequency offsets are discussed in Section 4. Finally in Section 5, the main advantages and disadvantages of OFDM systems are briefly concluded and the major wireless standards based on OFDM techniques are overviewed.

Table 2.2: Summary of OFDM based wireless standards

Standard	Frequency	Max Data Rate (Mbit/s)	Modulation Scheme	Range (meters)
802.11 a	5.25, 5.6 and 5.8 GHz	Up to 54Mbps in the 5GHz band	BPSK, QPSK 16QAM, 64QAM	20 m
802.11 g	2.4 - 2.4835 GHz	Up to 54Mbps in the 2.4GHz band	OFDM above 20Mbps, DSSS with CCK below 20Mbps	30m
802.11 n	2.4 - 2.4835 GHz 5.15 - 5.35 GHz	108+ Mbps	Up to 64 QAM on 108 OFDM	50 m
802.16 WiMAX	IEEE 802.16 - 10GHz-66GHz 802.16a-e - 2GHz-11GHz Licensed: 2.3 GHz, 2.5 GHz, 3.3 GHz US: 2.3 GHz, Asia/India: 2.5 GHz, 3.3 GHz	Up to 75 Mbps	Fixed Access : OFDM with BPSK, QPSK, 16 QAM, 64 QAM Mobile Access : OFDMA with BPSK, QPSK, 16 QAM, 64 QAM	30 m
802.22 (Draft)	54-698 MHz (USA)	72.6 Mbps	QPSK, 16QAM, 64QAM	33 km

### 3.1 Signal Cyclostationarity

## Chapter 3

# Algorithms for Blind Estimation of OFDM System Parameters

As OFDM system has been adopted in many different communications standards in recent years, cognitive OFDM signal reception capable of supporting multiple standards becomes increasingly important, which necessitates a need for blind OFDM system parameter estimation. In this chapter, OFDM system parameters (i.e., the sampling frequency, number of subcarriers, symbol duration, CP length as well as CFO) are estimated without any prior information. Based on the inherent cyclostationarity of the received oversampled OFDM signal, a two-step algorithm with low computational complexity is proposed to blindly estimate the original OFDM sampling rate at the transmitter and the oversampling ratio of the receiver. With this estimated oversampling ratio, other OFDM system parameters such as the number of subcarriers, symbol duration and length of CP are estimated based on the cyclic property induced by the CP. Simulation results confirm the high precision and efficient computations provided by the proposed algorithm.

### 3.1 Signal Cyclostationarity

Signal cyclostationarity has been used as a statistical tool in many different applications, including signal identification, blind equalization, parameter estimation and

modulation recognition [25] [26] [27]. Communication signals in general exhibit cyclostationarity associated with the symbol period, carrier frequency, chip rate and a combination of these factors [28]. Before discussing the cyclostationarity in OFDM signals, the fundamental concepts of cyclostationary processes will be first introduced.

### 3.1.1 Cyclostationary Process

A cyclostationary signal is a signal having statistical properties which vary cyclically with time. Define the mean and time-varying autocorrelation function (ACF) of a stochastic process  $x(t)$  (e.g., an OFDM communication signal) as

$$\mu_x(t) = E\{x(t)\}, \quad (3.1)$$

and

$$R_x(t_1, t_2) = E\{x(t_1)x^*(t_2)\}. \quad (3.2)$$

Here  $E\{\cdot\}$  is the standard expectation operator and  $*$  is the conjugation of the corresponding complex process.

The stochastic process  $x(t)$  is wide-sense cyclostationary if its mean and time-varying ACF are periodic in time [29] [30] with a period  $T_x$ . Namely, for any given integer  $m$ ,

$$\mu_x(t) = \mu_x(t + mT_x), \quad (3.3)$$

and

$$R_x(t_1, t_2) = R_x(t_1 + mT_x, t_2 + mT_x). \quad (3.4)$$

Without loss of generality, define  $t_1 = t + \tau/2$  and  $t_2 = t - \tau/2$ . An alternate

definition of the time-varying ACF for a cyclostationary process is

$$R_x(t, \tau) = E\{x(t + \frac{\tau}{2})x^*(t - \frac{\tau}{2})\}. \quad (3.5)$$

$R_x(t, \tau)$  is referred to as the symmetric form of the time-varying ACF since it considers two points in time separated by  $\tau$  and centered at  $t$ . For its clearness and simplicity, (3.5) will be used in the following for further explanation about cyclostationarity.

Analogous to (3.4), wide-sense cyclostationarity in (3.5) can be expressed as

$$R_x(t, \tau) = R_x(t + mT_x, \tau). \quad (3.6)$$

For any cyclostationary process  $x(t)$  that satisfies (3.6), the time-varying ACF can be expressed as a Fourier series over the corresponding period  $T_x$

$$R_x(t, \tau) = \sum_{\alpha} R_x^{\alpha}(\alpha, \tau) e^{j2\pi\alpha t}, \quad (3.7)$$

where the Fourier series coefficients in (3.7) are given as

$$R_x^{\alpha}(\alpha, \tau) = \frac{1}{T_x} \int_{-T_x/2}^{T_x/2} R_x(t, \tau) e^{-j2\pi\alpha t} dt. \quad (3.8)$$

$R_x^{\alpha}(\alpha, \tau)$  is referred to as the CCF where  $\alpha$  is the cyclic frequency (CF) [31]. If a process is wide-sense stationary, the CCF is identically zero for all  $\alpha$  other than  $\alpha = 0$  [30]. In other words, for a stationary process,  $R_x(t, \tau) = R_x^0(0, \tau)$  and  $R_x(t, \tau)$  can be shortened as  $R_x(\tau)$  because it is no longer dependent upon  $t$ .

The CCF can also be obtained by extending the period of integration in (3.8)



to infinite as follows

$$R_x^\alpha(\alpha, \tau) = \lim_{T \rightarrow \infty} \frac{1}{T} \int_{-T/2}^{T/2} R_x(t, \tau) e^{-j2\pi\alpha t} dt, \quad (3.9)$$

This expression together with the definition of  $R_x(t, \tau)$  given in (3.5), provide a method for estimating the CCF from observed waveforms. Suppose that samples from the process  $x(t)$  are observed during any observation interval  $T_{ob}$  which is symmetrical with respect to the time origin. An estimate for  $R_x^\alpha(\tau)$  is then given by

$$\hat{R}_x(\alpha, \tau) = \frac{1}{T_{ob}} \int_{-T_{ob}/2}^{T_{ob}/2} x(t+\tau/2) I_{T_{ob}}(t+\tau/2) x^*(t-\tau/2) I_{T_{ob}}(t-\tau/2) e^{-j2\pi\alpha t} dt, \quad (3.10)$$

where  $I_{T_{ob}}$  is the indicator function defined as

$$I_{T_{ob}} = \begin{cases} 1, & |t| \leq T_{ob}/2; \\ 0, & \text{elsewhere,} \end{cases} \quad (3.11)$$

and  $\{\cdot\}$  stands for an estimated value.

Moreover, define the Fourier transform of the CCF with respect to  $\tau$  as the cyclic spectrum (CS)

$$S_x(\alpha, f) = \int_{-\infty}^{\infty} R_x^\alpha(\tau) e^{-j2\pi f \tau} d\tau. \quad (3.12)$$

When  $\alpha = 0$ , CS is equal to the power spectrum (or spectral density) defined in the conventional manner [29]. For any wide sense stationary process, the CS is identically zero for all  $\alpha$  other than  $\alpha = 0$ . This follows directly from the equivalence of  $R_x^{\alpha=0}$  to  $R(\tau)$  for such a process.

### 3.1.2 An Interpretation of the Cyclic Correlation Function

To help the understanding of the signal cyclostationarity, a specific example is given below. Suppose there are two signals  $v(t)$  and  $v'(t)$  with opposite frequency shifts as

$$v(t) = x(t)e^{-j\pi\alpha t}, \quad (3.13)$$

and

$$v'(t) = x(t)e^{j\pi\alpha t}. \quad (3.14)$$

The cross-correlation of  $v(t)$  and  $v'(t)$  is

$$R_{vv'}(t, \tau) = E\{v(t + \frac{\tau}{2})v'^*(t - \frac{\tau}{2})\}. \quad (3.15)$$

Substituting (3.13) and (3.14) into (3.15) gives,

$$\begin{aligned} R_{vv'}(t, \tau) &= E\{x(t + \frac{\tau}{2})e^{-j\pi\alpha(t + \frac{\tau}{2})}x^*(t - \frac{\tau}{2})e^{-j\pi\alpha(t - \frac{\tau}{2})}\} \\ &= E\{x(t + \frac{\tau}{2})x^*(t - \frac{\tau}{2})\}e^{-j2\pi\alpha t} \\ &= R_x(t, \tau)e^{-j2\pi\alpha t}, \end{aligned} \quad (3.16)$$

which upon rearranging yields

$$R_x(t, \tau) = e^{j2\pi\alpha t}R_{vv'}(t, \tau). \quad (3.17)$$

By application of (3.9), the CCF therefore is

$$R_x^\alpha(\alpha, \tau) = R_{vv'}(\tau). \quad (3.18)$$

It can be seen from (3.18) that the CCF of a cyclostationary process is the cross-correlation of frequency-shifted versions of the original process.

## 3.2 Second-Order Cyclostationarity of Received Oversampled OFDM Signals

Based on the introduction of the signal cyclostationarity in the previous section, the inherent cyclostationarity of received oversampled OFDM signal will be analyzed in this section.

### 3.2.1 Signal Model

We assume the transmitted continuous-time OFDM signal is given by [5]

$$s(t) = \frac{1}{\sqrt{N}} \sum_{l=-\infty}^{\infty} \sum_{k=0}^{N-1} d_l(k) e^{j2\pi k \Delta f_k (t-lT)} g(t-lT), \quad (3.19)$$

where  $N$  is the number of subcarriers;  $l$  represents the  $l$ th symbol;  $k$  denotes the  $k$ th subcarrier;  $d_l(k)$  is the symbol transmitted within the  $l$ th symbol period and the  $k$ th subcarrier. Symbols from different subcarriers are considered as independent and identically distributed (i.i.d.) random variables with zero mean and variance of  $\sigma_d^2$ , drawn from either a QAM or PSK constellation;  $\Delta f_k$  is the subcarrier frequency spacing;  $T$  is the sampling period at the transmitter which equals to  $T = T_u/N$ , with  $T_u = 1/\Delta f_k$  as the useful symbol duration;  $g(t)$  is the combined effect of the

transmitter pulse shaping and receiver match filtering given by

$$g(t) = \begin{cases} 1, & 0 \leq t \leq T; \\ 0, & \text{otherwise.} \end{cases} \quad (3.20)$$

The received continuous time baseband signal with perfect time synchronization can be written as

$$\begin{aligned} r(t) &= \frac{1}{\sqrt{N}} e^{j2\pi\Delta f_c t} \sum_{k=0}^{N-1} \sum_{l=-\infty}^{\infty} \sum_{m=1}^{M_c} d_l(k) h(\xi_m) e^{j2\pi k \Delta f_k (t - \xi_m - lT)} \\ &\times g(t - \xi_m - lT) + w(t), \end{aligned} \quad (3.21)$$

where  $\Delta f_c$  stands for the CFO;  $h(\xi_m)$  is the channel coefficient at delay  $\xi_m$ ,  $m = 1, \dots, M_c$ ;  $w(t)$  represents AWGN with variance  $\sigma_w^2$ .

The discrete-time OFDM signal  $r(nT_b)$  obtained by oversampling  $r(t)$  can be denoted as

$$\begin{aligned} r(nT_b) &= \frac{1}{\sqrt{N}} e^{j2\pi\Delta f_c nT_b} \sum_{k=0}^{N-1} \sum_{l=-\infty}^{\infty} \sum_{m=1}^{M_c} d_l(k) h(\xi_m) e^{j\frac{2\pi N}{\rho T_b} k(nT_b - \xi_m - l\rho T)} \\ &\times g(nT_b - \xi_m - lT) + w(nT_b) \\ &= \frac{1}{\sqrt{N}} e^{j2\pi\Delta f_c nT_b} \sum_{k=0}^{N-1} \sum_{l=-\infty}^{\infty} \sum_{m=1}^{M_c} d_l(k) h(\xi_m) e^{j\frac{2\pi N}{\rho} k(n - \frac{\xi_m}{T_b} - \frac{l\rho T}{T_b})} \\ &\times g[T_b(n - \frac{\xi_m}{T_b} - \frac{lT}{T_b})] + w(nT_b), \end{aligned} \quad (3.22)$$

where  $T_b$  is the sampling period at the receiver and  $\rho = T/T_b$  denotes the oversampling ratio.

### 3.2.2 Cyclostationarity in Oversampled OFDM Signals

The time-varying ACF of the signal given by (3.21) can be written as (see Appendix A for the detailed derivation of (3.23)-(3.26)) [32]

$$\begin{aligned}\tilde{R}(t, \tau) &= \frac{\sigma_d^2}{N} e^{-j2\pi\Delta f_c \tau} \sum_{k=0}^{N-1} e^{-j2\pi k \Delta f_k \tau} \sum_{m_1=1}^{M_c} h(\xi_{m_1}) e^{-j2\pi k \Delta f_k \xi_{m_1}} g(t - \xi_{m_1}) \\ &\times \sum_{m_2=1}^{M_c} h^*(\xi_{m_2}) e^{j2\pi k \Delta f_k \xi_{m_2}} g^*(t - \xi_{m_2} + \tau) \otimes \sum_{l=-\infty}^{\infty} \delta(t - lT) + \tilde{R}_w(t, \tau),\end{aligned}\quad (3.23)$$

where  $\tilde{R}_w(t, \tau)$  is the time-varying ACF of the AWGN.

The CCF of (3.23) at CF  $\alpha$  and delay  $\tau$  can be obtained by taking Fourier transform of (3.23) with respect to  $t$  [28] [32]

$$\begin{aligned}\tilde{R}(\alpha, \tau) &= \frac{\sigma_d^2}{NT} e^{-j2\pi\Delta f_c \tau} \sum_{k=0}^{N-1} e^{-j2\pi k \Delta f_k \tau} \int_{-\infty}^{\infty} \sum_{m_1=1}^{M_c} h(\xi_{m_1}) e^{-j2\pi k \Delta f_k \xi_{m_1}} \\ &\times g(t - \xi_{m_1}) \sum_{m_2=1}^{M_c} h^*(\xi_{m_2}) e^{j2\pi k \Delta f_k \xi_{m_2}} g^*(t - \xi_{m_2} + \tau) \\ &\times e^{-j2\pi\alpha t} dt \times \sum_{l=-\infty}^{\infty} \delta(\alpha - \frac{l}{T}) + \tilde{R}_w(\alpha, \tau),\end{aligned}\quad (3.24)$$

where  $\tilde{R}_w(\alpha, \tau)$  is the CCF of the AWGN and

$$\alpha = \frac{l}{T}, \quad l \text{ integer.} \quad (3.25)$$

Taking Fourier transform of (3.24) with respect to  $\tau$ , the CS of the signal at

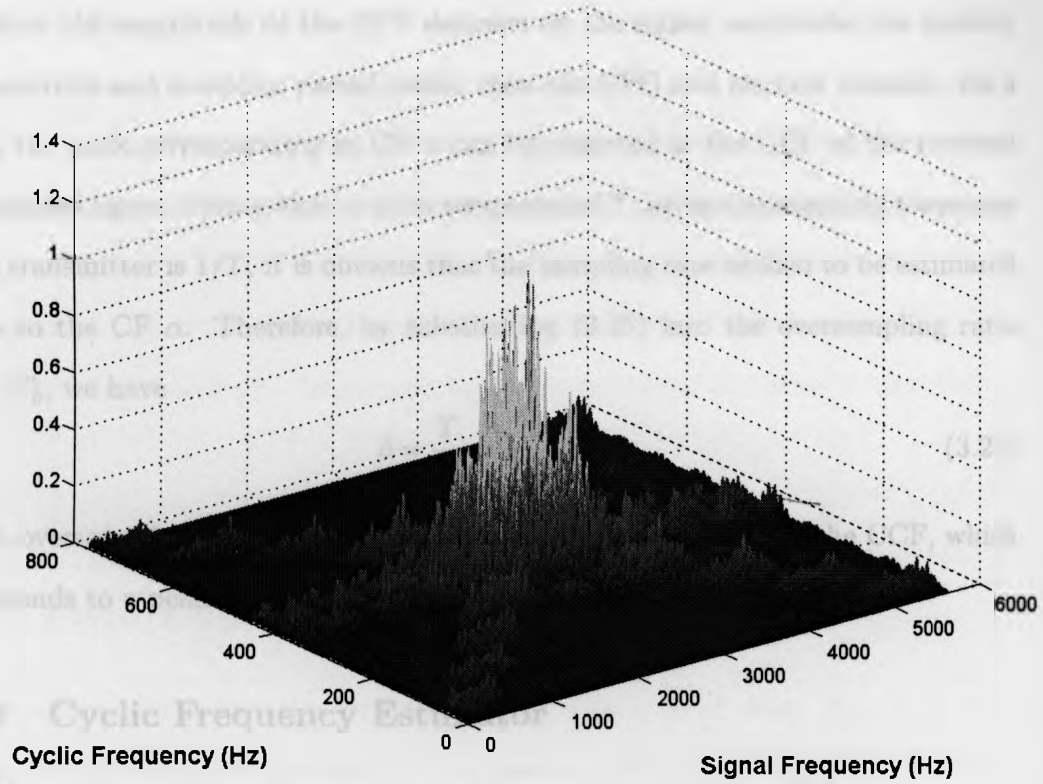


Figure 3.1: Cyclic spectrum of an oversampled OFDM signal.

CF  $\alpha$  and signal frequency  $f$  can be determined as

$$\begin{aligned} \bar{S}(\alpha, f) = & \frac{\sigma_d^2}{NT} \sum_{k=0}^{N-1} H^*(-f - \Delta f_c) G^*(-(f + \Delta f_c + k\Delta f_k)) \\ & \times H(\alpha - \Delta f_c - f) G(\alpha - f - \Delta f_c - k\Delta f_k) + \bar{S}_w(\alpha, f), \end{aligned} \quad (3.26)$$

where  $H(f)$  and  $G(f)$  are the Fourier transform of  $h(t)$  and  $g(t)$  respectively,  $\bar{S}_w(\alpha, f)$  is the CS of the AWGN. Fig. 3.1 shows the CS of the oversampled OFDM signal, the non-zero CF proves the existing cyclostationarity in oversampled OFDM signals since that a stationary signal has no CF.

It can be seen from (3.24) that  $\tilde{R}(\alpha, \tau) \neq 0$  only if  $\alpha = lT^{-1}$ , with  $l$  as an integer. Note that the magnitude of the CCF depends on the signal amplitude, the number of subcarriers and sampling period rather than the CFO and channel impacts. As a result, the peak corresponding to CF  $\alpha$  can be observed in the CCF of the received oversampled signal. Notice that  $\alpha$  is the reciprocal of  $T$ , given the sampling frequency at the transmitter is  $1/T$ , it is obvious that the sampling rate needed to be estimated equals to the CF  $\alpha$ . Therefore, by substituting (3.25) into the oversampling ratio  $\rho = T/T_b$ , we have

$$\hat{\rho} = \frac{T}{T_b} = \frac{1}{\alpha T_b}. \quad (3.27)$$

Hence, oversampling ratio  $\rho$  can be obtained by estimating CF  $\hat{\alpha}$  in the CCF, which corresponds to a peak in the CCF of the oversampled signals.

### 3.2.3 Cyclic Frequency Estimator

The CF estimator is given by maximizing the cost function below [33]

$$\hat{\alpha} = \arg \max_{\alpha} [|\hat{R}'(\alpha, \tau) + \hat{R}'^*(-\alpha, \tau)|^2], \quad (3.28)$$

where  $\alpha > 0$ ,  $\hat{R}'(\alpha, \tau)$  is the positive frequency part and  $\hat{R}'(-\alpha, \tau)$  is the negative frequency part of the CCF respectively. By adding these two components to reduce noisy frequency spikes, the performance of the CF estimator can be enhanced. Compared with the previous work proposed by Dandawaté and Giannakis in [34], this estimator is more robust and efficient for implementation.

It is obvious that the CCF  $R(\alpha, \tau)$  is a function with two variables  $\alpha$  and  $\tau$ . To search for the optimal CF  $\alpha$ , large amount of data and intensive computations are needed. Notice that for different  $\tau$ , the peak in CCF locates at the same position

which can be seen from (3.24). Therefore, it is much more efficient to search for the optimal  $\alpha$  with a fixed  $\tau$ . Furthermore, simulation shows that the optimal time delay  $\tau$  is dependent on the pulse shaping filter, which is also confirmed in [35]. However, the pulse shaping function is unknown in advance for blind estimation. Due to these reasons, a solution of setting the time lag as 1 (i.e.,  $\tau = 1$ ) is applied, which provides the best estimation results according to simulation and is also supported by [33]. Consequently, two dimensional search over function  $R(\alpha, \tau)$  can be simplified into one dimensional search and the complexity of the estimator decreases drastically.

### 3.3 Sampling Frequency Estimation by A

#### Two-Step Algorithm

In this section, CF estimation based on (3.28) with a fixed delay (i.e.  $\tau = 1$ ) is presented. A conventional one-step CF estimation is first presented as bench mark. The conventional method requires a large Fourier transform size to provide high estimation precision, which leads to high computational complexity for implementation. To reduce the computational complexity in the one-step scheme, a two-step algorithm based on zoom fast Fourier transform (ZFFT) is proposed for OFDM sampling frequency and oversampling ratio estimation.

##### 3.3.1 Conventional One-Step CF Estimation

Based on (3.28), CCF can be obtained by taking Fourier transform of the time-varying ACF and the optimal CF  $\alpha$  is the corresponding frequency which maximizes (3.28). In practice, FFT is always applied for spectral analysis due to its computational efficiency compared with DFT, especially when long data set and intensive computations



are required [36] [37]. Under this circumstance, the estimation of oversampling ratio by (3.27) can be given as

$$\hat{\rho} = \frac{1}{\hat{\alpha}T_b} = \frac{f_b}{\hat{K} \cdot \frac{f_b}{M}} = \frac{M}{\hat{K}}, \quad (3.29)$$

where  $M$  is the FFT size and  $\hat{K}$  is the estimated index of the CF.

Since OFDM signals are highly sensitive to frequency offsets, the estimated sampling frequency must be precise enough for signal recovery. For an example, in IEEE 802.11a standard, the symbol clock frequency tolerance shall be  $\pm 20$  ppm maximum. That is to say, the maximum tolerant offset is 6.25Hz with a symbol clock frequency of 0.3125MHz [17], which poses a high requirement for the sampling frequency estimation. As the estimation accuracy is determined by the resolution in the frequency domain, which corresponds to the observation duration and the utilized FFT size. By using a larger FFT size with a fixed observation period, the sampling in the frequency domain becomes denser. Consequently, a more precise CF estimate can be provided as the sampled frequency bin becomes closer to the exact CF in the CCF.

Large FFT size can be used to improve estimation precision of the oversampling ratio. However, it is impractical to increase the estimation accuracy by simply increasing FFT size due to hardware capability and power consumption limitations. Furthermore, large FFT size leads to a long processing time, which is not practical in real-time signal processing. Note that our aim is to search the optimal CF  $\alpha$  by locating the maximum FFT bin. It is more efficient to zoom in on the frequency range containing the desired CF rather than observing the whole frequency spectrum. Inspired by the zoom-in idea, algorithms for spectrum analysis over the desired frequency segment with high resolution are developed.

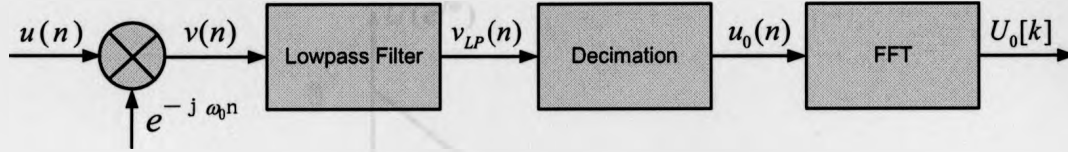


Figure 3.2: Block diagram of ZFFT.

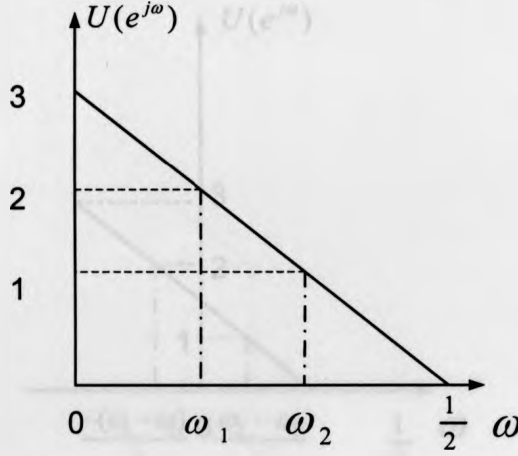
### 3.3.2 Zoom Fast Fourier Transform

ZFFT algorithm is a technique capable of zooming in on a segment of the spectrum in the same manner as a zoom lens on a camera does in photography [38]. It was first brought up by Hoyer [38] and Yip [39] with the aim to improve the efficiency in terms of storage size and computation time for the realistic implementation of Fourier transforms. By using ZFFT, only the resolution of a specific frequency segment is increased, which is suitable for the case where only the frequency segment containing the desired CF is of interest.

The frequency zoom-in effect is achieved by ZFFT shown in Fig. 3.2. It includes four steps: the original signal spectrum is first frequency shifted, then the resultant signal is lowpass filtered and decimated. These three function blocks of ZFFT are processed in the time domain. Finally, the decimated signal is transformed to the frequency domain by FFT.

Assume a  $K_2$ -point signal  $u(n)$  is sampled from a continuous signal  $u(t)$  with the sampling frequency  $F_u = 1$  Hz, after FFT, the corresponding frequency spectrum is  $U(e^{j\omega})$  with a frequency range  $[-1/2, 1/2]$  Hz as shown in Fig. 3.3. Assume the frequency interval  $[\omega_1, \omega_2]$ , which has a length of  $1/D$  ( $D$  is an integer) of the whole frequency range, is the frequency segment of interest. By ZFFT, the segment can be magnified as follows

- Frequency Shift

Figure 3.3: The frequency spectrum of  $U(e^{j\omega})$ .

To zoom in on the interested frequency segment ranging from  $\omega_1$  to  $\omega_2$ , frequency shift is first used to shift the original spectrum to a proper position, resulting in a frequency shifted signal  $v(n)$ .

$$v(n) = u(n)e^{-j\omega_0 n}, \quad (3.30)$$

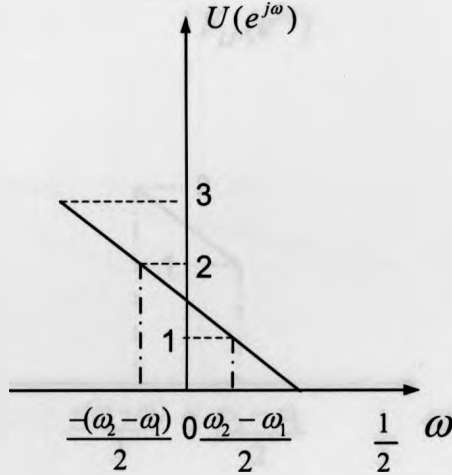
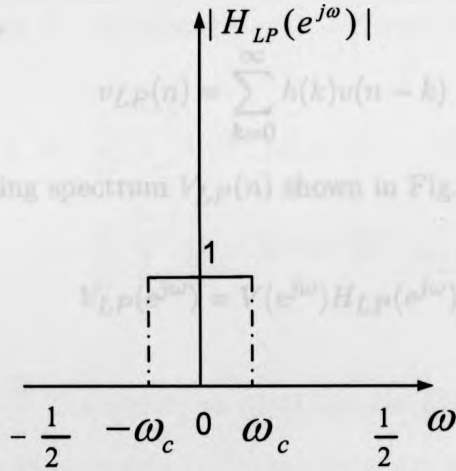
and the corresponding spectrum is

$$V(e^{j\omega}) = DFT[u(n)e^{-j\omega_0 n}] = U(e^{j(\omega+\omega_0)}), \quad (3.31)$$

where  $V(e^{j\omega})$  denotes the spectrum of  $v(n)$  and  $\omega_0 = \frac{\omega_1 + \omega_2}{2}$  is the shifted center frequency required by the system. The spectrum of the shifted signal is shown in Fig. 3.4.

- Ideal Lowpass Filter

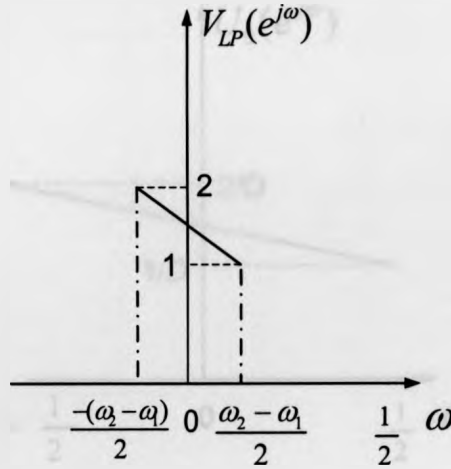
An ideal lowpass filter  $H_{LP}(e^{j\omega})$  as shown in Fig. 3.5 is utilized to filter out

Figure 3.4: The spectrum of  $v(n)$  after frequency shifting of  $u(n)$ .Figure 3.5: The ideal lowpass filter  $H_{LP}(e^{j\omega})$ .

the uninterested frequency part to eliminate frequency aliasing.

$$H_{LP}(e^{j\omega}) = \begin{cases} 1, & -\omega_c < \omega < \omega_c, \\ 0, & \text{otherwise.} \end{cases}$$

The cutoff frequency of the ideal lowpass filter should be  $\frac{\omega_2 - \omega_1}{2}$ , so that the frequency range of the filtered signal is  $\omega_1$  to  $\omega_2$ . The signal after lowpass filter

Figure 3.6: The spectrum of  $u_0(n)$  after decimation.

is  $v_{LP}(n)$  given by

$$v_{LP}(n) = \sum_{k=0}^{\infty} h(k)v(n-k) \quad (3.32)$$

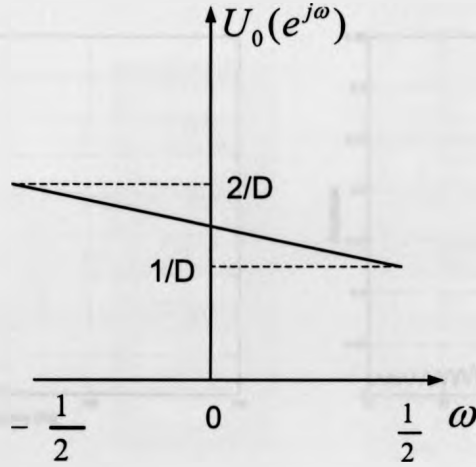
and the corresponding spectrum  $V_{LP}(n)$  shown in Fig. 3.6 is

$$V_{LP}(e^{j\omega}) = V(e^{j\omega})H_{LP}(e^{j\omega}). \quad (3.33)$$

- Decimation

The signal is then decimated by an integer factor  $D$  which means the new sampling frequency reduces to  $1/D$  of the original sampling frequency and the downsampled output, a  $K_1$ -point signal  $u_0(n)$  is

$$u_0(n) = v_{LP}(nD) = \sum_{k=0}^{\infty} h(k)v(nD-k), \quad (3.34)$$

Figure 3.7: The spectrum of  $u_0(n)$  after decimation.

and the spectrum of the decimated signal as shown in Fig. 3.7 is [40]

$$\begin{aligned}
 U_0(e^{j\omega}) &= \frac{1}{D} \sum_{l=0}^{D-1} V(e^{j\omega}) H_{LP}(e^{j\omega - 2\pi l}) \\
 &= \frac{1}{D} \sum_{l=0}^{D-1} U(e^{j(\frac{\omega}{D} + \omega_0 - \frac{2\pi l}{D})}) H_{LP}(e^{j(\frac{\omega}{D} - \frac{2\pi l}{D})}). \quad (3.35)
 \end{aligned}$$

Given  $H_{LP}(e^{j(\frac{\omega}{D} - \frac{2\pi l}{D})})$  denoting an ideal lowpass filter which removes the out of range frequency components, (3.35) can be rewritten as

$$U_0(e^{j\omega}) = \frac{1}{D} U(e^{j(\frac{\omega}{D} + \omega_0)}) H_{LP}(e^{j\frac{\omega}{D}}) = \frac{1}{D} U(e^{j(\frac{\omega}{D} + \omega_0)}). \quad (3.36)$$

Since the new sampling rate changes to  $F_{u_0} = \frac{F_u}{D}$ , the frequency range  $0 \leq |F_u| \leq \frac{1}{2D}$  is stretched to the corresponding frequency range  $0 \leq |F_{u_0}| \leq \frac{1}{2}$  by the decimation.

- FFT

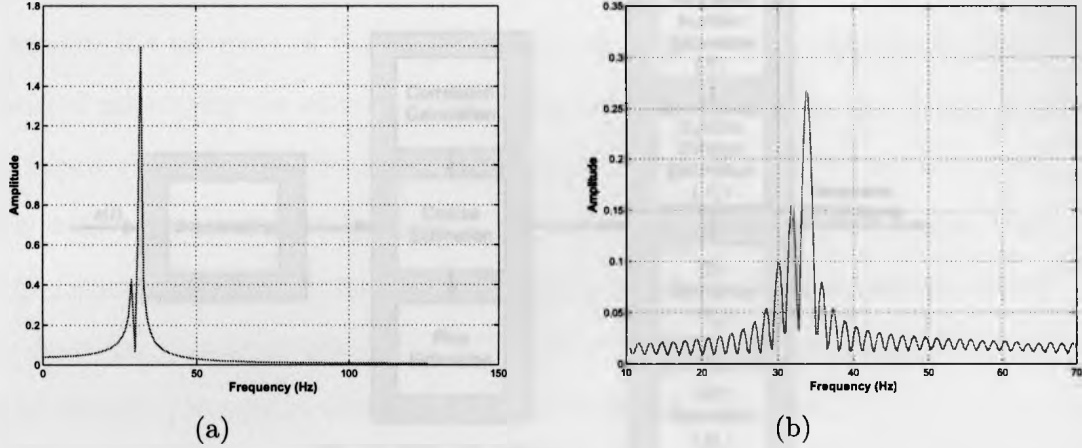


Figure 3.8: Spectrum of a signal with closely spaced frequency components processed with a)FFT and b)ZFFT.

The  $K_1$ -point FFT of the new signal  $u_0(n)$  therefore is given by

$$\begin{aligned}
 U_0(k) &= U_0(e^{j\omega})|_{\omega=\frac{2\pi}{K_1}k} = \frac{1}{D}U(e^{j(\frac{2\pi}{DK_1}k+\omega_0)}) \\
 &= \frac{1}{D}U(e^{j(\frac{2\pi}{K_2}k+\omega_0)}). \quad (3.37)
 \end{aligned}$$

It is demonstrated by (3.37) that to obtain the same resolution, a conventional  $K_2$ -point FFT is required when the entire spectrum is computed, where  $K_2 = DK_1$ . However, by ZFFT, only a  $K_1$ -point FFT is employed to achieve the same frequency resolution. In this sense, ZFFT can be used to calculate the interested frequency segment with high resolution without increasing FFT size, thereby reducing the computational complexity.

Fig. 3.8 shows an example of signal spectrum analysis from FFT and ZFFT. Assume the input original sequence consists of three sinusoidal signals: 30Hz to 1.0V,

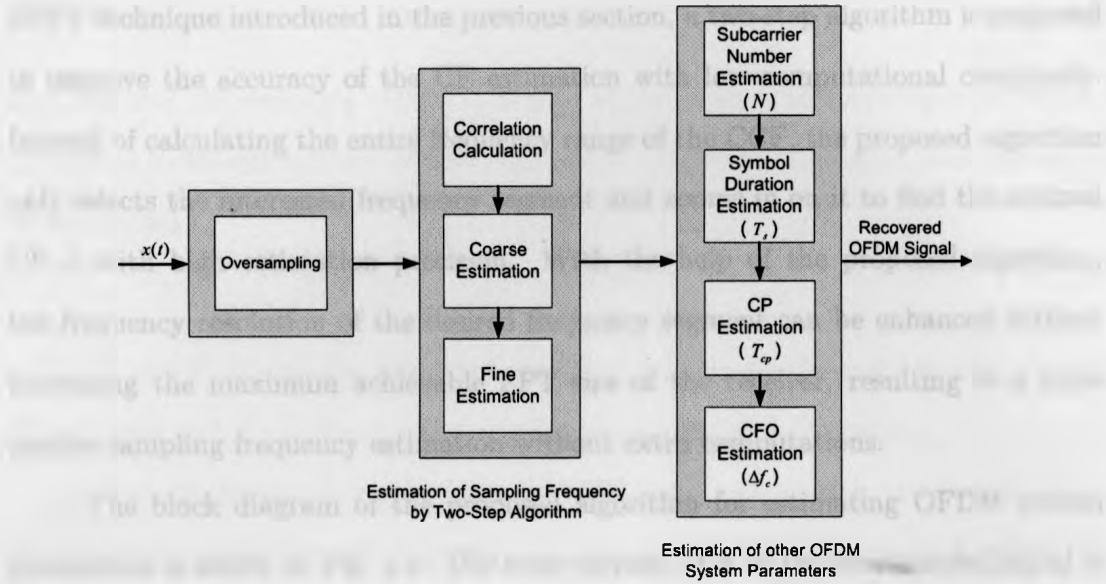


Figure 3.9: Block diagram of blind estimation of OFDM system parameters.

32Hz to 2.0V, 34Hz to 3.0V which are sampled at 500Hz, i.e.,

$$u(t) = \sin(2\pi \cdot 30t) + 2\sin(2\pi \cdot 32t) + 3\sin(2\pi \cdot 34t). \quad (3.38)$$

The spectrum of the original signal with 256 point FFT is plotted in Fig. 3.8(a). The three frequency components are undistinguishable because the frequency resolution is less than the frequency interval between two adjacent frequency components. Fig. 3.8(b) depicts the zoomed in spectrum with a decimation factor of  $D = 6$ . Benefitting from the zoom-in ability of ZFFT technique, without increasing the FFT size, the three frequency components can be identified clearly.

### 3.3.3 Proposed Two-Step CF Estimator Based on ZFFT

In practical implementations, the maximum achievable FFT size is often constrained, which limits the frequency resolution of the CCF obtained by FFT. Based on the



ZFFT technique introduced in the previous section, a two-step algorithm is proposed to improve the accuracy of the CF estimation with low computational complexity. Instead of calculating the entire frequency range of the CCF, the proposed algorithm only selects the interested frequency segment and zooms in on it to find the optimal CF  $\alpha$  with high estimation precision. With the help of the proposed algorithm, the frequency resolution of the desired frequency segment can be enhanced without increasing the maximum achievable FFT size of the receiver, resulting in a more precise sampling frequency estimation without extra computations.

The block diagram of the proposed algorithm for estimating OFDM system parameters is shown in Fig. 3.9. The time-varying ACF of the oversampled signal is calculated and then the CF is estimated with two steps. In the first step, a coarse estimation based on a small size FFT of ACF is obtained, with the aim of finding the approximate CF location and the frequency segment to be zoomed in. In the second step, the interested frequency segment is magnified by ZFFT to obtain a more precise CF estimation. In the sequel, other OFDM system parameters (i.e., the number of subcarriers, symbol duration, CP length and CFO) are estimated based on the estimated sampling frequency and oversampling ratio.

Given the minimum and maximum achievable FFT sizes ( $M_1$  and  $M_2$ ) of the receiver, the parameters in ZFFT for the proposed algorithm, i.e., the decimation factor, shifted center frequency and the range of the segment to be magnified, will be discussed in detail. To achieve the required precision, the selection of the decimation factor  $D$  is analyzed first. The selection of the zoomed-in frequency range is discussed later.

### 3.3.3.1 Selection of the Decimation Factor

Suppose that the sampling rate  $1/T_b$  is used at the receiver to oversample the signal. According to the system requirement, the bias of the estimated symbol clock frequency should satisfy

$$\left| \frac{1}{\hat{T}} - \frac{1}{T} \right| \leq \Delta_f, \quad (3.39)$$

where  $\hat{T}$  and  $T$  denote the estimated sampling period and the real sampling period respectively and  $\Delta_f$  is the required symbol clock frequency tolerance.

When the frequency resolution of the FFT is not high enough, the real CF of the CCF may lie in between two adjacent FFT bins and cannot be exactly represented. Assume that the true CF  $\alpha$  is located between the  $\hat{K}$ th and the  $(\hat{K} + 1)$ th bins as

$$\hat{\alpha} = \frac{(\hat{K} + \delta)}{M_2 D T_b}, \quad (3.40)$$

where  $\delta$  denotes the gap between the exact CF bin and the nearest FFT bin due to resolution limitation.  $\delta$  ranges from  $(-0.5, 0.5]$ , where the lower and upper bounds are decided by the worst case when the true CF lies exactly in the middle of two FFT bins.

Substituting (3.40) into (3.39) gives,

$$\left| \frac{\hat{K}}{M_2 D T_b} - \frac{(\hat{K} + \delta)}{M_2 D T_b} \right| \leq \Delta_f. \quad (3.41)$$

Finally, the decimation factor can be determined by

$$D \geq \max \frac{|\delta|}{M_2 T_b \Delta_f}. \quad (3.42)$$

The maximum value of  $\delta$  which equals to 0.5 is chosen for deriving the infimum of

the decimation factor  $D$  according to the precision requirements.

### 3.3.3.2 Selection of the Zoomed-in Segment Range

An  $M_1$ -point FFT is used in the first step to compute the CCF, the approximated CF  $\hat{\alpha}^*$  is then obtained by searching for the maximum FFT bin according to (3.28). Since the sampling clock is  $T_b$ , the frequency range of the CCF in the first step is  $[0, 1/T_b]$ . Depending on the decimation factor in the second step, the frequency segment to be zoomed in is  $\frac{1}{D}$  of the whole spectrum. Therefore, the range of the frequency segment for magnification in the second step is  $\frac{1}{DT_b}$ .

By obtaining the approximated CF  $\hat{\alpha}^*$  from the first step, the frequency segment to be observed around the center  $\hat{\alpha}^*$  is

$$[\hat{\alpha}^* - \frac{1}{2DT_b}, \hat{\alpha}^* + \frac{1}{2DT_b}]. \quad (3.43)$$

$\hat{\alpha}^*$  is the shifted frequency, which is used in the first block of ZFFT as shown in Fig. 3.8.

## 3.4 Estimation of Other System Parameters

With the previously estimated oversampling ratio, other OFDM system parameters, i.e., the number of subcarriers, symbol duration, length of CP and CFO can be estimated based on the previously estimated oversampling ratio.

### 3.4.1 Estimation of the Number of Subcarriers

As CP is copied from the last part of the OFDM data symbol, high correlation exhibits between CP and the last part of the data symbol. The ACF of the oversampled signal

can be expressed as follows [41]

$$R(\tau) = E\{r(n)r^*(n+\tau)\} = \begin{cases} \frac{\sigma_d^2}{N} + \sigma_\omega^2, & l = 0, \\ \frac{\sigma_d^2}{N}, & l = \rho N, \\ 0, & \text{otherwise,} \end{cases}$$

where  $\sigma_d^2$  and  $\sigma_\omega^2$  are the variances of OFDM symbol and AWGN, respectively.  $\tau$  is the time lag in the range of  $[0, \rho L]$  and  $\rho L$  is the length of the signal employed for estimation.

Obviously, the number of subcarriers can be estimated by searching the peak of the ACF which occurs at a time lag of  $\rho N$ . The location of the correlation peak is different from the one in [41] which occurs at the delay corresponding to  $N$ . In our case, the peak occurs at  $\rho N$  [42] due to oversampling and the correlation test is

$$\hat{N} = \arg \max_{\tau} \frac{1}{\hat{\rho}L} \sum_{n=0}^{\hat{\rho}L-1} r(n)r^*(n+\tau), \quad \tau = 0, 1, 2, \dots, \hat{\rho}L, \quad (3.44)$$

where  $\hat{\rho}$  is the oversampling ratio estimated before.

Combined with the sampling frequency estimated in the last section, the data part duration of an OFDM symbol is given by

$$\hat{T}_u = \hat{N}\hat{T}. \quad (3.45)$$

$R(\tau)$  is the special case of  $R(\alpha, \tau)$  when  $\alpha = 0$ , that is to say, OFDM signal itself is a cyclostationary signal due to the CP redundancy. This property will be used for the estimation of CP length in the following.

### 3.4.1.1 Estimation of the Length of CP

The duration of one OFDM symbol  $T_s$  consists of two parts, the period of useful data part  $T_u$  and the period of CP part  $T_{cp}$ , i.e.,  $T_s = T_u + T_{cp}$ . Since the CP part introduces cyclostationarity to OFDM signals at delay  $\tau = \hat{T}_u$ , the CCF at delay  $\tau = \hat{T}_u$  is given by

$$\begin{aligned} \tilde{R}(\alpha, \hat{T}_u) &= \frac{\sigma_d^2}{NT_s} e^{-j2\pi\Delta f_c \hat{T}_u} \sum_{k=0}^{N-1} e^{-j2\pi k \Delta f_k \hat{T}_u} \int_{-\infty}^{\infty} \sum_{m_1=1}^{M_c} h(\xi_{m_1}) e^{-j2\pi k \Delta f_k \xi_{m_1}} \\ &\quad \times g(t - \xi_{m_1}) \sum_{m_2=1}^{M_c} h^*(\xi_{m_2}) e^{j2\pi k \Delta f_k \xi_{m_2}} g^*(t - \xi_{m_2} + \hat{T}_u) \\ &\quad \times e^{-j2\pi\alpha t} dt \times \sum_{l=-\infty}^{\infty} \delta(\alpha - \frac{l}{T_s}) + \tilde{R}_w(t, \hat{T}_u), \end{aligned} \quad (3.46)$$

which is periodic of  $T_s$ . Therefore, by substituting (3.46) into (3.28), the symbol duration  $\hat{T}_s$  is equal to the reciprocal of the estimated CF. Since  $\hat{T}_u$  has been estimated in the previous section,  $\hat{T}_{cp}$  is then given by

$$\hat{T}_{cp} = \hat{T}_s - \hat{T}_u. \quad (3.47)$$

### 3.4.1.2 CFO Estimation

As discussed in Section 4 of Chapter 2, ICI caused by CFO leads to the loss of orthogonality among subcarriers in OFDM. Therefore, the estimation of CFO and further compensations are particularly important.

Frequency offset estimators can be classified into three categories: data-aided (DA), decision-directed (DD) and non-data-aided (NDA). Both DA and DD techniques assume that the transmitted symbol sequence is known. The DA method is normally employed for estimating the frequency offset based on a known training

sequence, whereas DD method performs the estimation by using the decoded output symbols as additional pilots. In contrast, NDA method acquires no knowledge of the transmitted signal. In the sequel, an NDA method exploiting the CP redundancy is proposed.

At the receiver, the CFO is modeled as a phase distortion of the received data in the time domain. According to [43] [44], the phase rotation between the CP and the last part of data symbol where CP duplicated is proportional to the CFO, from which the CFO can be estimated.

Assume channel fading is slow so that the channel impulse response does not change within one OFDM symbol. Therefore, the CFO can be estimated as [43]

$$\Delta f_c = \frac{1}{2\pi\hat{N}} \sum_n \text{angle}[r(n)r^*(n + \hat{N})], \quad n = 0, 1, 2, \dots, \hat{N}_{cp} - 1, \quad (3.48)$$

where  $\hat{N}$  stands for the number of subcarriers estimated in the previous part and  $\hat{N}_{cp} = \frac{\hat{T}_{cp}}{\hat{T}_u} \hat{N}$  denotes the number of CP samples in one OFDM symbol. The function  $\text{angle}[\cdot]$  calculates the phase of the given input.

### 3.5 Complexity Analysis of the Proposed

#### Algorithm for Oversampling Ratio

#### Estimation

As presented in the previous section, the proposed algorithm for oversampling ratio estimation consists of two steps. In the following the computational complexity associated with both Step 1 and Step 2 will be compared with the conventional algorithm used in [45].

In Step 1, a course estimation of CF  $\alpha$  is accomplished by  $M_1$ -point FFT,  $M_1$  is the minimum FFT size at the receiver. Therefore, it includes  $M_1 \log_2 M_1$  complex additions and  $\frac{M_1}{2} \log_2 M_1$  complex multiplications. In Step 2, a fine estimation of CF  $\alpha$  is accomplished by ZFFT with the maximum FFT size of the receiver is  $M_2$ . Thus there are  $M_2 \log_2 M_2$  complex additions and  $\frac{M_2}{2} \log_2 M_2$  complex multiplications in this step.

Table 3.1: Computational complexity comparisons between the proposed algorithm and the conventional algorithm

Proposed Algorithm			Conventional Algorithm
Step 1	Number of Complex Additions	384	-
	Number of Complex Multiplications	192	-
Step 2	Number of Complex Additions	$0.05 \times 10^6$	-
	Number of Complex Multiplications	$0.025 \times 10^6$	-
Total Number of Complex Computations		$0.075 \times 10^6$	$1.48 \times 10^6$

For the conventional FFT algorithm, to achieve the same estimation precision, the FFT size used is  $DM_2$ . Hence, the total number of complex additions and complex multiplications increase to  $DM_2 \log_2 DM_2$  and  $\frac{DM_2}{2} \log_2 DM_2$ , respectively.

For example, with the settings given in Simulation Setups in next section,  $M_1 = 64$ ,  $M_2 = 4096$  and  $D = 22$ , the computational complexity comparisons between the proposed algorithm and the conventional algorithm are shown in Table 3.1. It is illustrated that the proposed two-step algorithm for oversampling ratio estimation

can retain lower computational complexity compared to the conventional algorithm.

## 3.6 Simulation Results

### 3.6.1 Simulation Setup

To evaluate the precision requirements achieved by the proposed algorithm, system parameters used in the simulation are in accordance with the typical IEEE 802.11a standard [17]. The FFT size of 64 is used in each symbol with cyclic prefix  $N_{cp} = 16$ . The useful symbol period is  $3.2 \mu s$  and the cyclic prefix period is  $0.8 \mu s$ . Transmitted symbols are generated from QPSK scheme with unit variance. The normalized carrier frequency offset is 0.3 and the oversampling ratio used in our test is set to be 3.6. The channel considered in simulation is a five-tap ( $M_c = 5$ ) time dispersive channel [46], with coefficients  $h(\xi_1) = 0.227$ ,  $h(\xi_2) = 0.460$ ,  $h(\xi_3) = 0.688$ ,  $h(\xi_4) = 0.460$ ,  $h(\xi_5) = 0.688$  and  $[\xi_1, \xi_2, \xi_3, \xi_4, \xi_5] = [0.1, 0.2, 0.3, 0.4, 0.5] \mu s$ . The minimum and maximum achievable FFT size at the receiver is supposed to be 64 and 4096, then the decimation factor in the proposed algorithm is 22 according to (3.42) and the IEEE 802.11a standard [17]. All the simulation results are obtained from 1000 independent Monte Carlo trials.

### 3.6.2 Numerical Results

The performance of the proposed estimators are evaluated under both AWGN and multipath channels. Fig. 3.10 illustrates the computational complexity of the proposed two-step algorithm and the conventional algorithm [45] for the oversampling ratio estimation with the same precision. It is obvious that the computational complexity of the proposed two-step algorithm is much less than that of the conventional



algorithm. Fig. 3.11 shows the normalized mean square error (NMSE) of oversampling ratio estimations using the conventional algorithm and the proposed algorithm. It is illustrated that the estimation of oversampling ratio based on cyclostationarity test is robust even at low signal-to-noise ratios (SNRs). Furthermore, the accuracy of the proposed algorithm is higher than the conventional algorithm when the SNR and the maximum achievable FFT size are the same. This is due to the performance improvement of the proposed algorithm obtained by magnifying the interested frequency segment where the CF lies in.

The probability of correct estimation of the number of subcarriers and the length of CP versus SNR are plotted in Fig. 3.12. It is noticed that both the estimations are precise enough under AWGN channel while its performance degrades under multipath channel as SNR decreases. The estimation of the number of subcarriers is accurate because of the high signal correlation introduced by the CP redundancy. The estimation of the CP length is based on the cyclostationarity of the OFDM signal itself, which is as robust as the estimation of oversampling ratio.

Fig. 3.13 shows the NMSE versus SNR of the CFO estimation. It is apparent that the estimator is capable of working under AWGN channel even at low SNR values while the performance degrades in multipath channels.

### 3.7 Summary

In this chapter, OFDM system parameters (i.e., the sampling frequency, number of subcarriers, symbol duration, CP length as well as CFO) are blindly estimated by exploiting the cyclostationarity of oversampled signals. In Section 3.1, the theory of the signal cyclostationarity is introduced. Following that, the cyclostationarity of the oversampled OFDM signal is investigated with a time dispersive channel corrupted by

AWGN. The analytical expressions for the CCF and CS are derived to demonstrate the existing cyclostationarity in Section 3.2. Based on this, a two-step algorithm for OFDM sampling frequency and oversampling ratio estimations is proposed in Section 3.3 to reduce the computational complexity. Furthermore, other OFDM system parameters, i.e., the number of subcarriers, symbol duration, CP length and CFO are estimated. The complexity of the proposed algorithm is compared with the conventional algorithm in Section 3.4. Finally, the estimations are evaluated and the results confirm the precision and computational efficiency of the proposed algorithm in Section 3.5.

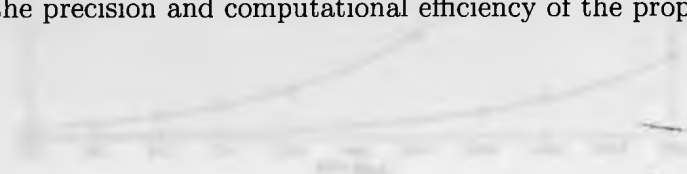


Figure 3.10: Computational complexity of the proposed algorithm compared to the conventional algorithm with AWGN channel condition.



Figure 3.11: RMSE of oversampling ratio estimation versus the proposed algorithm and conventional algorithm versus AWGN and multipath channel.

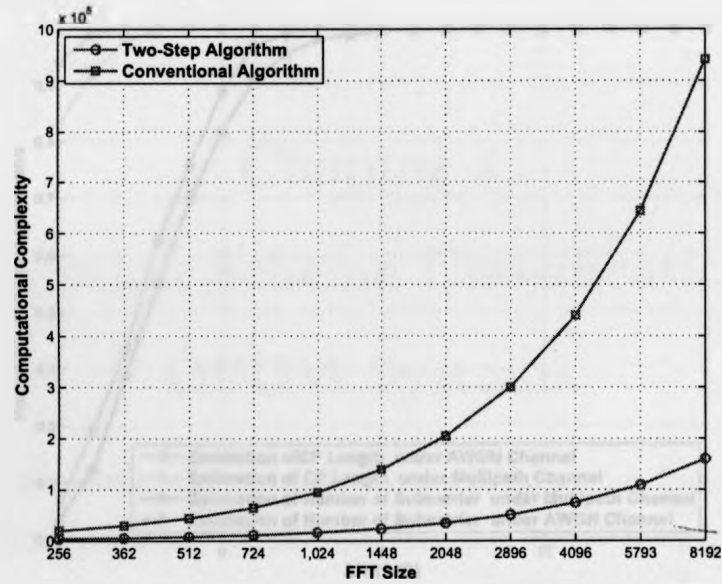


Figure 3.10: Computational complexity of the proposed algorithm compared to the conventional algorithm with the same estimation accuracy.

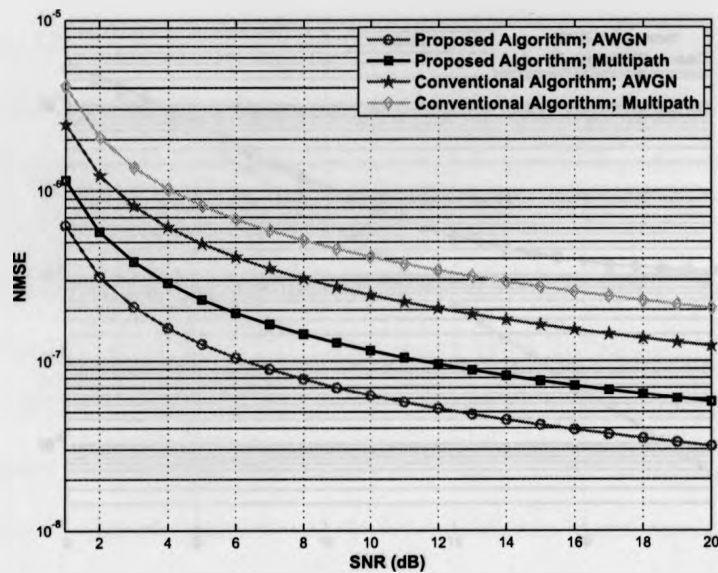


Figure 3.11: NMSE of oversampling ratio estimated from the proposed algorithm and conventional algorithm versus SNR under AWGN and multipath channels.

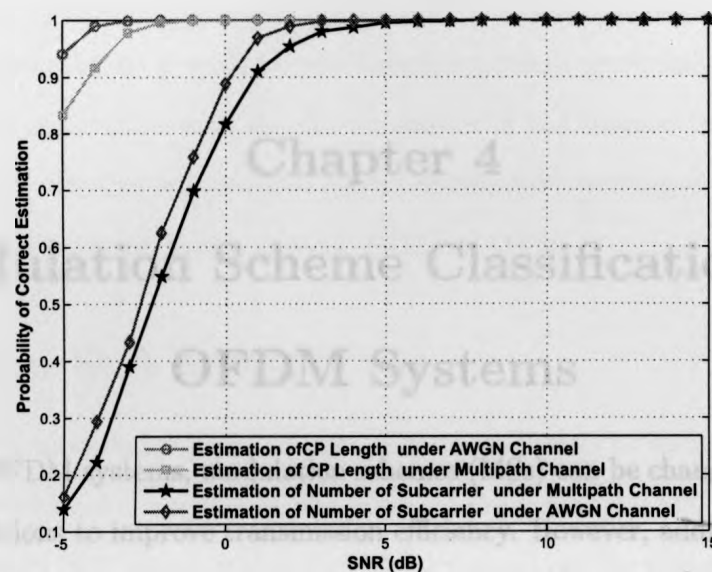


Figure 3.12: Correct estimation probability of number of subcarriers and CP length in multipath channel with AWGN under different SNRs.

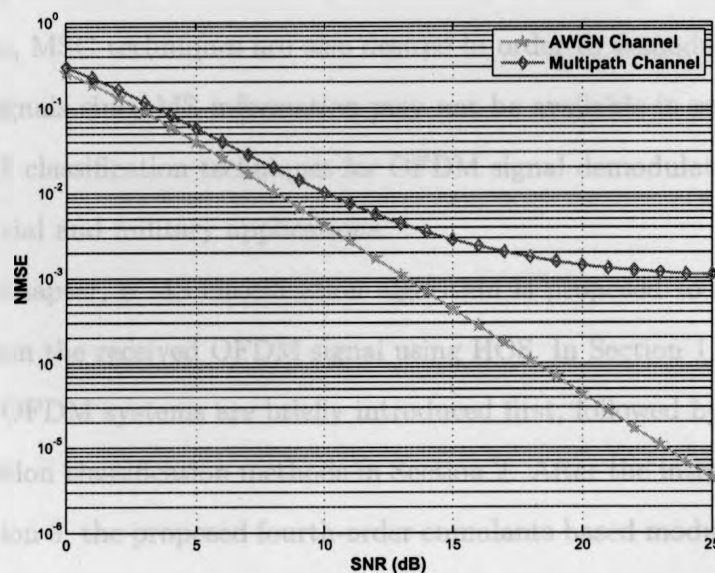


Figure 3.13: NMSE of the CFO estimation versus SNR under both AWGN and multipath channels.

## Chapter 4

# Modulation Scheme Classification for OFDM Systems

In adaptive OFDM systems, modulation schemes (MSs) can be changed according to channel conditions to improve transmission efficiency. However, additional signalling is often required to inform the receiver the employed MS, which lowers the bandwidth efficiency. Taking advantages of MS classification techniques, a smart receiver is able to automatically track and adapt to the employed MS, thereby avoiding additional signalling and saving the bandwidth. Furthermore, to intercept communications for S&R purposes, MSC techniques are also desired in order to demodulate and recover intercepted signals since MS information may not be available in such applications. Therefore, MS classification techniques for OFDM signal demodulation are useful in both commercial and military applications.

In this chapter, a MS classification algorithm is proposed to identify the employed MS from the received OFDM signal using HOS. In Section 1, MSs commonly employed by OFDM systems are briefly introduced first, followed by a review of existing modulation classification methods in Section 2. After the introduction of HOS basics in Section 3, the proposed fourth-order cumulants based modulation classification algorithm is presented in Section 4. Simulation results that confirm the accuracy of the proposed algorithm are given at the end of this chapter.

## 4.1 Digital Modulation Techniques

Digital modulation is the process by which digital symbols are transformed into waveforms that are compatible with the characteristics of the channel for the purpose of transmission [3]. In this section, two digital modulation techniques commonly used in OFDM systems are reviewed, namely, PSK and QAM.

### 4.1.1 Phase Shift Keying (PSK)

In  $M$ -ary PSK modulation,  $\log_2 M$  data bits are collected to form a symbol. The pattern of the symbol is encoded as the phase of the signal [47] [48].

The  $M$ -ary PSK signal within the  $k$ th subcarrier can be represented by

$$d_l(k) = e^{j2\pi\theta_l(k)}, \quad (4.1)$$

where  $d_l(k)$  is the symbol transmitted within the  $l$ th symbol period and the  $k$ th subcarrier;  $\theta_l(k)$  is the phase chosen from  $M$  possible values as follows

$$\theta_l(k) \in \{0, \frac{2\pi}{M}, \dots, \frac{(M-1)2\pi}{M}, k = 1, 2, \dots, M\}. \quad (4.2)$$

Different  $M$  values generate different kinds of PSK signals. Higher level PSK scheme has higher bandwidth efficiency, while it increases the complexity of demodulator and is more susceptible to noise. Binary PSK (BPSK) and QPSK are the most commonly used PSK schemes in OFDM systems, where  $M = 2$  for BPSK modulation and  $M = 4$  for QPSK modulation.

Fig. 4.1 shows a subset of binary data  $\{0, 1, 1, 0, 1, 1, 1, 0, 1, 1\}$  and the corresponding waveform of a BPSK signal. Fig. 4.2 shows a subset of binary data  $\{0, 0, 1, 0, 0, 1, 1, 0, 0, 0, 1, 0, 1, 0, 1, 1, 1, 0, 0\}$  and the corresponding waveform of a

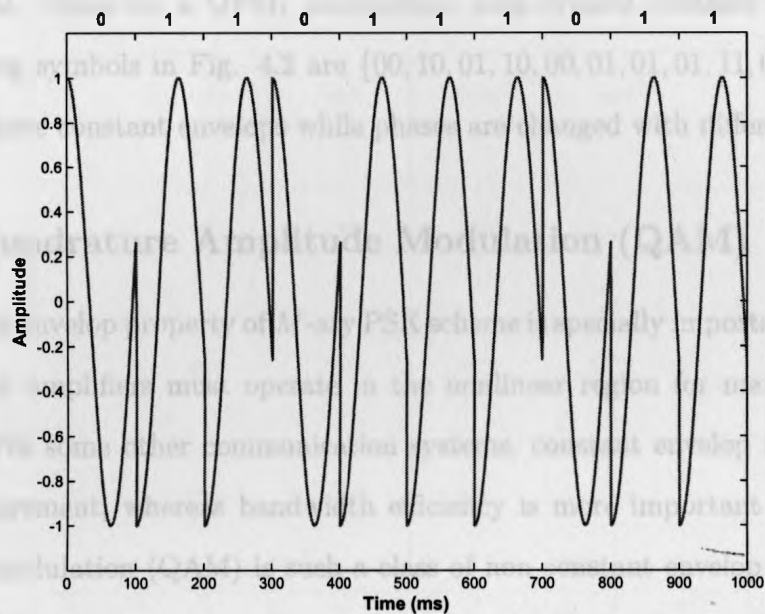


Figure 4.1: Binary data and the corresponding waveform of a BPSK signal.

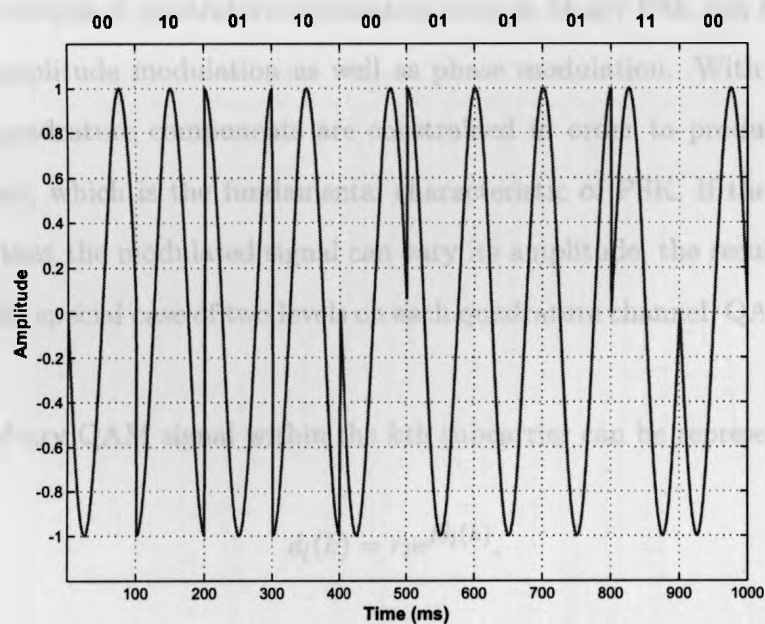


Figure 4.2: Binary data and the corresponding waveform of a QPSK signal.

QPSK signal. Since for a QPSK modulation, each symbol contains two bits, the corresponding symbols in Fig. 4.2 are {00, 10, 01, 10, 00, 01, 01, 11, 00}. All PSK waveforms have constant envelopes while phases are changed with different symbols.

### 4.1.2 Quadrature Amplitude Modulation (QAM)

The constant envelop property of  $M$ -ary PSK scheme is specially important to systems where power amplifiers must operate in the nonlinear region for maximum power efficiency. For some other communication systems, constant envelop may not be a crucial requirement, whereas bandwidth efficiency is more important. Quadrature amplitude modulation (QAM) is such a class of non-constant envelop schemes that can achieve higher bandwidth efficiency than  $M$ -ary PSK with the same average signal power.

The principle of quadrature modulation used in  $M$ -ary PSK can be generalized to include amplitude modulation as well as phase modulation. With PSK, the in-phase and quadrature components are constrained in order to produce a constant envelop signal, which is the fundamental characteristic of PSK. If the constraint is removed so that the modulated signal can vary its amplitude, the result is known as QAM. For the special case of two levels on each quadrature channel, QAM is identical to QPSK.

The  $M$ -ary QAM signal within the  $k$ th subcarrier can be represented by [49]

$$d_l(k) = r_l e^{j\theta_l(k)}, \quad (4.3)$$

where  $r_l = \sqrt{A_{li}^2 + A_{lq}^2}$ ,  $A_{li}$  and  $A_{lq}$  are the information-bearing signal amplitude;  $\theta_l(k) = \tan^{-1}(A_{lq}/A_{li})$  is the phase that is chosen from  $M$  possible values depending



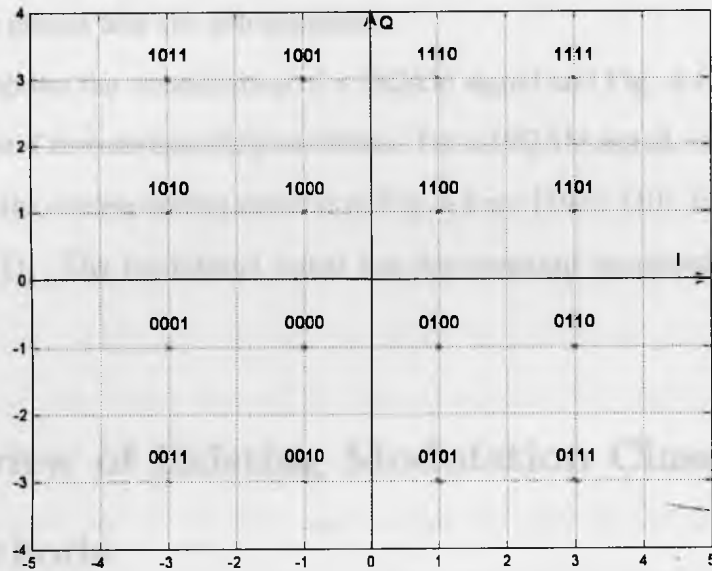


Figure 4.3: The constellation of 16QAM modulation scheme.

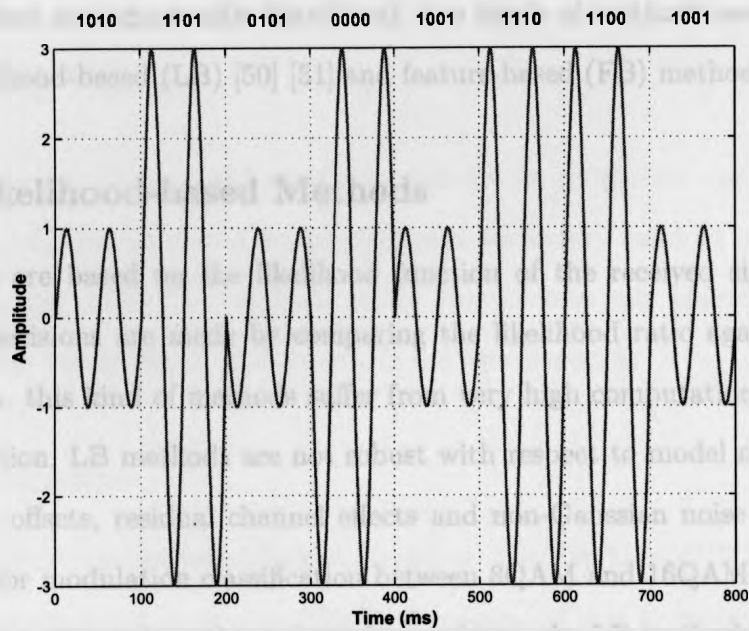


Figure 4.4: Binary data and the corresponding waveform of a 16QAM signal.

on the underlying symbols to be modulated;  $d_l(k)$  is the symbol transmitted within the  $l$ th symbol period and the  $k$ th subcarrier.

Fig. 4.3 shows the constellation of a 16QAM signal and Fig. 4.4 shows a subset of binary data and its corresponding waveform. For a 16QAM signal, each symbol contains four bits, the corresponding symbols in Fig. 4.4 are {1010, 1101, 0101, 0000, 1001, 1110, 1100, 1001}. The modulated signal has non-constant amplitude and different phases.

## 4.2 Review of Existing Modulation Classification

### Methods

MS classification techniques have been studied for decades, most of which are based on single carrier transmission schemes. Under the typical assumption that symbols are independent and identically distributed, two kinds of methods are widely used, namely, likelihood-based (LB) [50] [51] and feature-based (FB) methods [52].

#### 4.2.1 Likelihood-based Methods

LB methods are based on the likelihood function of the received signal and corresponding decisions are made by comparing the likelihood ratio against a threshold. However, this kind of methods suffer from very high computational complexity [53]. In addition, LB methods are not robust with respect to model mismatch such as frequency offsets, residual channel effects and non-Gaussian noise distributions. Specifically, for modulation classification between 8QAM and 16QAM which can be formulated as a binary hypothesis detection problem, the LB methods tend to favor the denser constellation (i.e., 16QAM), which are not robust as a classifier [54]. The

drawbacks of LB methods motivate the research of using statistical features for better classification performances with lower complexity.

## 4.2.2 Feature-based Methods

FB methods perform the modulation classification based on different statistical features in the received signal, such as the instantaneous amplitude, frequency, phase and so on [55]. In recent FB methods, the HOS of the received signal is exploited, including the fourth-, sixth-, and eighth-order cumulants [54] [56] [57] [58] [59] [60].

In this chapter, we utilize the fourth-order cumulant of the FFT demodulated signal as a powerful feature for MS classification due to their attractive properties: (a) cumulants provide natural measures of deviations from normality for a random variable or process; and more importantly, (b) higher-order cumulants of a stationary Gaussian process are zero which makes the classification immune to AWGN.

## 4.3 HOS Basics

Before introducing the proposed algorithm, definitions, properties and computations of the HOS (i.e., moments and cumulants) of a stationary random process will be discussed. In this thesis, the emphasis of the discussion is only placed on to fourth-order statistics, orders higher than four will not be considered.

### 4.3.1 Moments

For a collection of random variables  $\mathbf{x} = [x_1, x_2, \dots, x_k]$ , let  $\mathbf{I}_x = \{1, 2, \dots, k\}$  denote the set of components indices of  $\mathbf{x}$ . The joint moment of  $\mathbf{x}$  is given by

$$m_{\mathbf{x}}(\mathbf{I}) = E\{x_1 x_2 x_3 \cdots x_k\}. \quad (4.4)$$

According to (4.4), the  $k$ th moment of a set containing  $k$  random variables is the expectation of the product of these  $k$  random variables. It then follows that

$$m_1 = E\{x_1\}, \quad (4.5)$$

and the second, the third and the fourth moments are

$$m_2 = E\{x_1 x_2\}. \quad (4.6)$$

$$m_3 = E\{x_1 x_2 x_3\}, \quad (4.7)$$

$$m_4 = E\{x_1 x_2 x_3 x_4\}. \quad (4.8)$$

The foregoing equations are the basic moment equations which will be used for the derivation of fourth-order cumulant in the following subsection.

### 4.3.2 Cumulants

For a collection of random variables  $\mathbf{x} = [x_1, x_2, \dots, x_k]$  and the set of components indices  $\mathbf{I}_x = \{1, 2, \dots, k\}$  of  $\mathbf{x}$ , if we have  $\mathbf{I} \subseteq \mathbf{I}_x$ , then  $\mathbf{x}_I$  is the subvector consisting of those components of  $\mathbf{x}$  whose indices belong to  $\mathbf{I}$ . The “partition” of the set  $\mathbf{I}$  is the unordered collection of nonintersecting nonempty sets  $\mathbf{I}_p$  such that  $\cup_p \mathbf{I}_p = \mathbf{I}$  [61].

Denote the moment and cumulant of the subvector  $\mathbf{x}_I$  as  $m_x(\mathbf{I})$  and  $c_x(\mathbf{I})$ , the moment-to-cumulant (M-C) formula is [61]

$$c_x(\mathbf{I}) = \sum_{\cup_{p=1}^Q \mathbf{I}_p = \mathbf{I}} (-1)^{Q-1} (Q-1)! \prod_{p=1}^Q m_x(\mathbf{I}_p), \quad (4.9)$$

where  $\cup_{p=1}^Q \mathbf{I}_p = \mathbf{I}$ ,  $p = 1, \dots, Q$  denotes summation over all partitions of the set  $\mathbf{I}$ .

$Q$  is the number of the subsets of a partition. A partition of the set  $\mathbf{I}$  is a collection of nonintersecting and nonempty sets  $\mathbf{I}_p$ , such that  $\cup_p \mathbf{I}_p = \mathbf{I}$ . For example,  $Q = 1$  for  $\{(1, 2, 3)\}$ ,  $Q = 2$  for  $\{(1), (2, 3)\}$ ,  $\{(2), (1, 3)\}$  and  $\{(3), (1, 2)\}$ . Since we only investigate the fourth-order cumulant in this chapter, cumulants less than fourth-order are calculated in detail.

According to the M-C formula (4.9), the first cumulant is equal to the first moment, that is [61]

$$c_1 = m_1 = E\{x_1\}. \quad (4.10)$$

The second cumulant  $c_2$  is

$$c_2 = m_2 - m_1^2 = E\{x_1 x_2\} - E\{x_1\}E\{x_2\}. \quad (4.11)$$

The third cumulant,  $c_3$ , is

$$\begin{aligned} c_3 &= m_3 - 3m_1 m_2^2 + 2m_1^2 \\ &= E\{x_1\}E\{x_2\}E\{x_3\} - E\{x_1\}E\{x_2 x_3\} \\ &\quad - E\{x_2\}E\{x_1 x_3\} - E\{x_3\}E\{x_1 x_2\} + E\{x_1\}E\{x_2\}E\{x_3\}. \end{aligned} \quad (4.12)$$

The fourth cumulant,  $c_4$ , is [61]

$$\begin{aligned}
 c_4 &= m_4 - 4m_3m_1 - 3m_2^2 + 12m_1^2m_2 - 6m_1^4 \\
 &= E\{x_1x_2x_3x_4\} - E\{x_1\}E\{x_2x_3x_4\} - E\{x_2\}E\{x_1x_3x_4\} \\
 &\quad - E\{x_3\}E\{x_1x_2x_4\} - E\{x_4\}E\{x_1x_2x_3\} - E\{x_1x_2\}E\{x_3x_4\} \\
 &\quad - E\{x_1x_3\}E\{x_2x_4\} - E\{x_1x_4\}E\{x_2x_3\} + 2E\{x_1x_2\}E\{x_3\}E\{x_4\} \\
 &\quad + 2E\{x_1x_3\}E\{x_2\}E\{x_4\} + 2E\{x_1x_4\}E\{x_2\}E\{x_3\} + 2E\{x_2x_3\}E\{x_1\}E\{x_4\} \\
 &\quad + 2E\{x_2x_4\}E\{x_1\}E\{x_3\} + 2E\{x_3x_4\}E\{x_1\}E\{x_2\} \\
 &\quad - 6E\{x_1\}E\{x_2\}E\{x_3\}E\{x_4\}. \tag{4.13}
 \end{aligned}$$

For a random process with zero mean, the cumulants can be simplified as

$$c_1 = m_1 = E\{x_1\} = 0, \tag{4.14}$$

$$c_2 = m_2 = E\{x_1x_2\}, \tag{4.15}$$

$$c_3 = m_3 = E\{x_1x_2x_3\} = 0, \tag{4.16}$$

$$\begin{aligned}
 c_4 &= m_4 - 3m_2^2 \\
 &= E\{x_1x_2x_3x_4\} - E\{x_1x_2\}E\{x_3x_4\} \\
 &\quad - E\{x_1x_3\}E\{x_2x_4\} - E\{x_1x_4\}E\{x_2x_3\}. \tag{4.17}
 \end{aligned}$$

The second, third and fourth cumulants are usually called variance, skewness and kurtosis. In statistics and probability theory, kurtosis is a statistical measure of the “peakedness” of the probability distribution of a random variable [62]. It measures the flatness of a distribution density function near its center. Positive values are used to indicate that a density is more peaked around its center than a normal curve and negative values indicate that a density is more flat around its center than a normal

curve.

As to a Gaussian process, i.e., AWGN, all cumulants of order greater than two is identically zero. Non Gaussian processes do not have all zero cumulants. Thus, higher-order cumulant measurements have a natural tolerance to Gaussian noise.

## 4.4 Proposed Modulation Classification

### Algorithm for OFDM Systems

Since the shape of the distribution of different MS is characterized by kurtosis, it provides a statistical metric for MS classification. By calculating the higher-order cumulants of independent symbols over each subcarrier in OFDM systems, the corresponding MS can be classified according to the computed value and the theoretical value.

#### 4.4.1 Signal Model

Rewrite the received baseband continuous OFDM signal in Chapter 3 as follows

$$\begin{aligned}
 r(t) = & \frac{1}{\sqrt{N}} e^{j2\pi\Delta f_c t} \sum_{k=0}^{N-1} \sum_{l=-\infty}^{\infty} \sum_{m=1}^{M_c} d_l(k) h(\xi_m) e^{j2\pi k \Delta f_k (t - \xi_m - lT)} \\
 & \times g(t - \xi_m - lT) + \omega(t),
 \end{aligned} \tag{4.18}$$

where  $N$  is the number of subcarriers;  $l$  represents the  $l$ th symbol;  $k$  denotes the  $k$ th subcarrier;  $d_l(k)$  is the symbol transmitted within the  $l$ th symbol period and the  $k$ th subcarrier. Symbols from different subcarriers are considered as independent and identically distributed (i.i.d.) random variables with zero mean and variance of  $\sigma_d^2$ , drawn from either a QAM or PSK constellation;  $\Delta f_k$  is the subcarrier frequency

spacing;  $T$  is the sampling period at the transmitter which is equal to  $T = T_u/N$ , with  $T_u = 1/\Delta f_k$  as the useful symbol duration;  $g(t)$  is the combined effect of the transmitter pulse shaping and receiver match filtering;  $\Delta f_c$  stands for the CFO;  $h(\xi_m)$  is the channel coefficient at delay  $\xi_m$ ,  $m = 1, \dots, M_c$ ;  $w(t)$  represents AWGN with variance  $\sigma_w^2$ .

#### 4.4.2 Theoretical Cumulants for Different Constellations

According to [54], the  $n$ th-order/ $q$ -conjugate moment of the frequency domain symbol  $d_l(k)$  over the  $k$ th subcarrier can be calculated as

$$m_{k,n,q} = E\{(d_l^*(k))^q, (d_l(k))^{n-q}\} = \frac{1}{L} \sum_{l=0}^L (d_l^*(k))^q (d_l(k))^{n-q}, \quad (4.19)$$

where  $d_l(k)$  is the frequency domain symbol transmitted within the  $l$ th symbol period and the  $k$ th subcarrier and  $L$  is the number of total samples taking into computation.

By using the M-C formula (4.9), the  $n$ th-order/ $q$ -conjugate cumulant  $c_{k,n,q}$  of the constellation can be easily expressed in terms of moments as

$$\begin{aligned} c_{k,n,q} &= \text{Cum}[(d_l^*(k))^q, (d_l(k))^{n-q}] \\ &= \sum_{\cup_{p=1}^Q I_p=1} (-1)^{Q-1} (Q-1)! \prod_{p=1}^Q m_{k,n,q}. \end{aligned} \quad (4.20)$$

The theoretical values of the  $n$ th-order/ $q$ -conjugate cumulants,  $c_{k,n,q}$ , for the interested constellations are given in Table 4.1 [54] [58] [59]. These values were computed using the M-C formula in which the  $n$ th-order/ $q$ -conjugate moments calculated as ensemble averages over the noise-free constellations with equiprobable symbols under the constraint of unit energy. Due to the symmetry of the considered constella-



Table 4.1: Theoretical cumulants for constellations under constraints of unit variance.

$c_{k,n,q}$	BPSK	QPSK	16QAM	64QAM
$c_{k,2,0}$	1	0	0	0
$c_{k,2,1}$	1	1	1	1
$c_{k,4,0}$	-2	1	-0.68	-0.619
$c_{k,4,1}$	-2	0	0	0
$c_{k,4,2}$	-2	-1	-0.68	-0.619

tions, the  $n$ th-order/ $q$ -conjugate moments are equal to zero when  $n$  is odd. Therefore, only the  $n$ th-order/ $q$ -conjugate cumulants when  $n$  is even are given. These theoretical values will be used as the catalog patterns for decision making of the classifications in next subsection.

#### 4.4.3 Proposed Algorithm for OFDM Subcarrier MS

In this section, we propose a MS classification algorithm to classify modulation scheme for OFDM systems.

The algorithm consists of two steps. In Step 1, normalization of frequency domain samples is carried out to remove any scale factor. Afterwards, according to [54] and [58], the fourth-order/two-conjugate cumulant of symbols from the  $k$ th OFDM subcarrier are then computed as

$$\begin{aligned}
 \hat{c}_k &= \hat{m}_4 - 3\hat{m}_2^2 \\
 &= E\{(d_l^*(k))^2, (d_l(k))^2\} - 3[E\{(d_l^*(k)), (d_l(k))\}]^2 \\
 &= \frac{1}{L} \sum_{l=-\infty}^{\infty} \sum_{k=0}^{N-1} (d_l^*(k))^2 (d_l(k))^2 - 3 \left[ \frac{1}{L} \sum_{l=0}^L (d_l^*(k)) (d_l(k)) \right]^2, \quad (4.21)
 \end{aligned}$$

where  $d_l(k)$  is the frequency domain symbol with the  $l$ th symbol and the  $k$ th subcarrier and  $L$  is the number of total samples in the  $k$ th subcarrier taking into com-

putation. Then the feature vector  $\hat{\mathbf{c}} = [\hat{c}_1 \hat{c}_2 \cdots \hat{c}_N]^T$  which combines the fourth-order/two-conjugate cumulant of each subcarrier can be obtained, where  $N$  denotes the total number of subcarriers.

In Step 2, the calculated feature vector is compared with catalog pattern matrix given in Table 4.1 and the decision of the employed MS is made in accordance with the criterion

$$\hat{i} = \arg \min_{i=1,2,3,4} d(\mathbf{C}, \hat{\mathbf{c}}), \quad (4.22)$$

where  $i$  enumerates the candidate MSs;  $\hat{i}$  represents the decision on the MS of the estimated symbols;  $d(\cdot)$  represents the classic Euclidean distance;  $\hat{\mathbf{c}}$  is the measured feature vector and  $\mathbf{C}$  is the catalog matrix as follows

$$\mathbf{C} = [\mathbf{c}_1 \ \mathbf{c}_2 \ \mathbf{c}_3 \ \mathbf{c}_4] = \begin{bmatrix} -2 & -1 & -0.68 & -0.619 \\ -2 & -1 & -0.68 & -0.619 \\ \vdots & \vdots & \cdots & \vdots \\ -2 & -1 & -0.68 & -0.619 \\ \vdots & \vdots & \cdots & \vdots \\ -2 & -1 & -0.68 & -0.619 \end{bmatrix}. \quad (4.23)$$

Each column in  $\mathbf{C}$  stands for the fourth-order/two-conjugate cumulant of different MSs given in Table 4.1.

## 4.5 Simulation Results

In this section, simulations have been presented for performance evaluation of the proposed MS classification algorithm. Four MSs commonly employed in OFDM systems,

namely, BPSK, QPSK, 16QAM and 64QAM are to be classified.

#### 4.5.1 Simulation Setup

The same OFDM system parameters as in chapter 3 are employed to verify the proposed algorithm. The main parameters are as follows, the FFT size of 64 is used in each symbol with CP  $N_{cp} = 16$ ; The symbol period is  $4 \mu s$  and the CP period is  $0.8 \mu s$ . The normalized carrier frequency offset is 0.3 and the channel considered in simulation is a five-tap ( $M_c = 5$ ) time dispersive channel [46], with coefficients  $h(\xi_1) = 0.227$ ,  $h(\xi_2) = 0.460$ ,  $h(\xi_3) = 0.688$ ,  $h(\xi_4) = 0.460$ ,  $h(\xi_5) = 0.688$ , and  $[\xi_1, \xi_2, \xi_3, \xi_4, \xi_5] = [0.1, 0.2, 0.3, 0.4, 0.5] \mu s$ .

#### 4.5.2 Numerical Results

The classification performance is evaluated based on the average probability of correct classification  $P_c$ .

In Fig. 4.5, the correct classification probability of these four MSs is compared versus different SNR values. Classification performance improves as SNR increases for the reason that AWGN does not affect the fourth-order cumulant but their variance, which can be seen from (4.21). The higher the modulation order is, the more sensitive the corresponding constellation is to low SNRs. Therefore, the fourth-order/two-conjugate cumulant of the signal samples is more precise as SNR increases, which results in a more accurate classification.

Fig. 4.6 depicts the performance of the classifier with different number of samples when SNR = 10dB. It is illustrated that the number of samples required to attain excellent classification performance at a specific SNR depends on the investigated signals, i.e., at 10dB SNR, only a few hundreds samples is requested in case of

BPSK, while the data length increases for higher-order modulations such as 16QAM and 64QAM. Since the proposed algorithm classifies the MS based on the characteristics of constellation distributions, a larger number of samples is suggested in order to reduce the estimation bias.

Fig. 4.7 depicts the symbol error rates (SERs) of symbols demodulated according to classified modulation schemes compared with the theoretical SERs. By comparing with the theoretical SER of each MS, Fig. 4.7 illustrates that the classification of MS is accurate enough for demodulation and other processings.

## 4.6 Summary

In this chapter, modulation classification for OFDM systems is carried out using the fourth-order cumulant of the frequency domain signal. MSs which are usually employed in OFDM systems and the basic knowledge of the HOS of stationary random processes are described at the beginning of this chapter. Following that, the proposed algorithm for classifying four MSs commonly used in OFDM systems, namely, BPSK, QPSK, 16QAM and 64QAM is presented. Finally, the performance of this classifier is evaluated and the simulation results confirm the efficacy of the proposed algorithm.

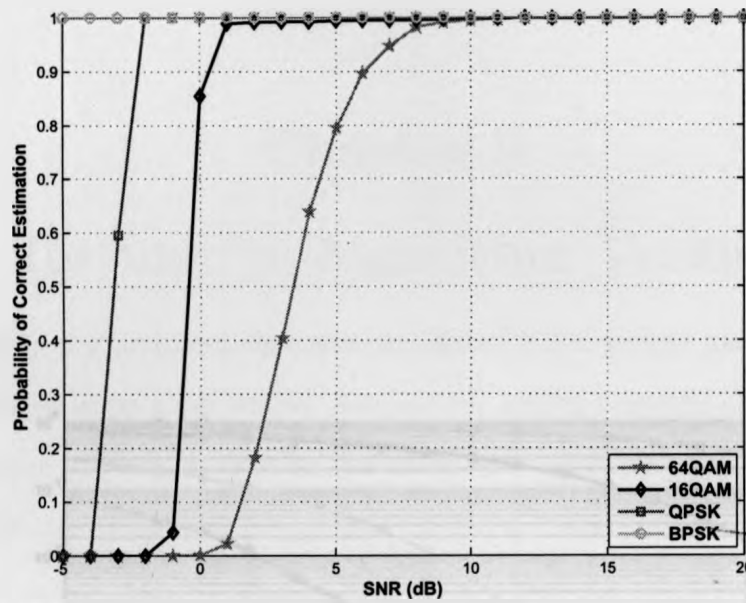


Figure 4.5: Correct classification probability of the proposed algorithm versus SNR.

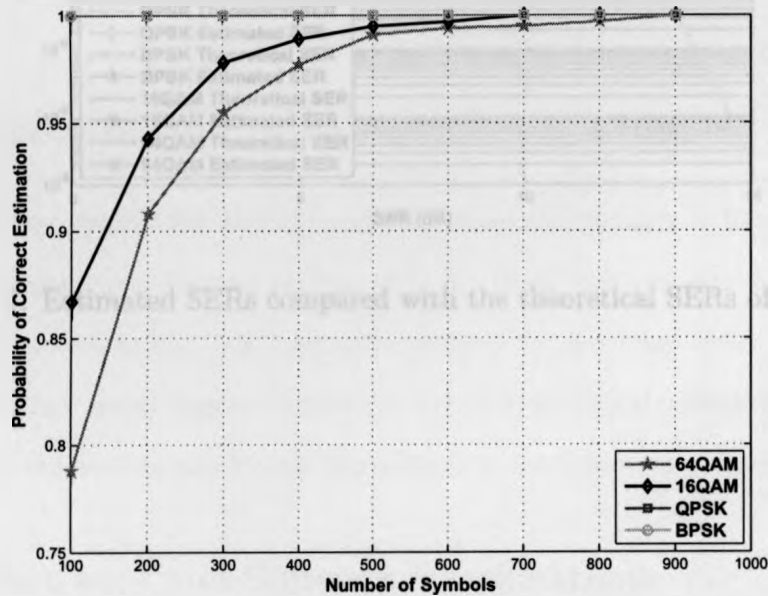


Figure 4.6: Correct classification probability of the proposed algorithm with different number of samples when SNR=10 dB.

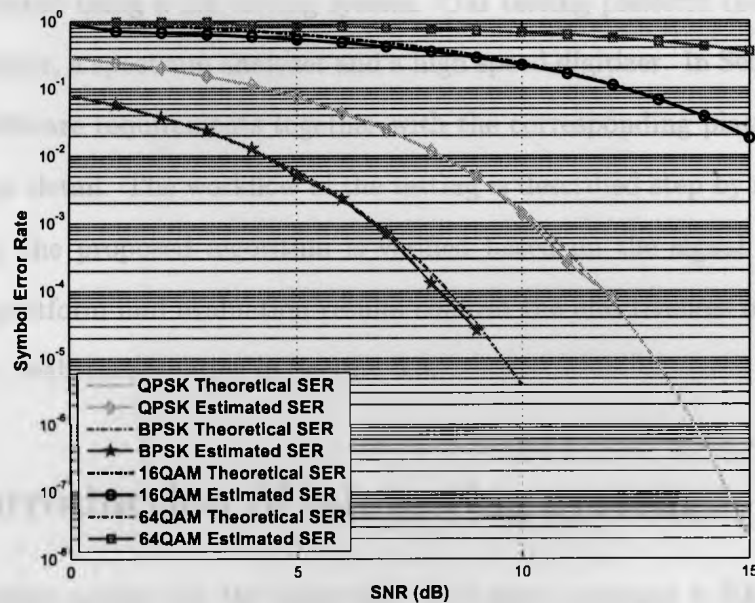


Figure 4.7: Estimated SERs compared with the theoretical SERs of four MSs.

## Chapter 5

### Lab Testing for Algorithm Verification

In this chapter, our proposed algorithm for blind OFDM system parameter estimation is evaluated using a lab testing system. Our testing platform includes a vector signal generator, a spectrum analyzer and a high speed digitizer. In Section 5.1, hardware and software requirements together with the corresponding platform setup are introduced in detail. The workflow of the testing is described step by step in Section 5.2. Finally the proposed algorithm is verified based on the signal obtained from the testing platform and evaluation results confirm the effectiveness of the proposed algorithm in realistic scenarios in Section 5.3.

#### 5.1 Introduction of lab testing system

The lab testing system for the algorithm verification contains a R&S<sup>®</sup> SMJ100A vector signal generator (shown in Fig. 5.1) for IEEE 802.11a signal generation, a R&S<sup>®</sup> FSP (shown in Fig. 5.2) spectrum analyzer for spectrum observation, and an NI PXI 5105 high speed digitizer (shown in Fig. 5.3) for signal collection and storage. The setup of the testing platform is introduced in the following section.

##### 5.1.1 Hardware and Software Specifications

The hardware and software specifications for the testing platform are shown in Table 5.1 and Table 5.2, respectively.



Figure 5.1: R&S<sup>®</sup> SMJ100A vector signal generator.

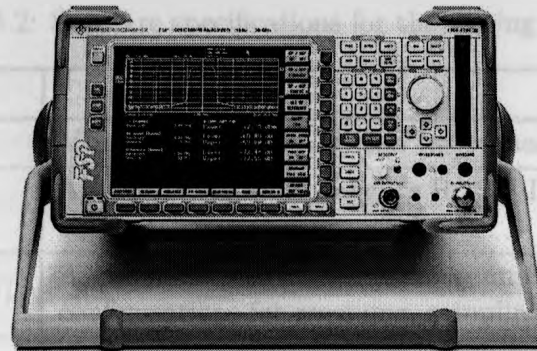


Figure 5.2: R&S FSP spectrum analyzer.

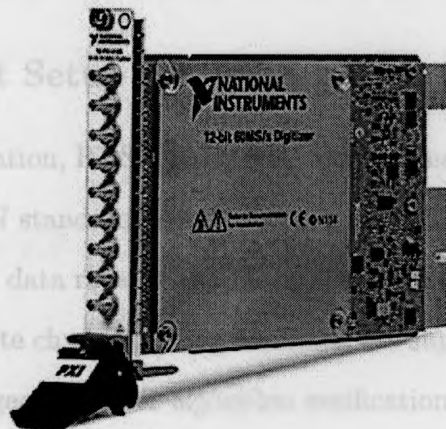


Figure 5.3: National instruments PXI 5105 high speed digitizer.



Table 5.1: Hardware specifications for the testing platform

Hardware	Characteristics
Computer	CPU with Pentium 1GHz or better.
R&S® SMJ100A	Baseband I/Q modulator and RF up to 6GHz.
R&S® FSP	Large frequency range from 9kHz to 30GHz and high measurement speed up to 1 $\mu$ s sweep time in time domain.
NI PXI 5105	High sampling rate up to 60MHz and fine resolution of 12 bits.
NI PXI 1031	Low noise emissions.

Table 5.2: Software specifications for the testing platform

Software	Characteristics
NI-VISA	VISA driver from National Instruments.
WinIQSIM	A software tool to configure R&S® I/Q modulator for signal generation.
NI LABVIEW/CVI	A graphical programming environment providing configurations for receiving, sampling and storing signals.
MATLAB	Signal processing environment.

### 5.1.2 Equipment Setup for Testing System

For OFDM signal generation, R&S® SMJ100A vector signal generator is used. It can support multiple WLAN standard specifications such as IEEE 802.11a, 802.11b and 802.11g. Specifically, all data rates in the IEEE 802.11a standard range from 6 Mbps to 54 Mbps with complete channel coding functions are supported. In our testing, an IEEE 802.11a signal is generated for algorithm verification.

For signal reception, NI PXI 5105 high speed digitizer is utilized. The PXI 5105 is capable of receiving 8 simultaneous channels of data at a rate of 60 Mega samples per second with a resolution of 12 bits. This high speed digitizer is inserted in NI PXI-1031 4-Slot 3U Chassis.

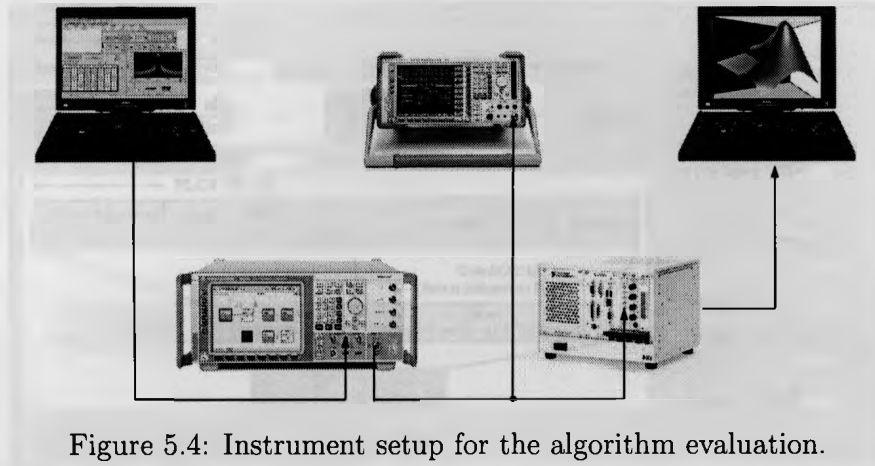


Figure 5.4: Instrument setup for the algorithm evaluation.

The interconnections of the equipments are shown in Fig. 5.4. As shown in the figure, the signal output from the vector signal generator is wired to the input of Channel 0 and Channel 1 of the digitizer plugged in the PXI chassis. The received signal is sampled and saved at the digitizer through the NI LABVIEW interface. Meanwhile, the generated signal is fed to the spectrum analyzer for signal observation and validation. The proposed blind system parameter estimation and modulation classification are performed on the saved data from the digitizer in MATLAB. The detailed workflow and configuration in each step of the testing are illustrated in the following section.

## 5.2 Workflow of the Lab Testing

The whole testing contains three steps as signal generation, validation and reception. As illustrated in Fig. 5.4, the generated signal is first configured in R&S® WinIQSIM on the PC, which is connected to R&S® SMJ100A through USB interface. Besides the setting of basic system parameters, realistic impairments such as multipath fading and CFO can also be introduced in the generated signal through the configuration in

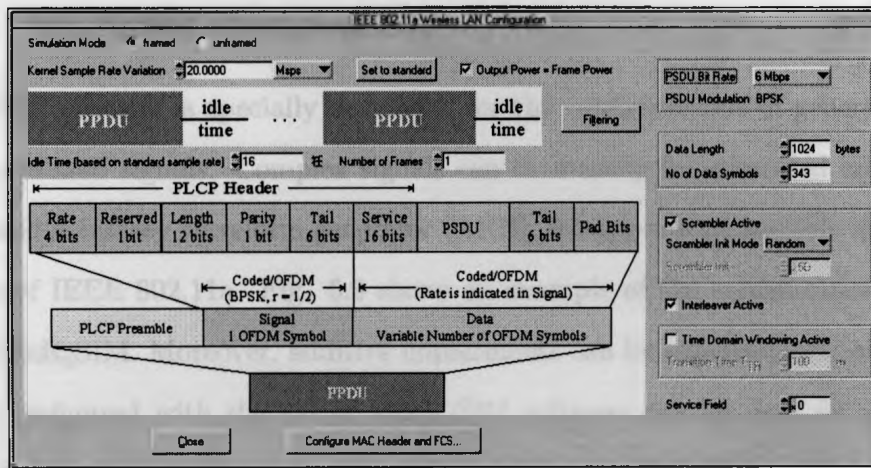


Figure 5.5: R&S<sup>®</sup> WinIQSIM configurations for generating IEEE 802.11a signals.

R&S<sup>®</sup> WinIQSIM.

Based on the configuration, actual signal waveforms with impairments generated by R&S<sup>®</sup> SMJ100A are fed to the spectrum analyzer and NI PXI 5105. The validity of the transmitted signal can be examined in the spectrum analyzer and the signals are captured and saved in NI PXI 5105 based on the specific reception configuration.

The configurations of each equipment and the setting of different signal parameters are presented step by step in the following.

### 5.2.1 Signal Generation

In our testing, configurations for generating IEEE 802.11a standard compatible signal are done in R&S<sup>®</sup> WinIQSIM software. R&S<sup>®</sup> SMJ100A then generates the corresponding signal waveforms according to these configurations.

### 5.2.1.1 WinIQSIM Configuration

WinIQSIM software is specially developed for the configurations of generating digitally modulated signals. Complex signals can thus easily be generated and tailored to the used arbitrary waveform generator (ARB). It supports all possible modulation schemes of IEEE 802.11a. Fig. 5.5 shows an example of the configuration diagram of the WinIQSIM. Moreover, additive impairments can be superimposed on a signal. Signals configured with the aid of WinIQSIM software can be used for generating signal waveforms at both baseband and RF band in the SMJ100A vector signal generator.

- Configuration for IEEE 802.11a Signal Generation

Signals configured by WinIQSIM are in accordance with IEEE 802.11a standard.

We begin with the introduction of IEEE 802.11a standard.

IEEE 802.11a WLAN supports 8 different OFDM based transmission data rates in the PHY. For each OFDM symbol, 64 carriers are defined and only the inner 52 carriers (-26 ... -1, 1 ... 26) are used for data transmission. Among the 52 used subcarriers, 4 subcarriers ( $\pm 21$  and  $\pm 7$ ) are used to transmit pilot with a fixed pattern, while the others are responsible for carrying data information. The subcarrier spacing of 312.5 kHz leads to a nominal signal bandwidth of 16.6 MHz. An OFDM symbol generated in this way has a period of 3.2  $\mu$ s. To compensate for multipath propagation, a CP with a duration of 0.8  $\mu$ s is attached to the beginning of each symbol so that a total symbol duration of 4  $\mu$ s is obtained. Major system parameters of the IEEE 802.11a PHY are shown in Table 5.3, followed by the rate-dependent parameters in Table 5.4.

Table 5.3: System parameter of IEEE 802.11a used in the testing

Parameter	Value
$N_{sd}$ : Number of data subcarriers	48
$N_{sp}$ : Number of pilot per sub-carrier	4
$N_{st}$ : Number of subcarriers, total	52
$\Delta_F$ : Subcarrier frequency spacing	0.3125 MHz
$T_{FFT}$ : IFFT/FFT period	3.2 $\mu s$
$T_{PREAMBLE}$ : PLCP preamble duration	16 $\mu s$
$T_{SIGNAL}$ : Duration of the SIGNAL BPSK-OFDM symbol	4.0 $\mu s$
$T_{GI}$ : GI duration	0.8 $\mu s$
$T_{GI2}$ : Training symbol GI duration	1.6 $\mu s$
$T_{SYM}$ : Symbol interval	4.0 $\mu s$
$B$ : Occupied bandwidth	16.6 MHz

Table 5.4: Modulation schemes and data rates in IEEE 802.11a

Data Rate (Mbits/s)	Modulation	Coding rate (R)	Coded bits per subcarrier ( $N_{BPSC}$ )	Coded bits per symbol ( $N_{CBPS}$ )	Data bits per symbol ( $N_{DBPS}$ )
6	BPSK	1/2	1	48	24
9	BPSK	3/4	1	48	36
12	QPSK	1/2	2	96	48
18	QPSK	3/4	2	96	72
24	16QAM	1/2	4	192	96
36	16QAM	3/4	4	192	144
48	64QAM	2/3	6	288	192
54	64QAM	3/4	6	288	216

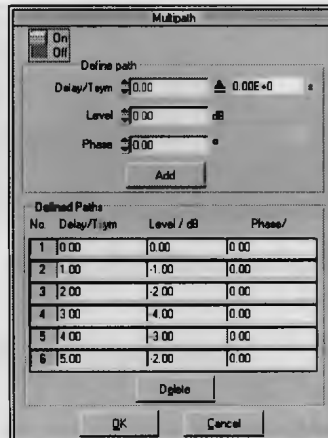


Figure 5.6: Multipath configuration panel.

In this evaluation, the raw data bits are convolutional-coded as specified and 16QAM modulation is selected for each non-null subcarriers. The detailed parameters of the generated signal are listed in Table 5.5.

Table 5.5: Signal configurations in WinIQSIM

Data Source	Pseudo Random Binary Sequence (PRBS)
Modulation type	16QAM
Symbol rate	0.25Mbps
PSDU rate	24Mbps
Sequence length	1024 bytes
Filter	Raised-Cosine Filter
Window function	Rectangular
Impulse length	32
Baseband Impulse	Rectangular

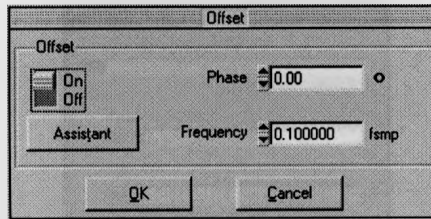


Figure 5.7: Frequency offset configuration panel.

- Configuration for Introduced Impairments

Additive impairments, i.e., multipath fading channel and CFO, in transmission can also be superimposed on the generated signal by WinIQSIM.

- Multipath Fading Channel

In the “Multipath Define” window in WinIQSIM, delay, level and the start phase can be defined as path parameters for multipath propagation as shown in Fig. 5.6. The delay time of the path is set normalized to the symbol duration.

- Frequency Offset

CFO can be configured in the “Offset panel” as shown in Fig. 5.7. In our testing, the normalized frequency offset is set to 0.1 with no phase offset.

### 5.2.1.2 Waveform Generation and Transmission

After setting all the signal parameters in WinIQSIM, an “\*.WV” file containing all the configurations is generated and transferred to SMJ100A as shown in Fig. 5.8.

The configuration file is then loaded to SMJ100A for generating and transmitting the desired continuous signal waveforms. Fig. 5.9 shows that AWGN is superimposed on the signal and then the complete impaired signal is sent to the *I*-channel and *Q*-channel.

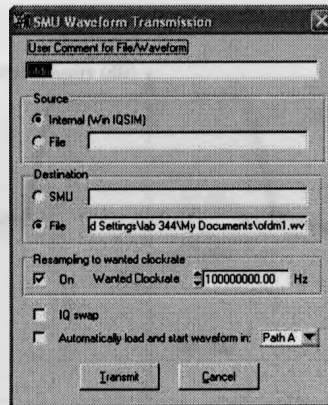


Figure 5.8: Configuration of waveform generation in WinIQSIM.

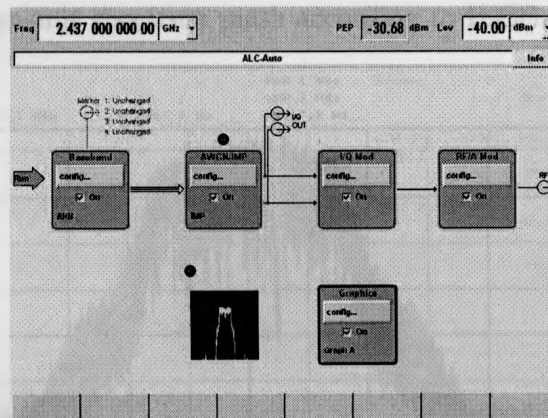


Figure 5.9: Setup for signal waveform transmission on R&amp;S® SMJ100A.

### 5.2.2 Signal Validation

The power spectrum of the transmitted signal according to IEEE 802.11a standard should fall within the spectral mask, as shown in Fig. 5.10. The spectrum of the transmitted signal observed from the spectrum analyzer is shown in Fig. 5.11, which has the same shape as the spectrum mask specified in IEEE 802.11a standard.



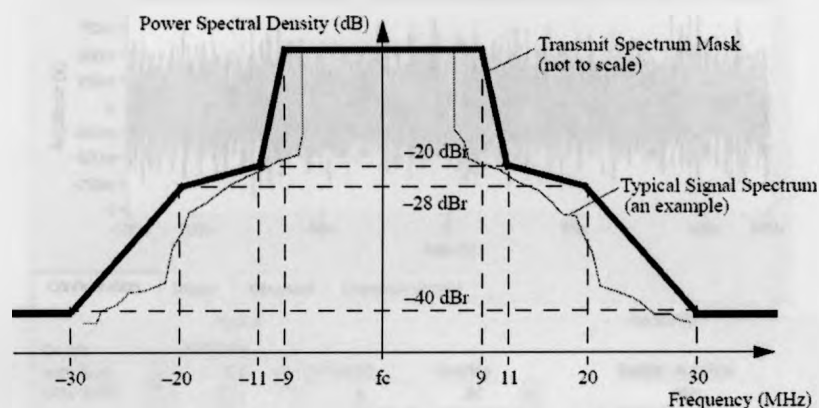
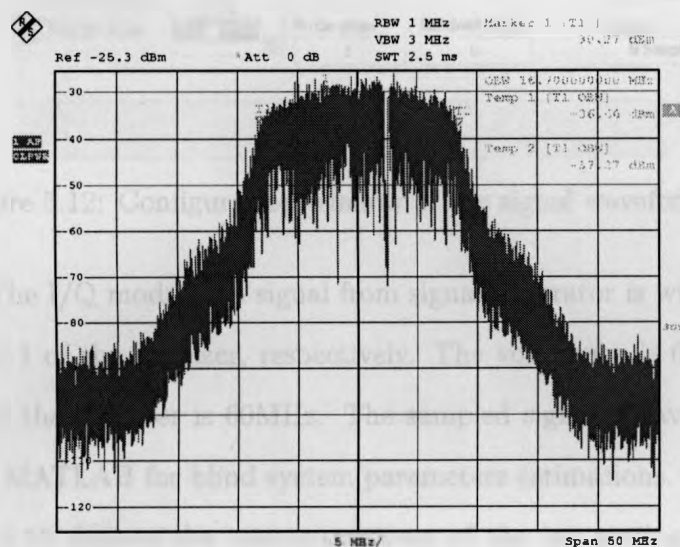


Figure 5.10: Transmit spectrum mask according to IEEE 802.11a standard.



Date: 8.MAY.2011 06:40:47

Figure 5.11: Power spectrum of the transmitted signal observed from spectrum analyzer.

### 5.2.3 Signal Reception

The high speed digitizer is wired to the vector signal generator with cables to receive and store the transmitted signal waveform. The setup for the digitizer is shown in

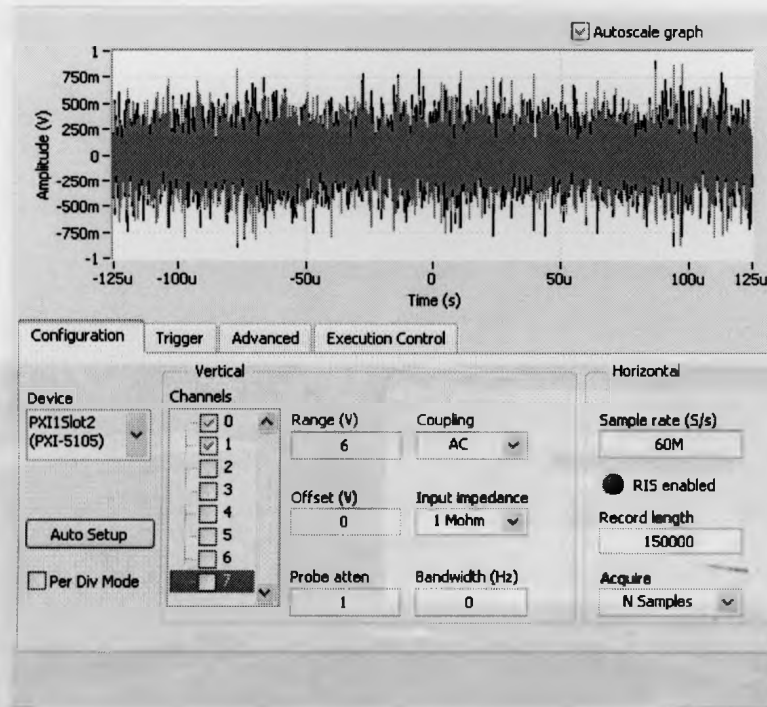


Figure 5.12: Configuration window of the signal waveform reception.

Fig. 5.12. The I/Q modulated signal from signal generator is wired to the channel 0 and channel 1 of the digitizer, respectively. The volt range is 6V and the sampling frequency of the digitizer is 60MHz. The sampled signal is saved so that it can be loaded into MATLAB for blind system parameters estimations.

Fig. 5.13 depicts the interconnections of the lab testing system. As shown in this figure, the vector signal generator placed at the bottom left is wired to the spectrum analyzer and digitizer.

### 5.3 Verification of the Proposed Algorithm

Fig. 5.14 shows the power spectrum of the signal received by the digitizer. Our proposed blind OFDM system parameter estimation algorithm is performed on this

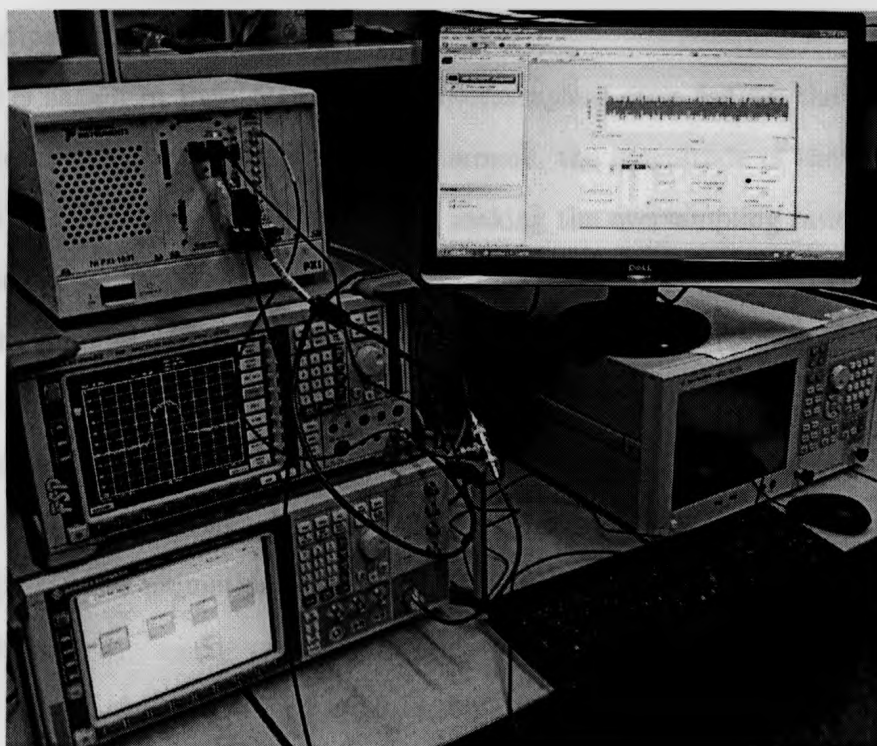


Figure 5.13: Lab testing system for the verification of the blind estimation algorithm.

signal. According to the IEEE 802.11a standard, the symbol clock frequency tolerance shall be  $\pm 20$  ppm maximum. Given the minimum and maximum FFT size at the receiver, 64 and 4096, the decimation factor derived from (3.42) therefore is 18 in the two-step algorithm for oversampling ratio estimation.

Fig. 5.16 - Fig. 5.19 depict the performance of the estimation, i.e., the oversampling ratio, number of subcarrier, CP length, CFO and the MS under both AWGN and multipath channels.

It is shown in Fig. 5.16 that the oversampling ratio follows the same trend as the results shown in Chapter 3. Furthermore, the magnitude of the CCF is not affected by frequency offsets and AWGN, making the oversampling ratio estimation robust under various realistic channels.

The number of subcarriers and CP length estimations (shown in Fig. 5.17) perform very well even at low SNRs under both AWGN and multipath channels. Although under multipath channel, there are some undesired peaks caused by multiple delayed replicas of the signal as shown in Fig. 5.15, the high correlation introduced by CP guarantees estimation accuracy as long as the multipath delay is less than the CP length.

It can be observed from Fig. 5.18 that the CFO estimation is quite accurate under AWGN, while it deteriorates under multipath channels because of the phase rotation induced from multiple delays. In addition, a large number of samples employed in estimation enhances the estimation accuracy.

Fig. 5.19 depicts the performance of the modulation classification algorithm for received signals versus different SNR values. The correct classification probability of these Classification performance improves as SNR increases for the reason that AWGN does not affect the fourth-order cumulant but their variance which is ex-

plained in Chapter 4. Therefore, increasing the SNR value improves the classification performance.

The performance of proposed algorithms for real IEEE 802.11a signals degrades due to the impairments in digitizing. Commercial high speed digitizers are typically composed of front-end analog circuitry to condition, scale and offset the input signal and a number of ADCs whose samples are interleaved to form the output. In an ideal ADC, a continuous input signal is transformed into discrete output values at equally spaced time intervals. However, in real world ADCs, a noisy signal is quantized at varying time intervals into unevenly spaced bins which causes quantization errors. Moreover, quantization errors can not be compensated for, thereby affecting the following estimation accuracy.

Another reason is the differences between OFDM symbol structure in one frame of IEEE 802.11a signals and simulated signals. For example, the structure of OFDM symbols in training sequences and preambles are different from them in data payloads. Therefore, OFDM system parameter estimations are interfered due to different OFDM symbol structures in the received signal. Moreover, for each OFDM symbol in IEEE 802.11a signal, four subcarriers are used to transmit pilots with a fixed pattern which are BPSK modulated, therefore two inherent modulations may exist in one symbol, which naturally affects MS classification results. Since a large number of data samples are employed in testing, the results in Fig. 5.17 and Fig. 5.19 are more stable than the simulation results obtained in Chapter 3.

## 5.4 Summary

In this chapter, the proposed algorithm for blind OFDM system parameter estimation is verified by a lab testing system. The hardware and software requirements of the

lab testing system, equipment interconnections and configurations are presented at the beginning of this chapter. The workflow for signal generation, validation and reception is described step by step in the sequel. Verification results given at last confirm the estimation accuracy and efficacy of the proposed algorithm in realistic scenarios.

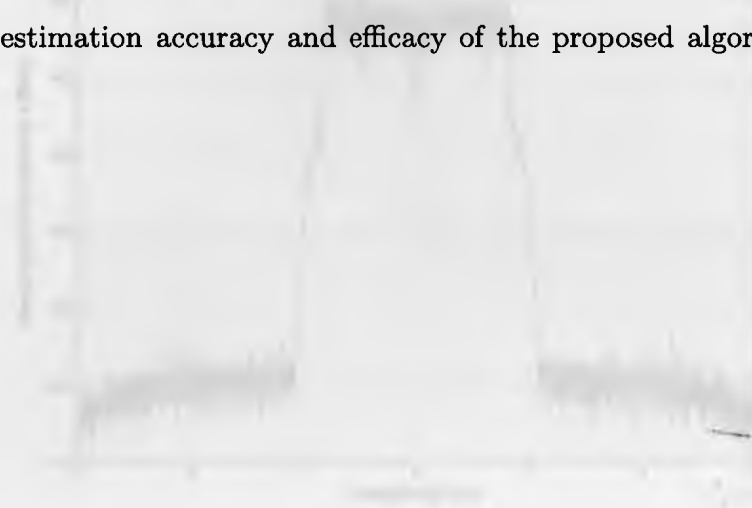


Figure 5.14: Power spectrum of the received signal. The signal is received by the antenna.



Figure 5.15: Comparison of the estimated and the actual values of the signal.

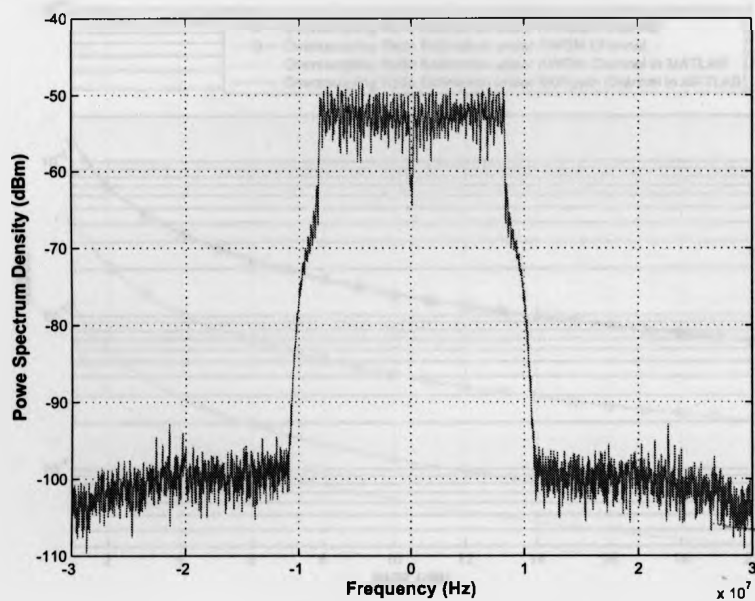


Figure 5.14: Power spectrum of the IEEE 802.11a signal received by NI PXI 5105 high speed digitizer.

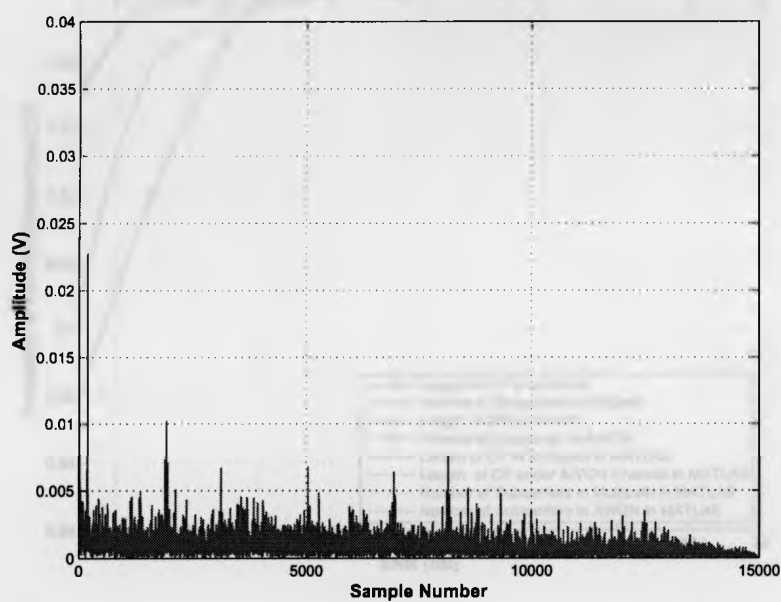


Figure 5.15: Correlation peaks in the estimation of the number of subcarriers.

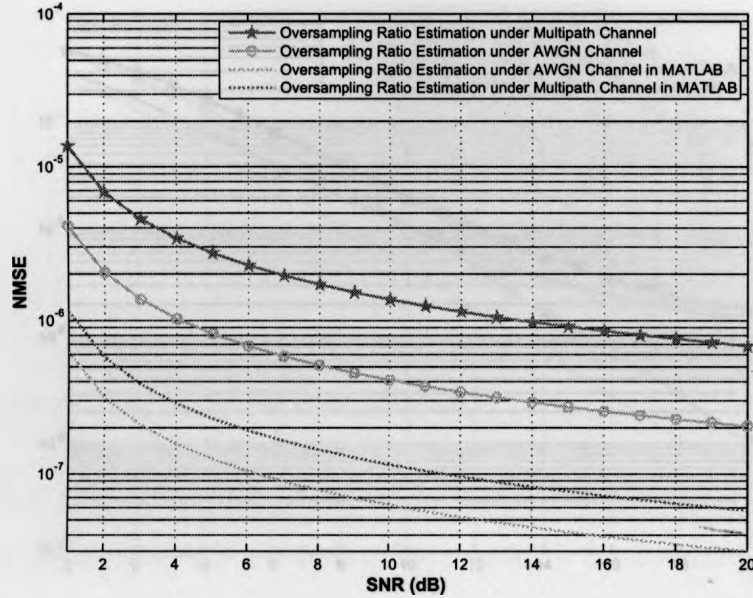


Figure 5.16: NMSE of oversampling ratio estimation of the proposed algorithm versus SNR under both AWGN and multipath channels.

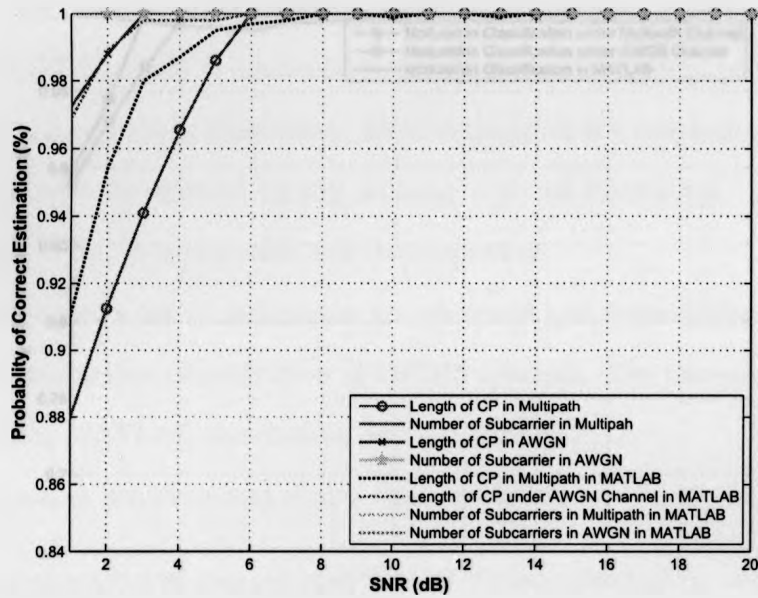


Figure 5.17: Probability of correct estimation of the number of subcarriers and CP length under both AWGN and multipath channels versus SNR.



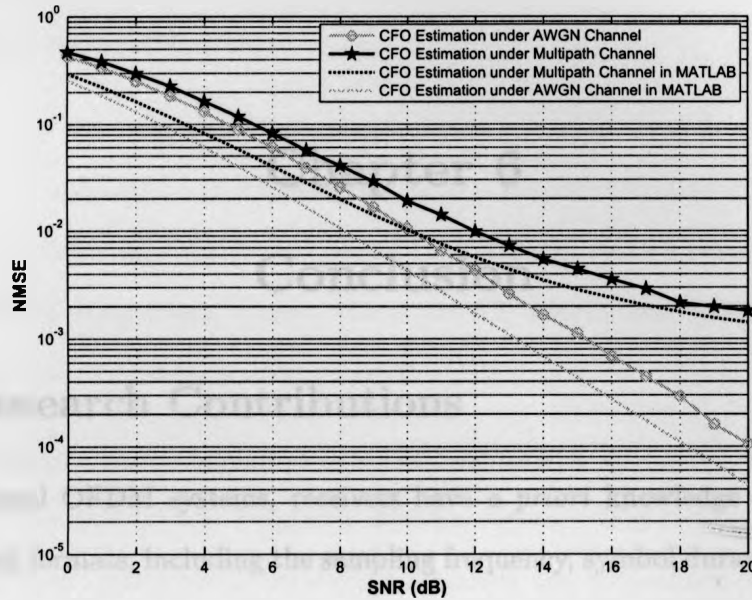


Figure 5.18: NMSE of the CFO estimation versus SNR under both AWGN and multipath channels.

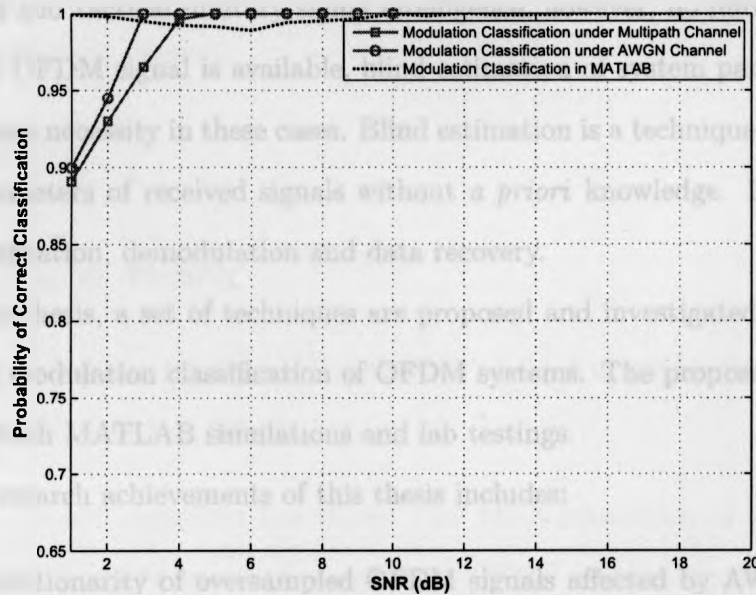


Figure 5.19: Modulation scheme classification versus SNR under both AWGN and multipath channels.

## Chapter 6

## Conclusion

### 6.1 Research Contributions

In conventional OFDM systems, receivers have *a priori* knowledge of transmitted OFDM signal formats, including the sampling frequency, symbol duration and modulation scheme. Since both transmitters and receivers are designed with known system parameters at system design stage, conventional communication studies generally focus on reliability, power/spectrum efficiency and transmission security.

In CR and tactical military signal intelligence, however, no information of the transmitted OFDM signal is available, blind estimation of system parameters therefore becomes a necessity in these cases. Blind estimation is a technique that estimates system parameters of received signals without *a priori* knowledge. It is crucial for signal identification, demodulation and data recovery.

In this thesis, a set of techniques are proposed and investigated for blind estimation and modulation classification of OFDM systems. The proposed algorithm is verified by both MATLAB simulations and lab testings.

The research achievements of this thesis includes:

- Cyclostationarity of oversampled OFDM signals affected by AWGN and multipath fading channels is investigated. The CCF and CS of the oversampled

OFDM signal are derived, which provide the foundations for the following oversampling ratio estimation.

- To reduce the computational complexity, a two-step algorithm for estimating sampling frequency and oversampling ratio is proposed by exploring the inherent signal cyclostationarity. In the sequel other OFDM system parameters, i.e., the number of subcarriers, symbol duration, CP length and CFO are estimated based on the correlation induced by the CP.
- Modulation schemes employed by OFDM subcarriers are classified by the fourth-order cumulant of the frequency domain signal. The resistance of HOS to AWGN and constellation rotation guarantees the robustness of the proposed algorithm.
- The proposed algorithm is verified through a lab testing platform. Testing results have proved the validity of the proposed algorithm under both AWGN and multipath channels.

•

## 6.2 Future Work

There are several topics related to the presented research worth further development. Some of them are listed as follows:

- The proposed algorithm has shown that blind estimation of OFDM system parameters can be achieved under both AWGN and multipath channels. In simulations, the received signal is assumed to be long enough so that the signal characteristics are obvious and stable for estimation. However, considering

more practical cases, the long observation interval of the interested signal at the receiver is not guaranteed, therefore, only limited samples of the signal is available for blind estimation. Consequently, both analytical and numerical studies on the stability of the proposed algorithm are desired under the circumstances that only limited samples are available for estimation.

- This thesis is focused on blindly estimating parameters of a detected OFDM signal of interest. For more realistic cases, interested OFDM signals should be detected first before applying the proposed algorithm. Consequently, a spectrum sensing algorithm with reliable performance is of importance as a prerequisite.

- [1] S. Haykin, *Adaptive Communication Systems*. Wiley, 2001.
- [2] S. Haykin, A. Pritchard, "Adaptive blind signal processing algorithms for an application classification," in *Adaptive Communications Conference, 1997. ADAPCOM 97. Conference Record*, 1997, pp. 1001-1007.
- [3] H. Töft, "Blind separation of overlaid binary and ternary frequency-shift keying (FSK) signals," *IEEE Transactions on Communications*, vol. 48, no. 6, pp. 980-990, 2000.
- [4] S. Haykin, H. Töft, H. Töft, H. Töft, H. Töft, and H. Töft, "A blind blind signal processing algorithm based on cyclic correlation," *IEEE Journal of Selected Areas in Communications*, vol. 19, no. 2, pp. 20-30, 2001.
- [5] M. Soderstrom, B. Soderstrom, and A. Soderstrom, "Blind signal classification: detection of two overlapping and a mixture of subcarriers," in *IEEE Workshop on Statistical Signal and Array Processing*, 1999, pp. 100-104.
- [6] M. Soderstrom and B. Soderstrom, "Blind signal classification: detection of two overlapping and a mixture of subcarriers," in *IEEE Workshop on Statistical Signal and Array Processing*, 1999, pp. 100-104.
- [7] K. S. Lee, "Spectrum of overlaid signals and its application to blind signal processing," *IEEE Trans. on Signal Process.*, vol. 46, pp. 1775-1786, 1998.
- [8] S. Soderstrom and B. Soderstrom, "Blind signal classification: detection of two overlapping and a mixture of subcarriers," *IEEE Transactions on Communications*, vol. 48, no. 6, pp. 980-990, 2000.

## References

- [1] "Ieee standard for information technology-telecommunications and information exchange between systems-local and metropolitan area networks-specific requirements - part 11: Wireless lan medium access control (mac) and physical layer (phy) specifications," *IEEE Std 802.11-2007 (Revision of IEEE Std 802.11-1999)*, pp. C1–1184, 12 2007.
- [2] E. T. Standard, "Digital video broadcasting (dvb): Framing structure, channel coding and modulation for digital terrestrial television (dvb-t)," *ETS 300401*, Feb. 1995.
- [3] B. Sklar, *Digital communications*. Prentice Hall, 2001.
- [4] C. Hwang and A. Polydoros, "Advanced methods for digital quadrature and offset modulation classification," in *Military Communications Conference, 1991. MILCOM '91, Conference Record, 'Military Communications in a Changing World'*, IEEE, nov 1991, pp. 841–845 vol.2.
- [5] H. Bolcskei, "Blind estimation of symbol timing and carrier frequency offset in wireless OFDM systems," *IEEE Transactions on Communications*, vol. 49, no. 6, pp. 988–999, 2001.
- [6] B. Park, H. Cheon, E. Ko, C. Kang, and D. Hong, "A blind ofdm synchronization algorithm based on cyclic correlation," *IEEE Signal Processing Letters*, vol. 11, no. 2, pp. 83–85, 2004.
- [7] W. Akmouche, E. Kerherve, and A. Quinquis, "Ofdm spectral characterization: estimation of the bandwidth and the number of sub-carriers," in *IEEE Workshop on Statistical Signal and Array Processing*. IEEE, 2000, pp. 48–52.
- [8] M. Oner and F. Jondral, "Cyclostationarity based air interface recognition for software radio systems," in *Radio and Wireless Conference, 2004 IEEE*. IEEE, 2004, pp. 263–266.
- [9] R. Chang, "Synthesis of band-limited orthogonal signals for multichannel data transmission," *Bell Sys. Tech. J.*, vol. 45, pp. 1775–1796, 1966.
- [10] S. Weinstein and P. Ebert, "Data transmission by frequency-division multiplexing using the discrete Fourier transform," *IEEE Transactions on Communication Technology*, vol. 19, no. 5, pp. 628–634, 1971.

- [11] L. Cimini Jr, "Analysis and simulation of a digital mobile channel using orthogonal frequency division multiplexing," *IEEE Transactions on Communications*, vol. 33, no. 7, pp. 665–675, 1985.
- [12] G. Li and G. Stber, *Orthogonal frequency division multiplexing for wireless communications*. Springer, 2006.
- [13] M. Speth, S. Fechtel, G. Fock, and H. Meyr, "Optimum receiver design for wireless broad-band systems using OFDM. I," *IEEE Transactions on Communications*, vol. 47, no. 11, pp. 1668–1677, 1999.
- [14] G. Santella, "A frequency and symbol synchronization system for OFDM signals: architecture and simulation results," *IEEE Transactions on Vehicular Technology*, vol. 49, no. 1, pp. 254–275, 2000.
- [15] S. Liu and J. Chong, "A study of joint tracking algorithms of carrier frequency offset and sampling clock offset for ofdm-based wlans," in *IEEE International Conference on Communications, Circuits and Systems and West Sino Expositions*, vol. 1. IEEE, 2002, pp. 109–113.
- [16] E. Ref, "ETSI: Digital Video Broadcasting (DVB); Implementation guidelines for DVB terrestrial services; Transmission aspects," Dec. 1997, tR Patent 101,190.
- [17] "Supplement to iee standard for information technology - telecommunications and information exchange between systems - local and metropolitan area networks - specific requirements. part 11: Wireless lan medium access control (mac) and physical layer (phy) specifications: High-speed physical layer in the 5 ghz band," *IEEE Std 802.11a-1999*, p. i, 1999.
- [18] "Ieee standard for information technology - telecommunications and information exchange between systems - local and metropolitan area networks - specific requirement. part 11: Wireless lan medium access control (mac) and physical layer (phy) specifications. amendment 2: Higher-speed physical layer (phy) extension in the 2.4 ghz band - corrigendum 1," *IEEE Std 802.11b-1999/Cor 1-2001*, p. 0.1, 2001.
- [19] "Ieee standard for information technology- telecommunications and information exchange between systems- local and metropolitan area networks- specific requirements part ii: Wireless lan medium access control (mac) and physical layer (phy) specifications," *IEEE Std 802.11g-2003 (Amendment to IEEE Std 802.11, 1999 Edn. (Reaff 2003) as amended by IEEE Std 802.11a-1999, 802.11b-1999, 802.11b-1999/Cor 1-2001, and 802.11d-2001)*, pp. i –67, 2003.
- [20] "Ieee standard for information technology–telecommunications and information exchange between systems–local and metropolitan area networks–specific requirements part 11: Wireless lan medium access control (mac) and physical

- layer (phy) specifications amendment 5: Enhancements for higher throughput," *IEEE Std 802.11n-2009 (Amendment to IEEE Std 802.11-2007 as amended by IEEE Std 802.11k-2008, IEEE Std 802.11r-2008, IEEE Std 802.11y-2008, and IEEE Std 802.11w-2009)*, pp. c1–502, 2009.
- [21] . W. Group, "802.16 working group. [online]," "http://www.ieee802.org/16".
- [22] S. Shepard, *WiMax crash course*. McGraw-Hill Osborne Media, 2006.
- [23] "Ieee standard for local and metropolitan area networks part 16: Air interface for fixed broadband wireless access systems," *IEEE Std 802.16-2004 (Revision of IEEE Std 802.16-2001)*, pp. 0.1 – –857, 2004.
- [24] C. Cordeiro, K. Challapali, D. Birru, S. Shankar *et al.*, "Ieee 802.22: the first worldwide wireless standard based on cognitive radios," in *IEEE International Symposium on New Frontiers in Dynamic Spectrum Access Networks*. Ieee, 2005, pp. 328–337.
- [25] M. Oner and F. Jondral, "Cyclostationarity based air interface recognition for software radio systems," in *IEEE Radio and Wireless Conference*. IEEE, 2004, pp. 263–266.
- [26] B. Wang and L. Ge, "A novel algorithm for identification of ofdm signal," in *2005 International Conference on Wireless Communications, Networking and Mobile Computing*, vol. 1. IEEE, 2005, pp. 261–264.
- [27] W. Akmouche, "Detection of multicarrier modulations using 4th-order cumulants," in *Military Communications Conference Proceedings, 1999. MILCOM 1999. IEEE*, vol. 1. IEEE, 1999, pp. 432–436.
- [28] W. Gardner, "Cyclostationarity in communications and signal processing," *STATISTICAL SIGNAL PROCESSING INC YOUNTVILLE CA*, Tech. Rep., 1994.
- [29] A. Papoulis and S. Pillai, *Probability, random variables and stochastic processes*. McGraw-Hill Education (India) Pvt Ltd, 2002.
- [30] W. Gardner, *Introduction to Random Processes: with applications to signals and systems*. McGraw-Hill, 1990.
- [31] —, *Statistical spectral analysis: a nonprobabilistic theory*. Prentice-Hall, Inc. Upper Saddle River, NJ, USA, 1986.
- [32] A. Punchihewa, Q. Zhang, O. Dobre, C. Spooner, S. Rajan, and R. Inkol, "On the cyclostationarity of ofdm and single carrier linearly digitally modulated signals

- in time dispersive channels: theoretical developments and application," *IEEE Transactions on Wireless Communications*, vol. 9, no. 8, pp. 2588–2599, 2010.
- [33] M. Shi, Y. Bar-Ness, and W. Su, "A Simple Method to Enhance the Detection of Second Order Cyclostationarity," in *IEEE Global Telecommunications Conference 2008*. IEEE, 2008, pp. 1–6.
- [34] A. Dandawate and G. Giannakis, "Statistical tests for presence of cyclostationarity," *IEEE Transactions on Signal Processing*, vol. 42, no. 9, pp. 2355–2369, 1994.
- [35] D. Reed and M. Wickert, "Minimization of detection of symbol-rate spectral lines by delay and multiply receivers," *IEEE Transactions on Communications*, vol. 36, no. 1, pp. 118–120, 1988.
- [36] J. Cooley and J. Tukey, "An algorithm for the machine calculation of complex Fourier series," *Math. Comput.*, vol. 19, no. 90, pp. 297–301, 1965.
- [37] J. Cooley, "How the FFT gained acceptance," in *Proceedings of the ACM conference on History of scientific and numeric computation*. ACM, 1987, pp. 97–100.
- [38] E. Hoyer and R. Stork, "The zoom FFT using complex modulation," in *IEEE International Conference on Acoustics, Speech, and Signal Processing*, vol. 2. IEEE, 1977, pp. 78–81.
- [39] P. Yip, "Some aspects of the zoom transform," *IEEE Transactions on Computers*, vol. 100, no. 3, pp. 287–296, 1976.
- [40] J. Proakis and D. Manolakis, *Introduction to digital signal processing*. Prentice Hall Professional Technical Reference, 1988.
- [41] H. Ishii and G. Wornell, "OFDM blind parameter identification in cognitive radios," in *IEEE 16th International Symposium on Personal, Indoor and Mobile Radio Communications, 2005.*, vol. 1. IEEE, 2005, pp. 700–705.
- [42] A. Bouzegzi, P. Ciblat, and P. Jallon, "New algorithms for blind recognition of OFDM based systems," *Signal Processing*, vol. 90, no. 3, pp. 900–913, 2010.
- [43] P. Moose, "A technique for orthogonal frequency division multiplexing frequency offset correction," *IEEE Transactions on Communications*, vol. 42, no. 10, pp. 2908–2914, 1994.
- [44] F. Daffara and O. Adami, "A new frequency detector for orthogonal multicarrier transmission techniques," in *IEEE 45th Vehicular Technology Conference, 1995*, vol. 2. IEEE, 1995, pp. 804–809.



- [45] M. Shi, Y. Bar-Ness, and W. Su, "Blind OFDM systems parameters estimation for software defined radio," in *New Frontiers in Dynamic Spectrum Access Networks, 2007. DySPAN 2007. 2nd IEEE International Symposium on*. IEEE, pp. 119–122.
- [46] S. Mak and A. Aghvami, "Detection of trellis-coded modulation on time-dispersive channels," in *Global Telecommunications Conference*, vol. 3. IEEE, 1996, pp. 1825–1829.
- [47] J. Anderson, *Digital transmission engineering*. Wiley-IEEE Press, 2005.
- [48] J. Anderson, T. Aulin, and C. Sundberg, *Digital phase modulation*. Plenum Publishing Corporation, 1986.
- [49] B. Sklar, *Digital communications*. Prentice Hall, 2001.
- [50] K. Chugg, C.-S. Long, and A. Polydoros, "Combined likelihood power estimation and multiple hypothesis modulation classification," in *Signals, Systems and Computers, 1995. 1995 Conference Record of the Twenty-Ninth Asilomar Conference on*, vol. 2, oct-1 nov 1995, pp. 1137–1141 vol.2.
- [51] W. Wei and J. Mendel, "A new maximum-likelihood method for modulation classification," in *1995 Conference Record of the Twenty-Ninth Asilomar Conference on Signals, Systems and Computers, 1995.*, vol. 2, oct-1 nov 1995, pp. 1132–1136 vol.2.
- [52] J. Reichert, "Automatic classification of communication signals using higher order statistics," in *IEEE International Conference on Acoustics, Speech, and Signal Processing, 1992.*, vol. 5, mar 1992, pp. 221–224 vol.5.
- [53] W. Wei and J. Mendel, "A new maximum-likelihood method for modulation classification," in *Signals, Systems and Computers, 1995. 1995 Conference Record of the Twenty-Ninth Asilomar Conference on*, vol. 2. IEEE, 1995, pp. 1132–1136.
- [54] A. Swami and B. Sadler, "Hierarchical digital modulation classification using cumulants," *IEEE Transactions on Communications*, vol. 48, no. 3, pp. 416–429, 2000.
- [55] K. Assaleh, K. Farrell, and R. Mammone, "A new method of modulation classification for digitally modulated signals," in *IEEE Military Communications Conference*. IEEE, 1992, pp. 712–716.
- [56] C. Spooner, "Classification of co-channel communication signals using cyclic cumulants," in *asilomar*. Published by the IEEE Computer Society, 1995, p. 531.

- [57] —, "On the utility of sixth-order cyclic cumulants for RF signal classification," in *Conference Record of the Thirty-Fifth Asilomar Conference on Signals, Systems and Computers*, vol. 1. IEEE, 2001, pp. 890–897.
- [58] O. Dobre, Y. Bar-Ness, and W. Su, "Robust QAM modulation classification algorithm using cyclic cumulants," in *IEEE Wireless Communications and Networking Conference*, vol. 2. IEEE, 2004, pp. 745–748.
- [59] —, "Higher-order cyclic cumulants for high order modulation classification," in *IEEE Military Communications Conference*, vol. 1. IEEE, 2003, pp. 112–117.
- [60] C. Nikias and J. Mendel, "Signal processing with higher-order spectra," *IEEE Signal Processing Magazine*, vol. 10, no. 3, pp. 10–37, 1993.
- [61] J. Mendel, "Tutorial on higher-order statistics (spectra) in signal processing and system theory: Theoretical results and some applications," *Proceedings of the IEEE*, vol. 79, no. 3, pp. 278–305, March 1991.
- [62] B. Everitt and A. Skrondal, *The Cambridge dictionary of statistics*. Cambridge University Press New York, 2002.

## Appendix A

### Time-varying ACF, CCF and CS of OFDM Signals

The expression for the time-varying ACF, CCF and CS of the received OFDM signal given by (3.21) are derived here, the AWGN component does not take into computation.

$$\begin{aligned}
 \tilde{R}(t, \tau) &= E[r(t)r^*(t + \tau)] \\
 &= \frac{\sigma_d^2}{N} e^{-j2\pi\Delta f_c \tau} \sum_{k=0}^{N-1} \sum_{l=-\infty}^{\infty} \sum_{m_1=1}^{M_c} h(\xi_{m_1}) e^{j2\pi k \Delta f_k (t - \xi_{m_1} - lT)} g(t - \xi_{m_1} - lT) \\
 &\quad \times \sum_{m_2=1}^{M_c} h^*(\xi_{m_2}) e^{-j2\pi k \Delta f_k (t - \xi_{m_2} - lT + \tau)} g^*(t - \xi_{m_2} - lT + \tau) \\
 &= \frac{\sigma_d^2}{N} e^{-j2\pi\Delta f_c \tau} \sum_{k=0}^{N-1} \sum_{l=-\infty}^{\infty} e^{-j2\pi k \Delta f_k \tau} \sum_{m_1=1}^{M_c} h(\xi_{m_1}) e^{-j2\pi k \Delta f_k \xi_{m_1}} \\
 &\quad \times g(t - \xi_{m_1} - lT) \sum_{m_2=1}^{M_c} h^*(\xi_{m_2}) e^{j2\pi k \Delta f_k \xi_{m_2}} g^*(t - \xi_{m_2} - lT + \tau) \\
 &= \frac{\sigma_d^2}{N} e^{-j2\pi\Delta f_c \tau} \sum_{k=0}^{N-1} e^{-j2\pi k \Delta f_k \tau} \sum_{m_1=1}^{M_c} h(\xi_{m_1}) e^{-j2\pi k \Delta f_k \xi_{m_1}} g(t - \xi_{m_1}) \\
 &\quad \times \sum_{m_2=1}^{M_c} h^*(\xi_{m_2}) e^{j2\pi k \Delta f_k \xi_{m_2}} g^*(t - \xi_{m_2} + \tau) \otimes \sum_{l=-\infty}^{\infty} \delta(t - lT). \quad (\text{A.1})
 \end{aligned}$$

The CCF of (A.1) at the CF  $\alpha$  and the time delay  $\tau$  can be obtained by taking Fourier transform of (A.1) with respect to  $t$  given as

$$\begin{aligned}
 \bar{R}(\alpha, \tau) &= \int_{-\infty}^{\infty} \bar{R}(t, \tau) e^{-j2\pi\alpha t} dt \\
 &= \frac{\sigma_d^2}{N} e^{-j2\pi\Delta f_c \tau} \int_{-\infty}^{\infty} \left[ \sum_{k=0}^{N-1} e^{-j2\pi k \Delta f_k \tau} \sum_{m_1=1}^{M_c} h(\xi_{m_1}) e^{-j2\pi k \Delta f_k \xi_{m_1}} \right. \\
 &\quad \times g(t - \xi_{m_1}) \sum_{m_2=1}^{M_c} h^*(\xi_{m_2}) e^{j2\pi k \Delta f_k \xi_{m_2}} g^*(t - \xi_{m_2} + \tau) \left. \right] e^{-j2\pi\alpha t} dt \\
 &\quad \otimes \sum_{l=-\infty}^{\infty} \delta(t - lT). \tag{A.2}
 \end{aligned}$$

By using the convolution theorem that

$$f(x) \otimes p(x) = \int_{-\infty}^{\infty} f(x) p(u - x) dx, \tag{A.3}$$

(A.2) can be written as

$$\begin{aligned}
 \bar{R}(\alpha, \tau) &= \frac{\sigma_d^2}{N} e^{-j2\pi\Delta f_c \tau} \sum_{k=0}^{N-1} e^{-j2\pi k \Delta f_k \tau} \int_{-\infty}^{\infty} \int_{-\infty}^{\infty} \sum_{m_1=1}^{M_c} h(\xi_{m_1}) e^{-j2\pi k \Delta f_k \xi_{m_1}} \\
 &\quad \times g(y - \xi_{m_1}) \sum_{m_2=1}^{M_c} h^*(\xi_{m_2}) e^{j2\pi k \Delta f_k \xi_{m_2}} g^*(y - \xi_{m_2} + \tau) \\
 &\quad \times \sum_{l=-\infty}^{\infty} \delta(t - y - lT) e^{-j2\pi\alpha t} dy dt. \tag{A.4}
 \end{aligned}$$

With the change of variables  $t - y = v$  and  $y = y$ , and by using the identity  $\mathfrak{F}\{\sum_{l=-\infty}^{\infty} \delta(t - lT)\} = T^{-1} \sum_{l=-\infty}^{\infty} \delta(\alpha - lT^{-1})$ ,  $\mathfrak{F}$  denotes Fourier transform, one

can easily show that

$$\begin{aligned}
 \bar{R}(\alpha, \tau) = & \frac{\sigma_d^2}{NT} e^{-j2\pi\Delta f_c \tau} \sum_{k=0}^{N-1} e^{-j2\pi k \Delta f_k \tau} \int_{-\infty}^{\infty} \sum_{m_1=1}^{M_c} h(\xi_{m_1}) e^{-j2\pi k \Delta f_k \xi_{m_1}} \\
 & \times g(y - \xi_{m_1}) \sum_{m_2=1}^{M_c} h^*(\xi_{m_2}) e^{j2\pi k \Delta f_k \xi_{m_2}} g^*(y - \xi_{m_2} + \tau) \\
 & e^{-j2\pi\alpha y} dy \times \sum_{l=-\infty}^{\infty} \delta(\alpha - lT^{-1}). \quad (A.5)
 \end{aligned}$$

It can be seen that  $\bar{R}(\alpha, \tau) \neq 0$  only at  $\alpha = lT^{-1}$ , with  $l$  as an integer. By using the notation  $y=t$ , (A.5) can be written as,

$$\begin{aligned}
 \bar{R}(\alpha, \tau) = & \frac{\sigma_d^2}{NT} e^{-j2\pi\Delta f_c \tau} \sum_{k=0}^{N-1} e^{-j2\pi k \Delta f_k \tau} \int_{-\infty}^{\infty} \sum_{m_1=1}^{M_c} h(\xi_{m_1}) e^{-j2\pi k \Delta f_k \xi_{m_1}} \\
 & \times g(t - \xi_{m_1}) \sum_{m_2=1}^{M_c} h^*(\xi_{m_2}) e^{j2\pi k \Delta f_k \xi_{m_2}} g^*(t - \xi_{m_2} + \tau) \\
 & e^{-j2\pi\alpha t} dt \times \sum_{l=-\infty}^{\infty} \delta(\alpha - lT^{-1}). \quad (A.6)
 \end{aligned}$$

The expression of the CS of (A.1) at the CF  $\alpha$  and spectral frequency vector  $f$

can be gained by taking Fourier transform of (3.24) with respect to  $\tau$  given by

$$\begin{aligned}
 \bar{S}(\alpha, f) &= \int_{-\infty}^{\infty} \bar{R}(\alpha, \tau) d\tau \\
 &= \frac{\sigma_d^2}{NT} \int_{-\infty}^{\infty} [e^{-j2\pi\Delta f_c\tau} \sum_{k=0}^{N-1} e^{-j2\pi k\Delta f_k\tau} \int_{-\infty}^{\infty} \sum_{m_1=1}^{M_c} h(\xi_{m_1}) e^{-j2\pi k\Delta f_k\xi_{m_1}} \\
 &\quad \times g(t - \xi_{m_1}) \sum_{m_2=1}^{M_c} h^*(\xi_{m_2}) e^{j2\pi k\Delta f_k\xi_{m_2}} g^*(t - \xi_{m_2} + \tau) \\
 &\quad \times e^{-j2\pi\alpha t} dt] e^{-j2\pi f\tau} d\tau \\
 &= \frac{\sigma_d^2}{NT} \int_{-\infty}^{\infty} \int_{-\infty}^{\infty} \sum_{k=0}^{N-1} \sum_{m_2=1}^{M_c} h^*(\xi_{m_2}) e^{j2\pi k\Delta f_k\xi_{m_2}} g^*(t - \xi_{m_2} + \tau) \\
 &\quad \times e^{-j2\pi\Delta f_c\tau} e^{-j2\pi k\Delta f_k\tau} e^{-j2\pi f\tau} d\tau \\
 &\quad \times \sum_{m_1=1}^{M_c} h(\xi_{m_1}) e^{-j2\pi k\Delta f_k\xi_{m_1}} g(t - \xi_{m_1}) e^{-j2\pi\alpha t} dt. \tag{A.7}
 \end{aligned}$$

With the change of variables, i.e.,  $t = t$ ,  $\nu = t + \tau$ , (A.7) becomes

$$\begin{aligned}
 \bar{S}(\alpha, f) &= \frac{\sigma_d^2}{NT} \int_{-\infty}^{\infty} \sum_{k=0}^{N-1} \sum_{m_2=1}^{M_c} h^*(\xi_{m_2}) e^{j2\pi k\Delta f_k\xi_{m_2}} g^*(t - \xi_{m_2} + \tau) \\
 &\quad \times e^{-j2\pi(f+\Delta f_c+k\Delta f_k)\nu} e^{j2\pi(f+\Delta f_c+k\Delta f_k)t} d\nu \\
 &\quad \times \int_{-\infty}^{\infty} \sum_{m_1=1}^{M_c} h(\xi_{m_1}) e^{-j2\pi k\Delta f_k\xi_{m_1}} \times g(t - \xi_{m_1}) e^{-j2\pi\alpha t} dt \\
 &= \frac{\sigma_d^2}{NT} \int_{-\infty}^{\infty} \sum_{k=0}^{N-1} \sum_{m_2=1}^{M_c} h^*(\xi_{m_2}) e^{j2\pi k\Delta f_k\xi_{m_2}} g^*(t - \xi_{m_2} + \tau) \\
 &\quad \times e^{-j2\pi(f+\Delta f_c+k\Delta f_k)\nu} d\nu \\
 &\quad \times \int_{-\infty}^{\infty} \sum_{m_1=1}^{M_c} h(\xi_{m_1}) e^{-j2\pi k\Delta f_k\xi_{m_1}} g(t - \xi_{m_1}) \\
 &\quad \times e^{j2\pi(f+\Delta f_c+k\Delta f_k)t} e^{-j2\pi\alpha t} dt. \tag{A.8}
 \end{aligned}$$

Notice that the fourth and sixth lines of (A.8) can be written as a Fourier transform of two convolved functions, and (A.8) becomes,

$$\begin{aligned} \tilde{S}(\alpha, f) = & \frac{\sigma_d^2}{NT} \sum_{k=0}^{N-1} \int_{-\infty}^{\infty} (h^*(\nu) e^{j2\pi k \Delta f_k \nu} \otimes g^*(\nu)) \\ & \times e^{-j2\pi(f + \Delta f_c + k \Delta f_k) \nu} d\nu \\ & \times \int_{-\infty}^{\infty} (h(t) e^{-j2\pi k \Delta f_k t} \otimes g(t)) e^{j2\pi(f + \Delta f_c + k \Delta f_k) t} e^{-j2\pi \alpha t} dt. \end{aligned} \quad (\text{A.9})$$

By using the Fourier transform of the convolution of two signals is multiplication of their Fourier transforms, and

$$\int_{-\infty}^{\infty} g(\tau) e^{-j2\pi f \tau} e^{j2\pi \Delta f \tau} d\tau = G(f - \Delta f), \quad (\text{A.10})$$

$$\int_{-\infty}^{\infty} g^*(\tau) e^{-j2\pi f \tau} e^{j2\pi \Delta f \tau} d\tau = G^*(-f + \Delta f), \quad (\text{A.11})$$

$$\int_{-\infty}^{\infty} h(\tau) e^{-j2\pi f \tau} e^{j2\pi \Delta f \tau} d\tau = H(f - \Delta f), \quad (\text{A.12})$$

$$\int_{-\infty}^{\infty} h^*(\tau) e^{-j2\pi f \tau} e^{j2\pi \Delta f \tau} d\tau = H^*(-f + \Delta f), \quad (\text{A.13})$$

with  $H(f)$  and  $G(f)$  as the Fourier transform of  $h(t)$  and  $g(t)$  respectively, and  $\Delta f$

as a frequency shift, (A.9) becomes

$$\begin{aligned}
 \tilde{S}(\alpha, f) &= \frac{\sigma_d^2}{NT} \sum_{k=0}^{N-1} H^*(-(f + \Delta f_c + k\Delta f_k) + k\Delta f_k) G^*(-(f + \Delta f_c + k\Delta f_k)) \\
 &\quad \times H(\alpha - \Delta f_c - f) G(\alpha - f - \Delta f_c - k\Delta f_k) \\
 &= \frac{\sigma_d^2}{NT} \sum_{k=0}^{N-1} H^*(-f - \Delta f_c) G^*(-(f + \Delta f_c + k\Delta f_k)) \\
 &\quad \times H(\alpha - \Delta f_c - f) G(\alpha - f - \Delta f_c - k\Delta f_k). \tag{A.14}
 \end{aligned}$$

Printed at State:

Copyright, Printed, India.

Year of birth:

1997

Publication:

John Wiley & Sons

Publication:

Thomson and Thomson Publishing

Diagram:

Issuing University of South and Communications

Testing, Theory, China

Publications:

- [1] M. J. Jones, B. Wang and D. E. C. "Time-varying Autocorrelation Functions of OFDM Signals and Frequency Estimation in OFDM Systems", *Proc. IEEE Veh. Tech. Conf.*, Atlanta, Georgia, Sept. 2000.
- [2] Q. Liang, B. Wang and D. E. C. "Time-varying Autocorrelation Functions of OFDM Signals and Frequency Estimation in OFDM Systems", *Proc. IEEE Veh. Tech. Conf.*, Atlanta, Georgia, Sept. 2000.